Influence of Solar Activity Cycles on Earth's Climate

Final Report

Task 700 – Summary Report
Conclusions and Recommendations

Freddy Christiansen, Danish National Space Center
Joanna D. Haigh, Imperial College
Henrik Lundstedt, Swedish Institute of Space Physics

ESTEC Contract no. 18453/04/NL/AR
Issue 1, September 4, 2007

Danish National Space Center
Scientific Report 2/2007

Influence of Solar Activity Cycles on Earth's Climate

Freddy Christiansen, Joanna D. Haigh, and Henrik Lundstedt

Danish National Space Center
Scientific Report 2/2007

ISBN-10: 87-91694-12-4
ISBN-13: 978-87-91694-12-7
http://www.space.dtu.dk

ESA STUDY CONTRACT REPORT - SPECIMEN

No ESA Study Contract Report will be accepted unless this sheet is inserted at the beginning of each volume of the Report.

ESA CONTRACT No 18453/04/NL/AR	***SUBJECT*** Influence of Solar Activity Cycles on Earth's Climate		**CONTRACTOR** Danish National Space Center
*** ESA CR( )No 18453**	*** STAR CODE**	**No of volumes 1** **This is Volume No 1**	**CONTRACTOR'S REFERENCE DNSC Scientific Report 2/2007**

ABSTRACT:
This summary report is presented as a condensation of the Tasks carried out under the ISAC (Influence of Solar Activity Cycles on Earth's Climate) study. The Tasks were:

1) Literary Survey on Sun-Earth Connection
2) Identification of Relevant Data
3) Data Interpretation
4) Quantification of Global Climate Modulations
5) Hypothetical Mechanisms
6) Investigation of Modelling Potentials
7) Conclusions and Recommendations

The report is a condensation of the ISAC study. Many details that were explained in the reports for each Task will necessarily have been omitted. The interested reader is referred to the individual reports.

The work described in this report was done under ESA Contract. Responsibility for the contents resides in the author or organisation that prepared it.

Names of authors: Freddy Christiansen, Joanna D. Haigh, and Henrik Lundstedt

**** NAME OF ESA STUDY MANAGER Chung-Chi Lin** **DIV: Instrument Pre-development (EOP-PIM)** **DIRECTORATE: Earth Observation Programmes**	**** ESA BUDGET HEADING G/1/100.060/600.5100/GE+/RD100/04s10**

Preface

This summary report is presented as a condensation of the Tasks carried out under the ISAC (Influence of Solar Activity Cycles on Earth's Climate) study. The Tasks were:

8) Literary Survey on Sun-Earth Connection
9) Identification of Relevant Data
10) Data Interpretation
11) Quantification of Global Climate Modulations
12) Hypothetical Mechanisms
13) Investigation of Modelling Potentials
14) Conclusions and Recommendations

In Section 1 of this report we present the background of the ISAC study along with the most prominent results of Task 1 and a summary of the data identified in Task 2.
In Section 2, 3 and 4 we present the solar-climate correlation work that was carried out in Tasks 3 and 4.
In Section 5 we evaluate hypothetical physical mechanisms for Sun-climate connections in the light of the climate correlations of the previous sections.
Modelling of the solar influence on climate is reviewed in Section 6.
Finally, conclusions from the ISAC study is given in Section 7 along with recommendations for further study, observations and modelling work.

This report is a condensation of the ISAC study. Many details that were explained in the reports for each Task will necessarily have been omitted. The interested reader is referred to the individual reports.

The ISAC study has been carried out by groups at the Danish National Space Center (now part of the Danish Technical University), Copenhagen, Denmark, the Swedish Institute of Space Physics (IRF), Lund, Sweden, and the Space and Atmospheric Physics Department, Imperial College, London, UK. Apart from the authors listed for this report the following have contributed to the ISAC study and therefore also to this summary: Nigel D. Marsh, Torsten Bondo, and Henrik Svensmark, DNSC, Peter Wintoft and Fredrik Boberg, IRF, and Wenya Zhong and Isla Simpson, IC.

Contents

1. INTRODUCTION.....7

1. 1 The variable Sun 7
1.2 The Sun-climate connection 11
1.3 Solar and Climate Data 25

2. SOLAR ACTIVITY.....31

3. STRATOSPHERIC INTERACTIONS 37

3.1 Regression technique 37
3.2 Temperature 37
3.3 Zonal wind 39
3.4 Polar modes of variability 39
3.5 A new index 42
3.6 Stratospheric ozone 44
3.7 Summary 46

4. TROPOSPHERIC INTERACTIONS AND SURFACE RESPONSE 48

4.1 Method of analysis 48
4.2 Tropospheric Response 53
4.3 Surface Response 66
4.4 Summary 78

5. MECHANISMS.....80

5.1 Solar signals through the stratosphere and troposphere 81
5.2 Solar variability and stratospheric ozone 84
5.3 Evidence for stratosphere-troposphere coupling 86
5.4 Mechanisms of stratosphere-troposphere coupling 88
5.5 Role of Ionisation 91
5.6 Role of TSI 99

6. MODELLING 106

7. CONCLUSIONS AND RECOMMENDATIONS.....119

Conclusions 119
Recommendations 120

REFERENCES.....122

1. Introduction

Never before has the state of Earth's climate been so much in the public's eye. Global warming is a major concern of the world with its potentially devastating effects on coastal areas and agricultural production. The steep rise in greenhouse gas emissions since the start of the industrial era has increased the CO_2 concentrations in the atmosphere by 30%. This is widely believed to be the dominant cause of the observed rise of about 0.6^{o}C in the global mean surface temperature during this period. A small systematic rise or fall in the global temperature is caused by a net imbalance in the Earth's radiation budget. The present net radiative forcing from manmade constituents (greenhouse gases and aerosols) is estimated to be about 1.2 Wm^{-2}. The climate models upon which the predictions of greenhouse warming depend provide a reasonable representation of the observed variations in global temperature over the last century. However, they remain subject to significant uncertainties, especially from feedback mechanisms and from the effects of anthropogenic aerosols.

In order to determine the influence of mankind on climate change it is important to understand the natural causes of climate variability. A natural effect that has been hard to understand physically is an apparent link between climate and solar activity. From historical and geological records there are strong indications that the sun has played an important role in the past climate of the Earth, but the physical mechanism is currently unknown. Whatever mechanism caused those earlier changes would most likely also be operating today and may have been active throughout the history of our planet. There have been several attempts to explain the link between solar activity and climate from variations in the sun's radiative output. These have tended to rely on simulations involving Global Climate Models (GCM), which are limited by our current understanding of the fundamental physics. The aim of this study has been to enhance this understanding and point to areas where further research and observations are needed.

1. 1 The variable Sun

Solar activity varies on time-scales from hours to billions of years. Solar variability originates from the solar interior. One aspect of solar variability is linked to solar evolution driven by nuclear conditions in the core. This is a relatively slow process with changes on time-scales of the order of several million years and above for parameters such as mass, radius and luminosity.

Another aspect of solar variability is related to solar magnetic fields generated below the convective zone in the interior. The evolution of magnetic fields results in many manifestations, on time-scales in the range of hours to several hundred even thousand years, such as the well-known sunspot cycle and its longer-period modulations, solar wind structures, and coronal mass ejections. Fourier studies of solar activity give certain periods and frequencies. However, wavelet studies show that the periods and frequencies change with time. Certain frequencies come and go. A much more complex picture therefore appears, than variability on only the 11-year sunspot cycle.

A third aspect of solar variability deals with periodicities due to orbital conditions such as solar rotation, changes in Earths orbit, or inclination of rotation axis with respect to the ecliptic plane.

Many are also the mechanisms by which the Sun can influence Earth and the climate. The influences from the variation of the electromagnetic radiation are most often considered. However, a changing solar wind and energetic particles can also influence Earth either directly or indirectly through modulating the cosmic ray flux. Probably many mechanisms influence Earth at the same time. With this very complex scenario it is not a surprise we detect many solar signals in climate records.
The literature contains a large number of solar-climate relations. Table 1 summarizes this giving solar origin of variability, corresponding time-scale, and suggested produced climate change.

Time-scale	Solar origin	Climate change	Reference
~ 10^9 years	Solar evolution and galactic arm transversing	Glaciation periods	Shaviv, 2003 Marcos, 2004
100,000 years	TSI variation due to eccentricity of Earth's orbit	Temperature, ice cores	Berger et al.,1984 Petit et al., 1999
41,000 years	TSI variation due to obliquity in Earth's rotational axis	Temperature, ice cores	-"- -"- -"-
23,000 years	TSI variation due to precession of Earth's rotational axis	Temperature, ice cores	-"- -"- -"-
2,300 years	Solar dynamo modulation of α, ω	Glaciation periods	Denton and Karlen, 1973
205 years	Solar dynamo modulation of α, ω	Temperature, atmospheric circulation, ice cores ^{14}C, ^{10}Be	Muscheler et al., 2003 Delmonte et al., 2005
88 years	Solar dynamo modulation of α, ω	Temperature, Precipitation	Hoyt and Schatten, 1997 Fairbridge, 1967
22 years	Solar dynamo main oscillation	Rhythm of drought in US	Mitchell et al., 1979
11 years	Solar dynamo main oscillation, meridional circulation speed change (SCL)	Stratosphere T and geopotential height Arctic Oscillation Low cloud coverage Sea surface temperature Land temperature northern hemisphere	Labitzke and Matthes, 2003 Shindell et al., 1999 Svensmark, 1998 Reid, 1991 Friis-Christensen and Lassen, 1991
1.3 years	Solar dynamo bifurcation of ω	Atmospheric circulation? (Geomagnetic activity) (Cosmic rays)	 Paularena et al., 1995 Kudela et al., 2002
27 days	Solar rotation	Stratospheric ozone	Williams et al.,2001

Table 1: A summary of processes behind solar variabilities with corresponding time-scales, and correlated climatic variations found in the literature.

Many different kinds of indicators for solar activity have been used in the literature. The most well known and most often used is the sunspot number that has been recorded since the early 17th century (Figure 1). The 11-year sunspot cycle (Schwabe, 1844) is also the most well known solar variability. This cycle results from active region migration, evolution, submerging, and annihilation. Although the period is 11 years on average, this sunspot cycle is varying in both length and amplitude. As a result of this cycle, the global solar magnetic polarity is reversed approximately every 11 years, giving a total solar magnetic cycle period of 22 years. Modulating the 11-year sunspot cycle is the Gleissberg cycle with a period around 88 years. The Gleissberg cycle has been detected in sunspot data (Frick et al., 1997; Ogurtsov et al., 2002), solar cosmic ray activity (McCracken et al., 2001), and in solar energetic particle events (Reames, 2004). By using cosmogenic isotopes it has been shown that the Gleissberg cycle is valid for extended time spans (Peristykh and Damon, 2003; Usoskin et al., 2004). Solar cycles with even longer periods have been proposed, such as the 205-year de Vries cycle (Beer, 2000; Wagner et al., 2001) and the 2,100-year Hallstatt cycle (Damon and Jirikowic, 1992).

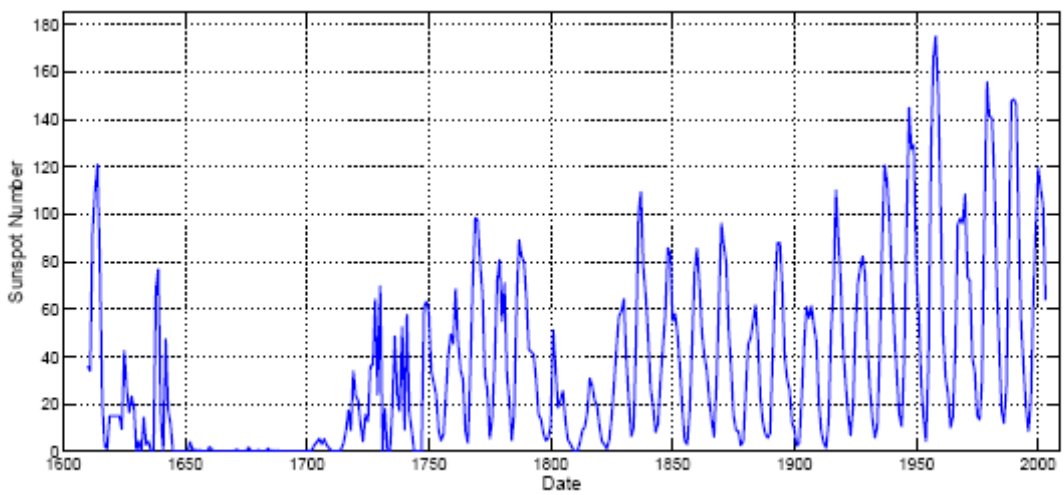

Figure 1: Smoothed yearly sunspot number for the period 1610 to 2003. The clear 11-year sunspot cycle is modulated with an 88-year Gleissberg cycle with the distinct Maunder Minimum (1645-1715) with almost no visible sunspots.

Changes in sunspot number are manifestations of the dynamics of the internal dynamics of the Sun and are accompanied by changes in virtually every other output from the Sun such as the radiated energy in the form of the Total Solar Irradiance (TSI, Figure 2) as well as in every part of the radiated spectrum (X-rays, gamma-rays, UV, or radio flux), particle streams from the Sun (solar wind, coronal mass ejections, solar energetic particles, or solar flares) and also influences solar modulated parameters such as galactic cosmic rays and cosmogenic isotopes; Figure 3 displays a few of these. This simultaneous variation of basically all solar and solar-modulated parameters is a significant problem when aiming to pin-point a single solar source to an observed climate variation. This is because the observed changes in various climate parameters correlate equally well with more than one solar-related index.

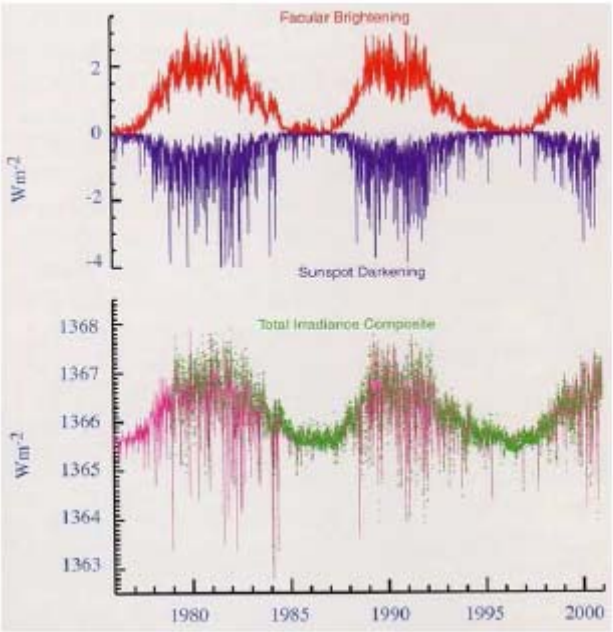

Figure 2: TSI variation with the solar cycle is shown. The contribution from the bright faculae and networks dominate the contribution from sunspots. That explains why the TSI is higher during solar maximum. Courtesy of J. Lean, NRL, USA.

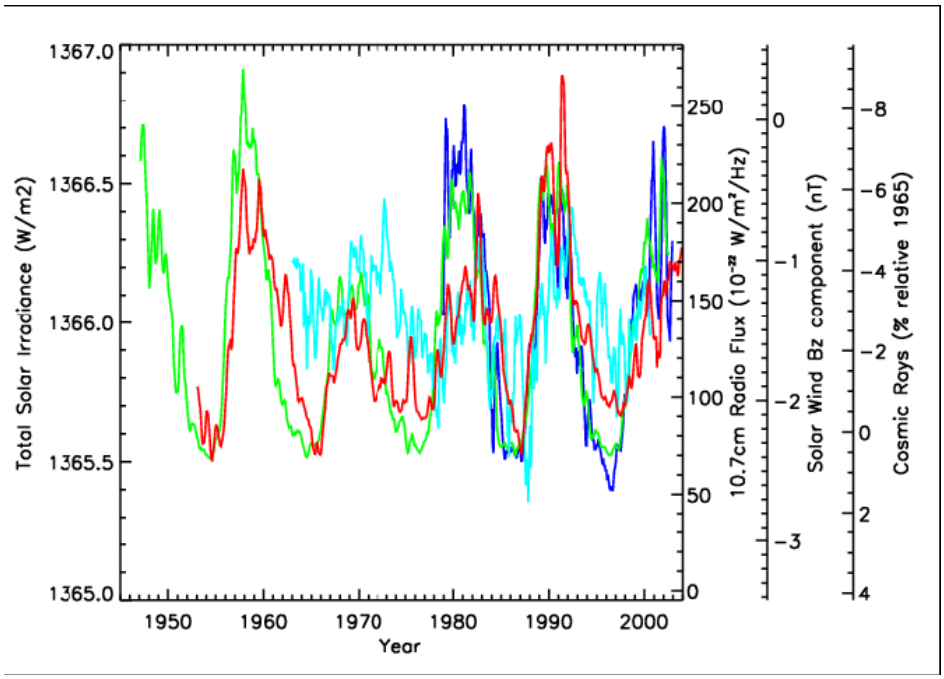

Figure 3: Monthly observations of TSI (blue) together with other solar parameters influencing Earth's environment: 10.7cm Radio Flux often used as a proxy for Solar UV (green), Solar Wind Bz component (light blue), and Cosmic Rays (red). All data have been smoothed with a 5-month running window.

1.2 The Sun-climate connection

The observation that warm weather seems to coincide with high sunspot counts and cool weather with low sunspot counts was made as long ago as two hundred years by the astronomer William Herschel (Herschel, 1801; Hoyt and Schatten, 1992). Herschel noticed that the price of wheat in England was lower when there were many sunspots, and higher when there were few (Figure 4).

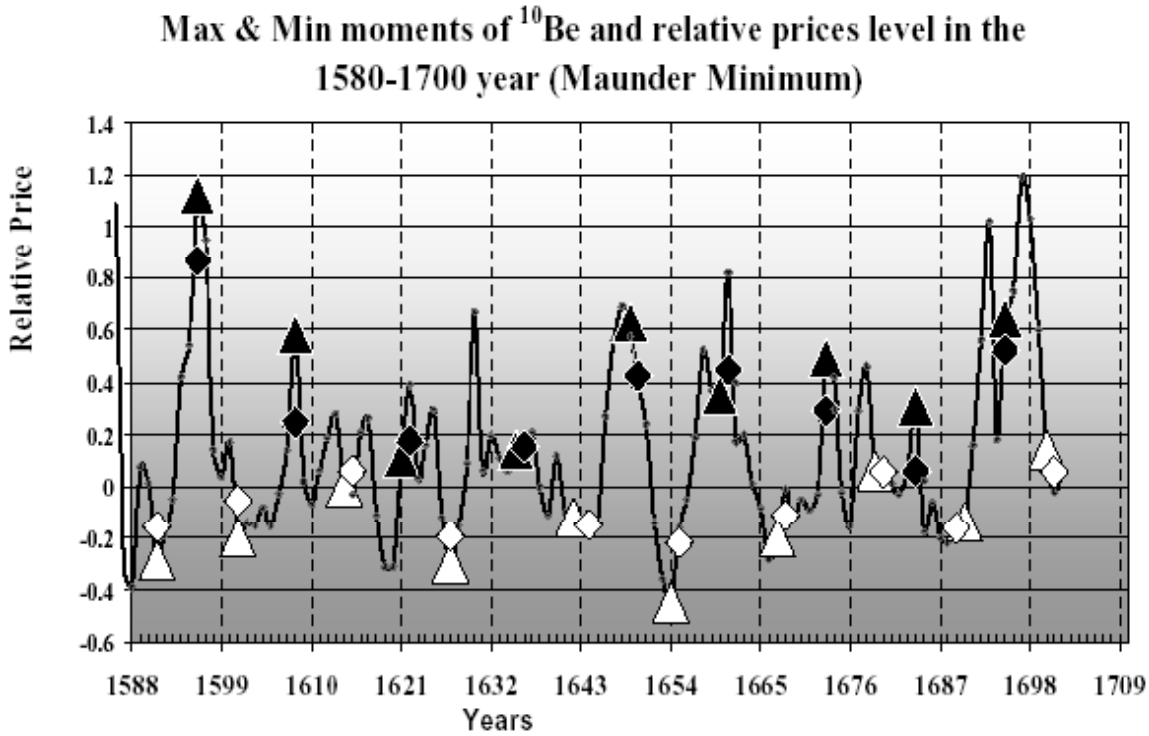

Figure 4: **Wheat prices in England during the 17th century compared with solar activity. White (black) triangles are prices at maximum (minimum) sunspot number, and white (black) diamonds are 3-year averages centred at maximum (minimum) sunspot number. Figure adapted from Pustilnik and Din (2003).**

Since the time of Herschel there have been numerous observations and non-observations of an apparent link between climate and the sunspot cycle, a large number of these have previously been recorded in various review articles and books on the subject (e.g., Dickinson, 1975; Herman and Goldberg, 1978; Hoyt and Schatten, 1997). Table 2 presents some examples of observations of solar influence on climate.

A solar influence on Earth's climate has been found in many climate parameters from the surface up to the top of the atmosphere. However, it is often global temperature that is used as the key parameter for demonstrating variability in the average state of Earth's climate. In the following a summary is given of changes in observed temperature that coincide with variations in solar activity.

YEAR	REFERENCE	SOLAR-CLIMATE RELATION
400 B.C.	Meton (Hoyt and Schatten, 1997)	High SA give increased P in Greece
1651	Riccoli (Hoyt and Schatten, 1997)	High R give increased T on Earth
1801	Herschel (1801)	Sunspots influence price of wheat
1875	Blanford (1875a,b)	Increase in insolation => increase evaporation => clouds and P
1878	Chambers (1878)	SLP low during sunspot maxima
1878	Broun (1878)	R anti-correlated with SLP over S. Asia
1879	Hill (1879)	T variations in India greatest near Rmin
1879	Archibald (1879a,b)	SLP in St. Petersburg correlated with R
1890	Brückner (1890)	30-year variations in T, SLP and P 34.8±0.7 year periodicity from Sun
1896	MacDowall (1896)	T extremes frequent around Rmax
1901	Lockyer and Lockyer (1901)	Variations in SCL
1902	Richter (1902)	T in Europe compares with R, northern lights, and declination of geomagnetic field
1903	Nordmann (1903)	11-years T-cycle in tropics anti- correlated with R
1906	Schuster (1906)	Sunspot cycle of 33.375, 13.57, 11.125, 8.38, 5.625, 4.81, 3.78, and 2.69 years
1908	Abbot and Fowle (1908)	T-variations probably directly related to variations in insolations
1908	Bigelow (1908)	11-year cycle in the geomagnetic field, T, humidity, and SLP over Europe
1913	Abbot and Fowle (1913)	Volcanic eruptions block out light
1974	Wilcox et al. (1974)	Influence of solar magnetic field on tropospheric circulation
1977	Kelly (1977)	SA influence on SLP
1987	Reid (1987)	SA influence on SST
1988	Labitzke and van Loon (1988)	SA, QBO and stratospheric T
1989	Tinsley et al. (1989)	SCL affect cyclogenesis
1991	Friis-Christensen and Lassen (1991)	SCL related to land surface T
1995	Lean et al. (1995)	Reconstruction of solar irradiation from 1610
1996	Haigh (1996)	Correlation between UV radiation and tropospheric jets
1997	Svensmark and Friis-Christensen (1997)	Cosmic rays flux and global cloud cover
1999	Thejll and Lassen (2000)	Variations in SCL and climate
2001	Neff et al. (2001)	P in Oman correlated with SA
2002	Boberg and Lundstedt (2002)	Solar wind and the NAO
2003	Gleisner and Thejll (2003)	Solar variability and the troposphere

Table 2: A summary of some found evidence of a solar influence on Earth. T=Temperature, R=sunspot number, SA=solar activity, SLP=sea level pressure, SCL=sunspot cycle length, SST=sea surface temperature, QBO=quasi-biennial oscillation, UV=ultra violet, NAO=North Atlantic Oscillation.

Ocean Temperatures

One example of a positive correlation is the apparent solar response of Sea Surface Temperatures (Reid, 1987; Reid, 1991; Reid, 2000). Sea Surface Temperatures (SSTs) have been obtained from ocean going ships since the middle of the 19th century. During the first part of the 20th century the observed SSTs increased, and then flattened out during the years 1940 and 1970, before continuing with the overall increasing trend. Figure 5 indicates that this long-term variability in SSTs is in phase with the 80-90 year envelope that modulates the approximately 11-year sunspot cycle.

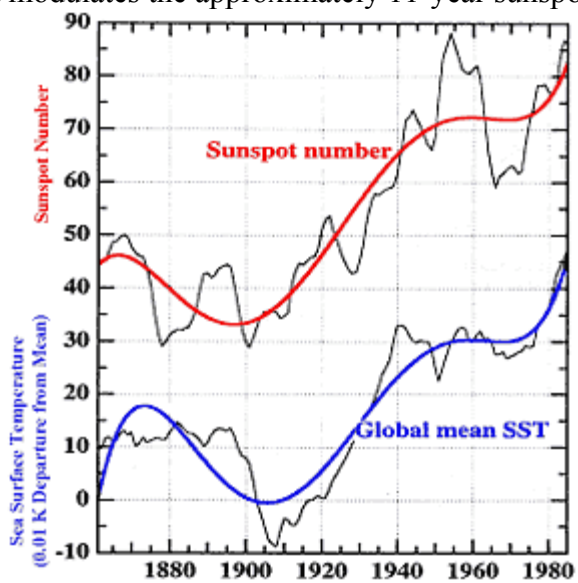

Figure 5: 11 year running mean of the annual sunspot numbers (upper thin curve), and the mean global sea-surface temperature anomaly (lower thin curve). The heavy curves represent a 7th degree polynomial least squares fit to the data. Units for the lower curves are 0.01K departures from the 1951-1980 average.

White et al (1997) confirmed this finding with two independent SST datasets, i.e., surface marine weather observations (1900-1991) and upper-ocean bathythermograph temperature profiles (1955-1994). They band-passed basin average temperatures, and found each frequency component to be in phase with changes in solar activity across the Indian, Pacific and Atlantic Oceans. Global averages yielded maximum changes of 0.08±0.02 K on decadal (ca. 11-year period) scales and 0.14±0.02 K on interdecadal (ca. 22-year period) scales in response to a 1 Wm^{-2} change in Total Solar Irradiance (TSI) at the top of the atmosphere. The highest correlations were obtained with ocean temperatures lagging solar activity by 1-2 years, which is roughly the time scale expected for the upper layers of the ocean (<100m) to reach radiative balance following a perturbation in TSI. From simple energy balance arguments White et al (1997) estimated climate sensitivities due to changes in TSI at the ocean surface to be 0.2-0.4^{o} K/(Wm^{-2}). This suggests that a 0.04-0.09^{o} K change in SSTs would be expected from a 1 Wm^{-2} change in TSI at the top of the atmosphere. While these estimates are of a similar order of magnitude to the observed changes in global SSTs, they are on the low side, suggesting a possible amplification of the solar signal exists within the climate system.

Land Temperatures

Another example of a positive observation is the correlation between solar activity and northern hemisphere land temperatures (Friis-Christensen and Lassen, 1991). They used the sunspot cycle length as a measure of the Sun's activity. The cycle length averages 11 years but has varied from 7 to 17 years, with shorter cycle lengths corresponding to a more magnetically active Sun. A correlation was found between the sunspot cycle length and the change in land temperature of the northern hemisphere over the period 1861 to 1989 (latest update in Figure 6). The land temperature of the northern hemisphere was used in order to avoid the lag by several years of air temperatures over the oceans, due to their large heat capacity. Of particular note is the dip between 1945 and 1970, which was also present in the Sea Surface Temperatures discussed above. This cannot easily be explained by the steadily rising greenhouse gas emissions but seems to coincide with a decrease in the Sun's activity. Clearly the correlation breaks down after 1990 and it has been suggested that this is an indication of the increasingly dominant effect greenhouse gas emissions have had on global warming (Thejll and Lassen, 2000).

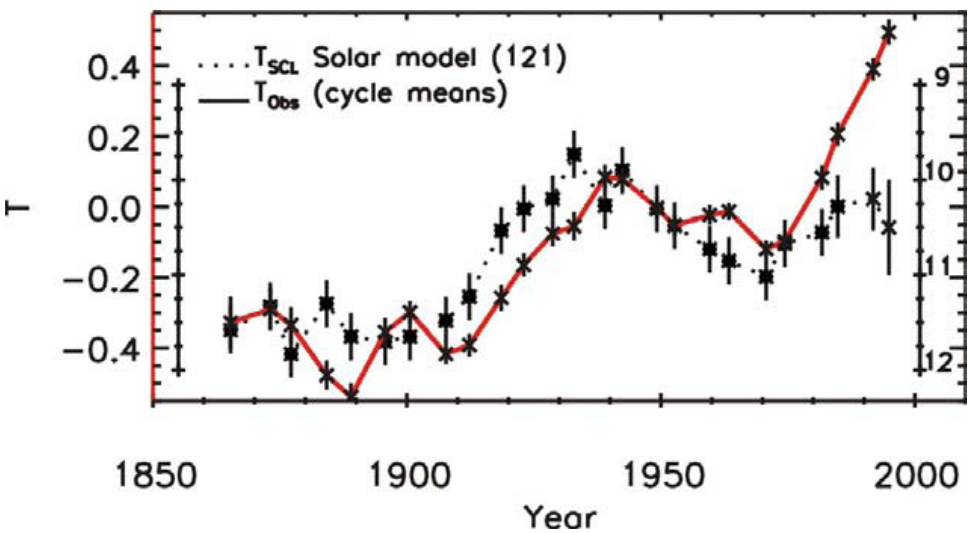

Figure 6: **Sunspot cycle length (black dotted curve) versus the northern hemisphere temperature anomaly over land (red solid curve).**

However, the physical significance of the solar cycle length and whether it reflects changes in solar properties that in turn affect Earth's environment are currently uncertain. Attempts have been made to attribute the solar cycle length with secular variations in the Sun's large-scale magnetic field, which influences the interplanetary shielding of cosmic rays arriving at Earth (Solanki et al., 2000), but there are still a number of open questions.

Tropospheric Temperatures

Radiosonde observations of tropospheric temperatures over the period 1958 - 2001 display significant variability at a number of different time-scales. From monthly data the effects of El Nino and volcanic eruptions are particularly evident. However, these features are largely removed when filtering with a three-year running mean, and the low pass Tropospheric temperatures show a remarkably good agreement with changes in reconstructed Total Solar Irradiance (TSI). Figure 7 indicates that an increase in

reconstructed TSI of 1 Wm^{-2} coincides with an increase of ~0.4° K in tropospheric temperatures.

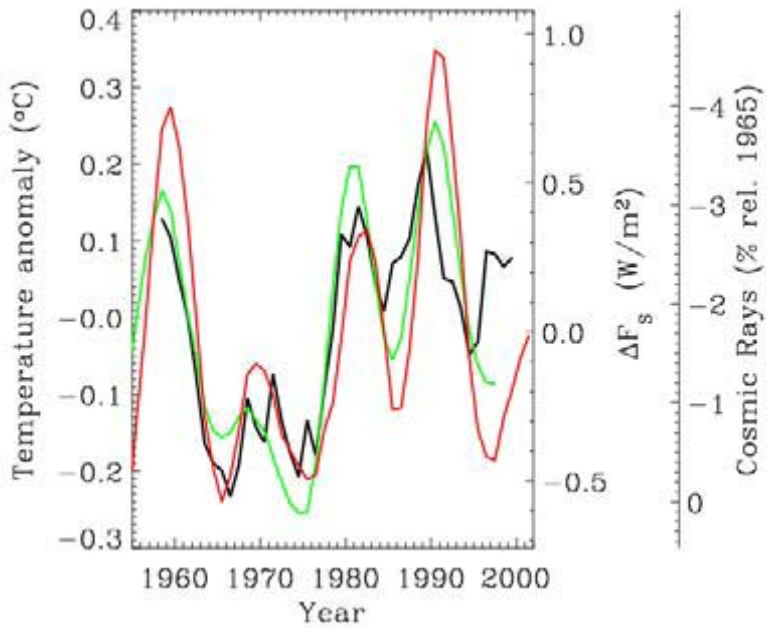

Figure 7: Tropospheric temperatures (black), obtained from radiosondes, shown together with reconstructed TSI (green), ΔF_s, using re-scaled sunspot numbers as a proxy and cosmic rays (red). Both data sets have been low pass filtered with a three year running mean (adapted from Marsh and Svensmark, 2003b).

An expected temperature response from the reconstructed changes in TSI can be estimated with a simple climate sensitivity analysis. Assuming a climate sensitivity of 0.6-0.8° K/(Wm^{-2}), estimated from the average response of climate models to a doubling of CO_2 (e.g., Appendix 9.1 - Houghton et al., 2001), predicts that a 1 Wm^{-2} change in TSI at the top of the atmosphere would result in only ~0.1°K change in temperature. Clearly, changes in TSI alone are too small to explain the observed Tropospheric temperature variability and an amplification factor is required (Marsh and Svensmark, 2003b).

Observational Evidence for Indirect Mechanisms

Although a solar influence on climate is apparent, model studies have indicated that variations in the Total Solar Irradiance (TSI) are too small to explain the observed changes in recent climate. Stott et al. (2003) found that current climate models underestimate the observed climate response to solar forcing over the twentieth century as a whole, and concluded that the climate system has a greater sensitivity to solar forcing than models currently indicate. This is consistent with other studies that show models underestimate the response to solar forcing in Tropospheric temperatures by a factor of 2 to 3 (Hill et al., 2001), and near-surface temperatures by a factor 2 (North and Wu, 2001). These studies assumed the solar imprint on climate originated from direct changes in TSI at the top of Earth's atmosphere and did not include any possible indirect mechanism. Clearly an amplification of the solar signal, via some indirect mechanism(s), is required

to explain the observed correlations with climate, and resolve the inconsistency with models.

There are three possible vectors between the Sun and the Earth that could lead to a solar imprint on climate; a) the electromagnetic radiation (Total Solar Irradiance) - or some component of it such as the ultra violet (UV), b) the direct influence of the solar wind, and c) the galactic cosmic radiation, which is modulated by the solar wind.

The ISAC team has identified five external forcing parameters that are modulated by solar variability and have the potential to influence Earth's lower atmosphere below 50km. These include: Total Solar Irradiance (TSI), the Ultra-Violet (UV) component of solar radiation, the direct input from the Solar Wind (SW), the total Hemispheric Power Input (HPI) reflecting properties of precipitating particles within the magnetosphere, and Galactic Cosmic Rays (GCR). In the table below, estimates of the energy input directly into Earth's environment is provided for each solar modulated parameter.

Solar Modulated Parameter	TSI	UV	SW	HPI	GCR
Number Density (cm^{-3})	-	-	6	-	$5\cdot10^{-10}$
Energy/Particle(eV)	-	-	10^3	10^4	10^8
Energy Density($eVcm^{-3}$)	$2.8\cdot10^7$	-	$6\cdot10^3$	-	0.5
Velocity(ms^{-1})	$3\cdot10^8$	$3\cdot10^8$	$4.5\cdot10^5$	-	$3\cdot10^8$
Energy Flux (Wm^{-2})	1366	15	$4.4\cdot10^{-4}$	$6\cdot10^{-5}$	$2.4\cdot10^{-5}$

Table 3: Energy received at Earth from 5 Solar Modulated Parameters. The total solar irradiance (TSI), ultra-violet (UV) radiation between 200-300nm, solar wind (SW) and galactic cosmic ray (GCR) quantities are estimates at the top of the atmosphere outside the magnetosphere. The precipitating energy of charged particles within the magnetosphere has been estimated from the Total Hemispheric Power Input (HPI). The energy input from cosmic rays is nearly isotropic, whereas the solar irradiance impinges only on the dayside. The solar wind impinges on the much larger area of the magnetosphere, compared to the surface of the Earth, but only in the region of open field lines (polewards of the cusp) can the solar wind penetrate directly down to the uppermost layers of the atmosphere.

The quantities in the three right hand columns of Table 3 are miniscule compared to the TSI. Their variations in absolute terms are even smaller over a solar cycle, where TSI varies by about 0.1%, and the variations in the other parameters are ~5% for UV and 3-20% for GCR. Observational and modelling studies have suggested that the response to TSI over a solar cycle is too small to have had a significant impact on climate. Therefore, for the other solar-modulated quantities to play a role in climate change, some mechanism for magnifying their effect must be in place. These are briefly outlined below.

A number of solar amplification mechanisms have been proposed, involving each of these three parameters. The mechanisms are reviewed below, together with a summary of the evidence that currently exists for each one.

Solar UV

According to various modelling studies, a response in atmospheric circulation can amplify the terrestrial effect of solar irradiance changes, possibly via the influence of

solar UV variability on ozone concentrations and a corresponding response in stratospheric temperatures (Haigh, 1996; Haigh, 1999; Haigh, 2003). Model results further suggest that this amplified stratospheric response to solar variability has the potential to influence tropospheric circulation patterns (Matthes et al., 2004).

a) b)

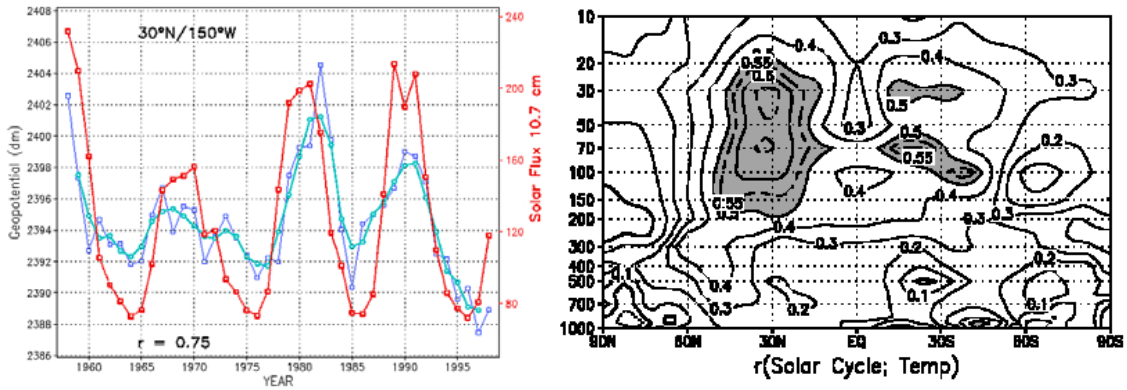

Figure 8: a) **Geopotential heights at 30 hPa (blue curve) at 30N, 150W versus 10.7cm solar flux (red curve).** b) **Correlation between zonally averaged annual mean detrended temperatures and 10.7cm solar flux, shaded regions are for correlations >0.5 (adapted from Labitzke and Matthes (2003)).**

Meteorological parameters in the stratosphere, e.g., temperature and geopotential height, are strongly correlated with the 11-year solar cycle (Labitzke, 1987; Labitzke and Matthes, 2003; Labitzke and van Loon, 1988). In particular, the zonally averaged temperatures in the stratosphere are found to be significantly correlated with changes in UV flux, and the 30hPa geopotential height, which is a measure of the mean temperature of the atmosphere below about 24 km, is seen to vary in phase with solar activity, preferentially at mid-latitudes (Figure 8). A general picture has now emerged in which the low-to-mid-latitude upper stratosphere warms by ~1° K at solar maximum with respect to solar minimum, the temperature signal is very small, or possibly negative near 50hPa and then larger, perhaps 0.5^{o} K in the lower stratosphere. Although changes in TSI over a solar cycle are too small, ~0.1%, to explain this observed temperature response, solar UV variations are much larger, ~5%, at wavelengths between 200nm to 300nm (Lean et al., 1997). At these wavelengths solar UV has a direct effect on the photochemistry generating stratospheric ozone, which in turn influences the radiative heating and dynamics of the upper stratosphere (Hood et al., 1993).

The ozone response to the 11-year solar cycle variability has been assessed from satellite datasets (e.g. SBUV/TOMS) and a similar picture emerges to that seen in the temperature structure with a mid-stratospheric minimum (Figure 9). That the same feature is also apparent from the influence of the 27-day solar rotation, for which statistically longer time series are available, suggests it is real (Williams et al., 2001).

Model studies have confirmed that solar UV will have an impact on the radiation, temperature, ozone budget, and dynamics of the stratosphere (Balachandran and Rind, 1995; Haigh, 1999; Shindell et al., 1999), but they have not been successful at reproducing the magnitude or structure of the response. However, very recent work has indicated that improvements are possible when correctly capturing the observed equatorial wind properties throughout the stratosphere, while taking into account the phase of the Quasi-Biennial Oscillation (Matthes et al., 2004).

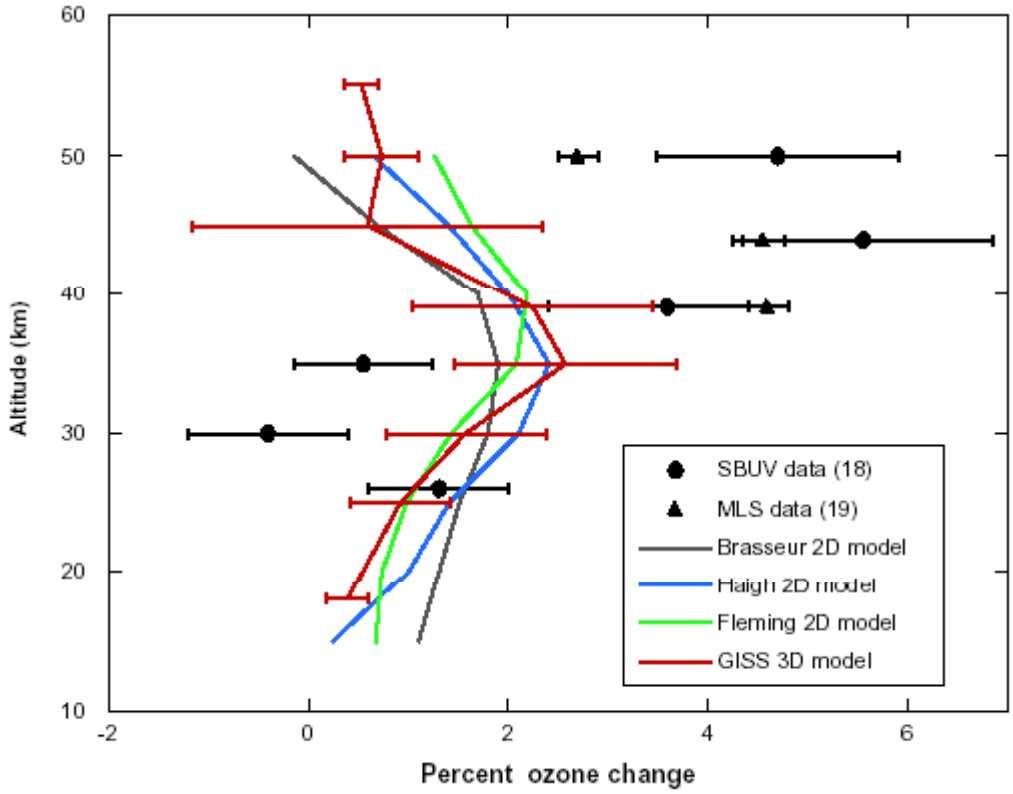

Figure 9: Annual average ozone differences between solar maximum and solar minimum between 60°S to 60°N in percent. Filled circles are from satellite observations covering 15 years for Solar Backscatter Ultraviolet (SBUV) data, and triangles are from 3 years for Microwave Limb Sounder (MLS) data. The coloured lines represent results obtained from various models of ozone photochemistry in the stratosphere (adapted from Shindell et al. (1999)).

Observations of various meteorological parameters in the Troposphere also demonstrate correlations with solar activity (Egorova et al., 2004; Gleisner and Thejll, 2003; Labitzke and van Loon, 1997; Labitzke and van Loon, 1995; Labitzke and van Loon, 1988). However, coupling of the solar induced stratospheric signal with the troposphere is currently not well understood, and there is still uncertainty as to the physical mechanism responsible for a tropospheric response to solar variability. Model studies do hint at a tropospheric circulation response (Balachandran et al., 1999; Haigh, 1999; Shindell et al., 1999; Tourpali et al., 2003), which can be seen in Figure 10 with a comparison between solar min and solar max differences of zonal wind speed obtained from observations and a Global Climate Model (GCM). While some of the general features revealed in the observations are captured in the GCM response, namely that the mid-latitude jets weaken and broaden at solar maximum, there are still significant differences in structure and magnitude of the tropospheric response.

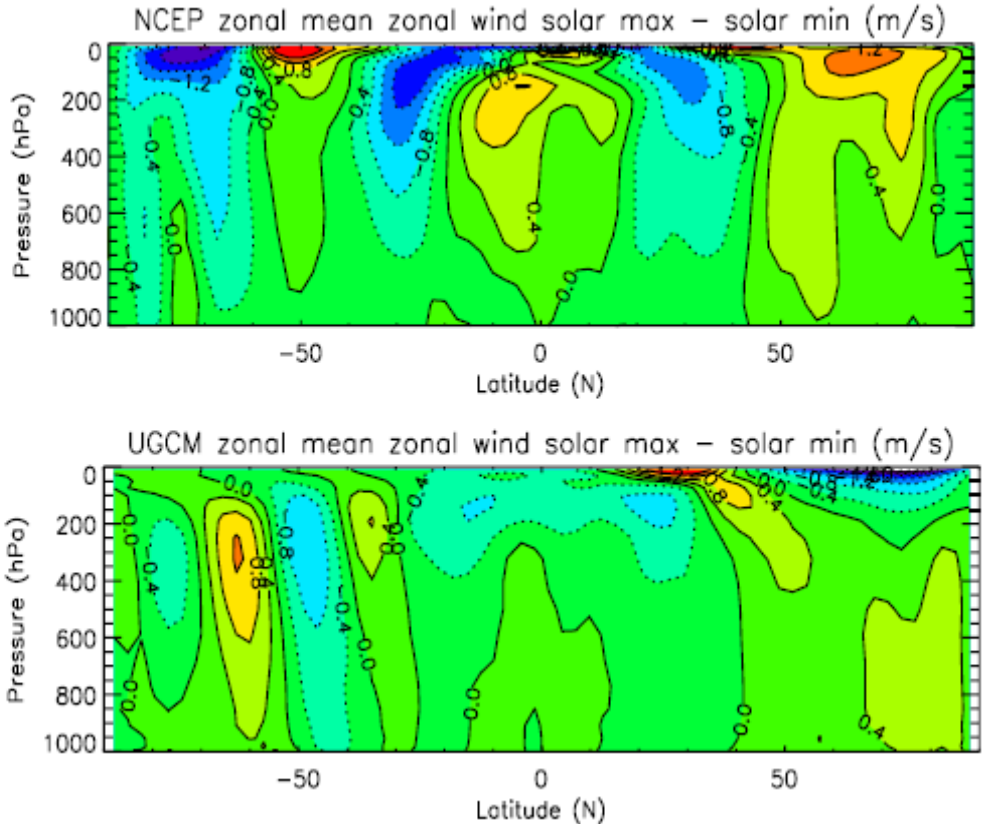

Figure 10: **Differences in zonal wind speed between solar max and min from a) a multi regression analysis of NCEP reanalysis data between 1979-2002 and b) a GCM simulation (adapted from Haigh (1996) and Haigh et al. (2005)).**

Direct Influence of the Solar Wind

The solar wind is able to generate significant heating of the lower thermosphere at high latitudes by direct particle precipitation, as well as generating upper atmospheric ionisation that may influence the global electric circuit. Through coupling with the magnetosphere the solar wind also drives ionospheric currents at high latitudes that in turn accelerate the neutral atmosphere.

Recent studies (Boberg and Lundstedt, 2003; Boberg and Lundstedt, 2002) have shown a strong relationship between the electric field of the solar wind and a pressure phenomena in the north Atlantic termed the North Atlantic Oscillation (NAO) (Marshall et al., 2001). A substantial portion of the climate variability in the Atlantic sector is associated with the NAO with variations occurring on a wide range of scales.

Model studies (Arnold and Robinson, 2001; Arnold and Robinson, 1998) indicate that the influence of geomagnetic activity on the stratosphere is comparable to that of ultraviolet flux variation between solar minimum and solar maximum and that planetary wave activity is a key process in determining the extent to which the stratosphere is able to respond to changes in the lower thermosphere.

Bucha and Bucha (1998) observe an intensification of both thermospheric and tropospheric flows following strong geomagnetic activity. They suggest a mechanism

where downward winds are generated in the polar cap of the thermosphere and penetrate to the stratosphere and troposphere.
A possible scenario for the solar wind/NAO interaction could include an electromagnetic disturbance induced by the solar wind in the global electric circuit of the ionosphere. This global disturbance could then dynamically propagate downwards through the atmosphere, a scenario similar to the one proposed by Baldwin and Dunkerton (2001). This downward motion takes several weeks and during this time it would be affected by different atmospheric circulations from the equator toward the poles (Peixoto and Oort, 1984) resulting in a pressure pattern more concentrated at high latitudes (Figure 11). Due to this slow, dynamic, propagation, one can make forecasts of the weather/climate in the Atlantic sector based on the solar wind state.

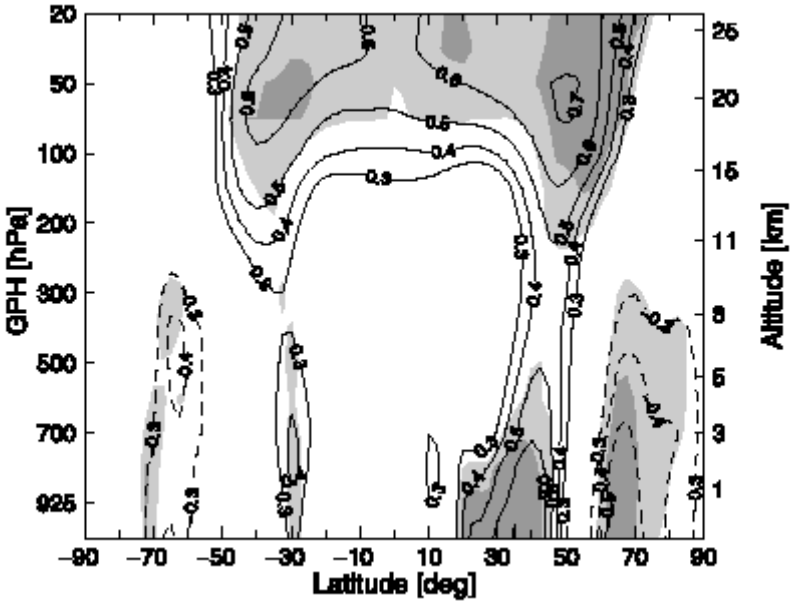

Figure 11: **Linear correlations between the electric field of the solar wind and geopotential height variations as function of latitude at the zero meridian and geopotential height (adapted from Boberg and Lundstedt, 2003).**

Magnetosphere/Ionosphere

The dynamics of the magnetosphere is driven by the solar wind, and thus is strongly correlated with solar activity. The physical state of the ionosphere is determined predominantly by solar illumination and precipitating charged particles, so it too reflects variations in solar activity, but it is also sensitive to changes in the atmosphere be-low. For there to be a significant effect on the climate of the lower atmosphere, a strong amplifying mechanism is required which couples the solar wind-magnetosphere-ionosphere-lower atmosphere. This coupling could take various forms, e.g., through precipitating particles or through magnetospheric current systems closing in the ionosphere thereby depositing Joule heating to the upper layers of the atmosphere. While precipitating particles fluctuate by several orders of magnitude between quiet times and magnetic storms/substorms, magnetospheric current systems are more persistent existing even during very quiet periods. However, the energies involved are extremely small compared to TSI or UV (see Table 3); thus, a currently unknown amplifying mechanism

is required if the magnetosphere – ionosphere system is to have a significant impact on the climate of the lower atmosphere.

Galactic Cosmic Rays

Cosmic rays are the main source of ionization in the troposphere (Bazilevskaya 2000), however, the energy they deposit into the Earth's atmosphere, ~10^{-5} Wm^{-2}, is negligible compared to that from changes in solar irradiance over an 11-year solar cycle,~0.34Wm^{-2}. Clearly some form of amplification mechanism is required if cosmic rays are to play a role in climate variability.

There is increasing evidence that the cosmic rays, which are modulated by the solar wind, can noticeably affect Earth's planetary albedo, and hence climate, via an influence on tropospheric cloud properties (Carslaw et al., 2002; Marsh and Svensmark, 2000b; Marsh and Svensmark, 2003a; Svensmark and Friis-Christensen, 1997).

Based on five different satellite observations, a link was proposed between total cloud amount and the number of Galactic Cosmic Rays (GCR) received at Earth between 1979-1996 (Svensmark, 1998; Svensmark and Friis-Christensen, 1997). Since clouds play an important role in the radiation budget of the atmosphere, by both reflecting solar radiation and trapping outgoing longwave radiation, the existence of a GCR-cloud link would introduce a previously unknown external forcing mechanism to the climate system. Marsh and Svensmark (2000b) found the correlation to be limited to low liquid water clouds below ~3.2km (rather than clouds at other altitudes) between 1983-1994 (Figure 12). They suggested that this was consistent with a mechanism involving ionisation and aerosol nucleation, which in turn could influence the activation of cloud droplets in the lower troposphere, and hence cloud radiative properties (Marsh and Svensmark, 2000a).

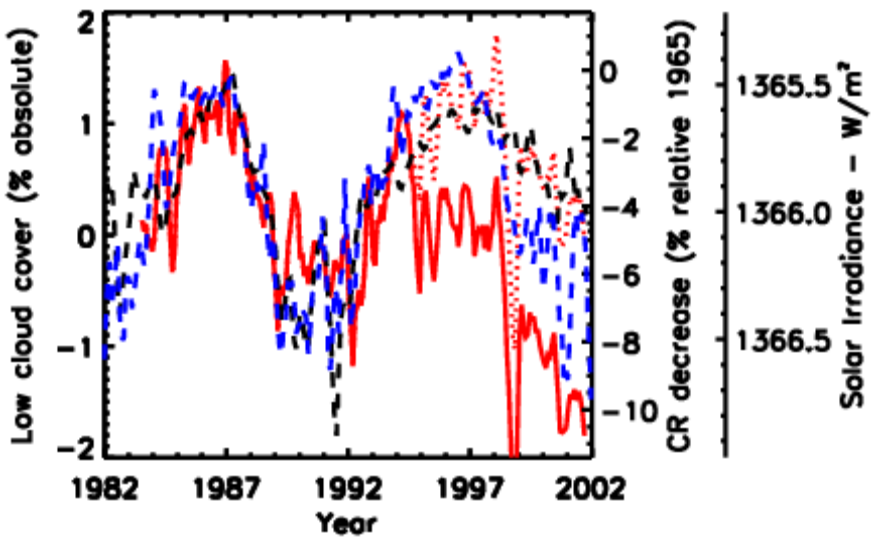

Figure 12: **Monthly averages of ISCCP-D2 IR global Low Cloud Amount (red) shown together with cosmic rays (black dashed), and solar irradiance (blue dashed). The red dashed curve includes an offset after 1994 that has been added to Low Cloud Amount, this accounts for a possible inter-calibration problem at the end of 1994.**

This basic result has subsequently been confirmed by other independent studies (Palle Bago and Butler, 2000; Yu, 2002a). More recently, Marsh and Svensmark (2003a) found

that the low cloud-cosmic ray correlation can be extended until 2001 (Figure 12), but only after the globally averaged cloud data are re-calibrated (Marsh and Svensmark, 2004b).

However, beyond the GCR-total cloud correlation there is currently no experimental confirmation to suggest that such processes has had a discernible effect on cloud properties (Marsh and Svensmark, 2003b). This has lead to suggestions that the correlation is fortuitous and might better be explained by internal climate processes, e.g., El-Nino Southern Oscillation (ENSO), such that any agreement with cosmic rays is purely coincidental. As a result a number of questions have been raised as to the validity of the GCR-cloud link.

Kernthaler et al (1999) found no clear relationship between individual cloud types and GCR, which became further degraded with the inclusion of polar-regions. However, their analysis relied on the individual cloud type derivations from the International Satellite Cloud Climatology Project monthly C2 data (ISCCP-C2) (Rossow and Schiffer, 1991) using an algorithm which was abandoned by ISCCP in 1990 due to its poor performance (Klein and Hartmann, 1993). The reanalysed D2 data (ISCCP-D2) using an improved algorithm (Rossow et al., 1996), differs considerably from the ISCCP-C2 derivation of individual cloud types. The results of Kernthaler et al (1999) cannot be reproduced using the ISCCP-D2 data (Marsh and Svensmark, 2000b). Kuang et al (1998) confirmed the GCR - total cloud correlation using the ISCCP-C2 data, but were unable to distinguish between the effects of GCR and ENSO on the mean cloud optical thickness. Jorgensen and Hansen (2000) raised a number of criticisms but of a more general nature which have been addressed in a comment by Svensmark and Friis-Christensen (2000). Farrar (2000) argued that trends in the globally averaged total cloud amount were the result of a composite of expected regional cloud responses to ENSO, and found little evidence to suggest a role for GCR. However, Marsh and Svensmark (2003a) have shown that in low cloud properties the ENSO signal is limited to equatorial regions, while the GCR-low cloud correlation appears to dominate global properties. Sun and Bradley (2002; 2004) expressed concern that the effects of high cloud would obscure the satellite view of low cloud. Marsh and Svensmark (2003a; 2004a) show that the correlation between low cloud and cosmic rays is a robust feature in regions not obscured by overlaying high cloud.

However, variability in low cloud amount (LCA) correlates equally well with total solar irradiance (Figure 10), and cannot be uniquely ascribed to a single mechanism when using globally averaged data. This has lead to suggestions that the cosmic ray-low cloud link is a result of a tropospheric circulation response to TSI or solar UV (Kristjansson et al., 2002). One way to distinguish between these two processes is to utilize the property that cosmic rays arriving at Earth are modulated by the geomagnetic field whereas solar irradiance is not. Recent observational evidence indicates that the solar cycle amplitude in LCA, over the period 1984–2000, increases polewards and possesses a similar latitudinal dependence to that found in cosmic ray induced ionization (CRII) of the troposphere (Figure 13). This supports a physical mechanism involving cosmic rays rather than TSI or solar UV.

There is also evidence for the reduction of cloud coverage during strong Forbush decreases at time scales of a few days (Pudovkin and Veretenenko, 1996). This implies that the proposed cloud-cosmic ray relation may also be significant at short-time scales. Recently, Kniveton and Todd (Kniveton, 2004; 2001) found a strong relationship

between GCR and precipitation over southern oceans at mid to high latitudes. They suggest this is more consistent with changes in the global atmospheric electric circuit according to Tinsley (1996a) rather than with tropospheric aerosols or ENSO.

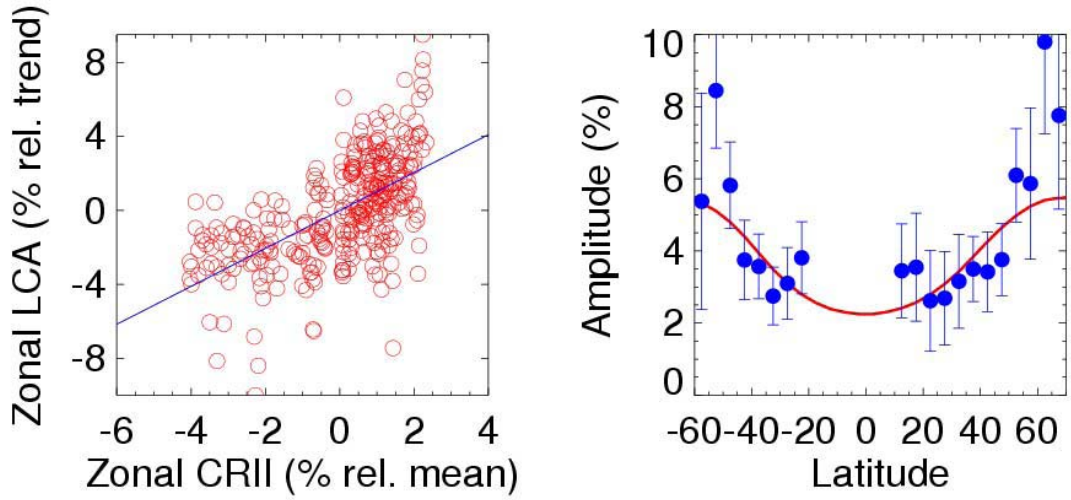

Figure 13: **Latitudinal relation between relative variations of Low Cloud Amount (LCA) and Cosmic Ray Induced Ionisation (CRII) for the period 1984–2000 within the latitude range 55° – 20° S and 10° – 70° N.** a) **Scatter plot of LCA vs. CRII, each dot representing an annual value within a 5° latitudinal bin. Solid blue line depicts the best linear.** b) **Latitudinal dependence of the amplitude of cyclic variations in LCA (blue dots) and CRII (red line). The amplitude is found by fitting a 10-year sinusoid to the respective time profiles. Adapted from Usoskin et al. (2004).**

The above evidence supports the suggestion that cosmic rays influence cloud properties, but a mechanism is required to physically link atmospheric ionization to clouds. Below two possible candidate mechanisms are briefly outlined.

Ion Induced Nucleation

Ions produced through the nucleonic cascade of cosmic rays in the troposphere rapidly interact with atmospheric molecules and are converted to complex cluster ions (aerosols) (Gringel et al., 1986; Hoppel et al., 1986). It is thought that these cluster ions grow through ion-ion recombination or ion-aerosol attachment and thus affect the number of aerosols acting as cloud condensation nuclei (CCN) at typical atmospheric super saturations of a few percent (Viggiano and Arnold, 1995). Recent atmospheric observations indicate a role for ion induced nucleation (IIN) in ultra-fine aerosol formation (sizes < 10 nm - Eichkorn et al., 2002; Lee et al., 2003). But it remains an open question as to whether aerosol concentrations at CCN sizes (~100 nm) are sensitive to a perturbation in ionisation and capable of significantly influencing cloud properties. Nucleation modelling studies suggest that it is the lower troposphere below 5 km that is most sensitive to changes in IIN (Yu, 2002b). Under such conditions, an increase in GCR would lead to an increase in aerosol and hence a decrease in cloud droplet sizes. Ferek et al. (2000) have shown that an increase in aerosol due to ship exhaust can lead to drizzle suppression which has implications for cloud lifetimes. If ionization from GCR can be shown to have a similar affect on the lower tropospheric aerosol distribution, and

subsequently prolong a clouds lifetime, it would be consistent with the cosmic ray - low cloud correlation outlined above. However, ship tracks are a large perturbation locally, whereas a possible GCR - CCN mechanism will be a small perturbation globally. The possible link between atmospheric ionization and aerosols acting as CCN requires confirmation by experiment to determine its potential implications for climate. Currently two such experimental efforts are underway at DNSC (http://www.dsri.dk/sun-climate/) and at CERN, Geneva (http://cloud.web.cern.ch/cloud/).

Global Atmospheric Electric Circuit

A further suggestion is that the amplification of cosmic rays on climate could be through changes in the global atmospheric electric circuit. Current flowing in the global atmospheric electrical circuit substantially decreased during the twentieth century, which has been quantitatively explained by a decrease in cosmic rays (CR) reducing the ionospheric potential as solar activity increased (Harrison, 2002). This potentially affects aerosol-cloud interactions at the edges of clouds, e.g., Tinsley (2000), (or a review of possible mechanisms in Harrison and Carslaw (2003)). Highly charged droplets are generated at cloud boundaries in the troposphere due to the weak vertical currents of the global electric circuit. Once these droplets have evaporated, highly charged CCN's remain, and the presence of this charge enhances collision efficiencies when interacting with other liquid droplets. The process of nucleation and evaporation repeats itself continuously and is thought to aid in the formation of ice particles in supercooled liquid water clouds, as a result it is referred to as 'Electroscavaging' (Tinsley, 1996b; Tinsley, 2000; Tinsley and Deen, 1991). There is some limited observational evidence to suggest that this process can have an additional influence on atmospheric dynamics (Roldugin and Tinsley, 2004; Tinsley, 1996b).

1.3 Solar and Climate Data

During the ISAC study the team having collected an extensive set of solar and climate data.

A very nearly exhaustive set of solar parameters were collected by the group at the Swedish Institute of Space Physics and organized in a web-accessible data base (for access to the data base, please contact Henrik Lundstedt). Figure 14 shows the solar parameters and their time span. The (group) sunspot number is available for nearly 4 centuries and the aa index of geomagnetic activity is available since 1868, but most parameters are only available for about 3 decades. Thus Total Solar Irradiance and solar UV are available since November, 1978.

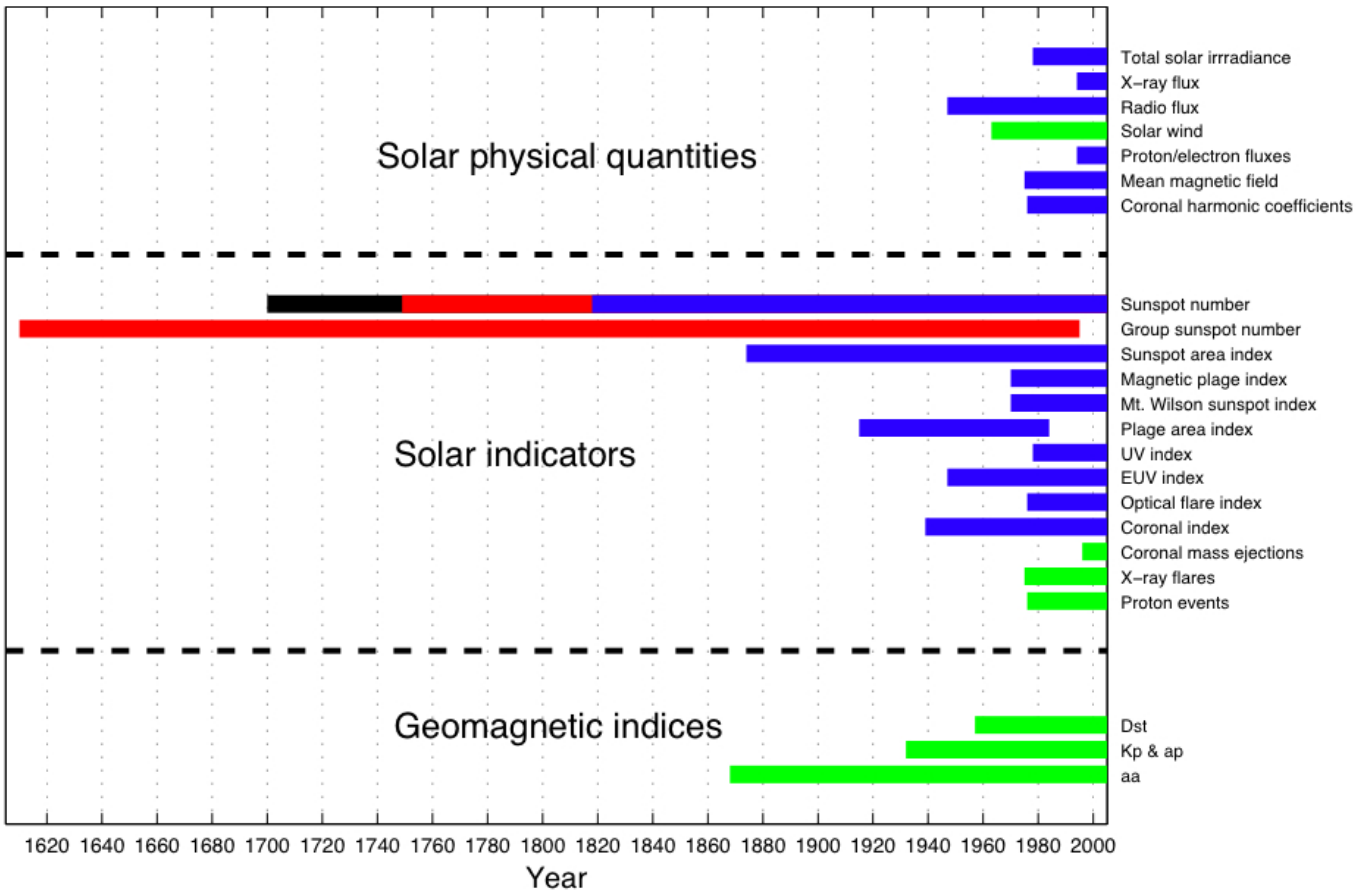

Figure 14: Time spans for solar data. Green, blue, red, and black bars for hourly, daily, monthly, and yearly values, respectively. The solar proxies are not included in this Figure.

Collecting a similarly exhaustive set of climate parameters would be an impossible task. Below are listed the parameters on which we concentrated our work. Surface measurements go back more than a century, but are only available as global grid from 1960. The International Geophysics Year in 1958 boosted many observations, among other things radiosonde temperature measurements and grid of neutron counters. The

satellite age took speed in November, 1978, from which time there are Microwave Sounding Units of atmospheric temperatures. This coincides with the beginning of measurements of solar TSI and UV. Satellite measurements have the advantage of continuous global coverage, but the short time span covering barely 2½ 11-year solar cycles limits any correlation study severely.

	Observation	Geographic coverage	Temporal coverage
Cosmic Rays			
	Neutron counts	World wide network 30-60 stations (1953-1956: 2-5 stations)	1953-present Hourly data
	Source: www.env.sci.ibaraki.ac.jp/ ftp/pub/WDCCR/ Available at DNSC: full data set		
	Muon counts	Single station Adelaide	1998-present 15 minute data
	Source: http://www.physics.adelaide.edu.au/astrophysics/index.html Available at DNSC: 1998-2001		
	Cosmic ray-induced ionisation	Global 5x5 degrees grid 16 vertical levels	1951-2000 Monthly data
	Source: I. G. Usoskin, Oulu, Finland Available at DNSC: full data set		

	Observation	Geographic coverage	Temporal coverage
***Magneto-/* ionosphere**			
	Total Power Input	Hemispheric average	1983-2003 app. 50 minute
	Source: spidr.ngdc.noaa.gov/spidr/dataset.do Available at DNSC: full data set		

	Observation	Geographic coverage	Temporal coverage
Temperatures			
	Microwave Sounding Units: temperature anomalies	Global Hemispheric, zonal or gridded (2.5 degree) 3 vertical layers	1979-present Daily or monthly data (gridded data only monthly)
	Source: http://www.nsstc.uah.edu/data/msu/ Available at DNSC: full monthly data		
	Surface stations: temperature	Global Hemispheric or gridded (5	1856-present Monthly data

	anomalies	degree)	(gridded data only from 1960)
	Source: http://www.cru.uea.ac.uk/cru/data/temperature/ Available at DNSC: full data set		
	Radiosonde: temperature anomalies	Global Gridded (5x10 degrees) 9 vertical levels	1958-present Monthly data
	Source: http://badc.nerc.ac.uk/data/hadrt/ Available at DNSC: full data set		

	Observation	Geographic coverage	Temporal coverage
Clouds			
	ISCCP data: type, amount, top temperature, top pressure, optical thickness and many others	Global Gridded (280 km) (Pixel level data at 30 km) 3 vertical levels (cloud types)	1983-present 3 hour, daily, monthly
	Source: http://isccp.giss.nasa.gov/index.html Available at DNSC: full monthly data set, parts of 3 hr data set		
	Nimbus-7: type, amount, radiance	Global Gridded (4.5 degree) 3 vertical levels (cloud types)	1979-1985 Monthly (twice daily)
	Source: http://www.cgd.ucar.edu/cas/catalog/satellite/cmatrix/ Available at DNSC: total cloud cover data set		
	HIRS: cloudiness	Global Gridded (2x3 degrees) 16 vertical levels	1989-1994 Monthly data (averages over the data period)
	Source: http://www.ssec.wisc.edu/~donw/PAGE/CLIMATE.HTM Also available: 22 year data set Available at DNSC: full 6.5 year data set		
	SSM/I: Cloud liquid water, precipitation, total precipitable water and others	Global Gridded (1 and 2.5 degree)	1987-present Monthly data
	Source: http://www.ncdc.noaa.gov/oa/satellite/ssmi/ssmiproducts Available at DNSC: full data set		

	Observation	Geographic coverage	Temporal coverage

Reanalysis			
	NCEP/NCAR: Meteorological variables	Global Gridded (200 km) 28 vertical layers	1948-present 4 times daily Monthly means
	Source: http://www.cdc.noaa.gov/cdc/reanalysis/ Available at DNSC: air temperatures and geopotential heights – monthly means		

	Observation	Geographic coverage	Temporal coverage
Aerosols			
	Aerosol index	Global Gridded (1.25 x 1 degree)	Nov 1978-present (gap June 1993 – July 1996) Daily
	Source: http://toms.gsfc.nasa.gov/aerosols/aerosols_v8.html Available at DNSC: full data set		
	Aerosols Optical Thickness	Global (over oceans) Gridded (1 degree)	1998-present Daily
	Source: http://www.osdpd.noaa.gov/PSB/EPS/Aerosol/Aerosol.html Available at DNSC: weekly data		

	Observation	Geographic coverage	Temporal coverage
Ozone			
	TOMS Total ozone	Global Gridded (1.25 x 1 degree)	Nov 1978-present (gap June 1993 – July 1996) Daily
	Source: http://toms.gsfc.nasa.gov/ozone/ozone_v8.html Available at DNSC: full data set		
	GOME Total ozone	Global Gridded (1.25 x 1 degree)	1995-2003 Daily
	Source: http://www-iup.physik.uni-bremen.de/gome/wfdoas/ Available at DNSC: full data set		

	Observation	Geographic coverage	Temporal coverage
Other data			
	NVAP: Water vapour	Global Gridded (1 degree) 4 vertical layers (from 2000 0.5 degree and	1988-2001 Daily (from 2000 twice daily)

		5 layers)	
	Source: http://www.cira.colostate.edu/climate/NVAP/climate_wvsci.html Available at DNSC: 1988-1997		
	Berlin data: Geopot. height, temperature	Northern hemisphere Gridded (5 degrees) 3 vertical layers	Nov 1964-Jun 2001 Daily data (twice daily in Summer)
	Source: http://strat27.met.fu-berlin.de/products/ Available at DNSC: full data set		

	Observation	Geographic coverage	Temporal coverage
Surface data			
	Precipitation	Global – over land Gridded (5 degree or 2.5 x 3.75 degree)	1900-1998 Monthly data
	Source: http://www.cru.uea.ac.uk/~mikeh/datasets/global/ Available at DNSC: full data set		
	Precipitation	Tropics – below 30° Gridded (2.5 x 3.75)	1974-1994 Monthly data
	Source: http://www.cru.uea.ac.uk/~mikeh/datasets/global/ Available at DNSC: full data set		
	Precipitation	USA (20N-60N, 220E-297.5E) Gridded (2 x 2.5 degree)	1948-2002 Hourly data
	Source: http://www.cdc.noaa.gov/cdc/data.cpc_hour.html Available at DNSC: full data set		
	Pressure	Northern hemisphere Gridded (5 x 10 degree)	1873-2000 Monthly data
	Source: http://www.cru.uea.ac.uk/cru/data/pressure.htm Available at DNSC: full data set		
	Temperature	Global (1856-1869 only over land) Hemispheric or gridded (5 degree)	1856-present Monthly data
	Source: http://www.cru.uea.ac.uk/cru/data/temperature/ Available at DNSC: full data set		
	Temperature (sea surface), sea ice coverage	Global over oceans Gridded (1 degree)	1870-present Monthly data
	Source: http://badc.nerc.ac.uk/data/hadisst/ Available at DNSC: full data set		

	Temperature, precipitation, cloud cover, vapour pressure, frost and wet day frequencies	Global over land Gridded (0.5 degree)	1901-2002 Monthly data
	Source: http://www.cru.uea.ac.uk/~timm/grid/CRU_TS_2_0.html Available at DNSC: full data set		
	NAO and SOI	Single index	1821-2000 (NAO) 1866-2004 (SOI) Monthly data
	Source: http://www.cru.uea.ac.uk/cru/data/nao.htm and http://www.cru.uea.ac.uk/cru/data/soi.htm Available at DNSC: full data set		

	Observation	Geographic coverage	Temporal coverage
Snow and Ice			
	Nimbus-7 snow cover and depth	Global – over land Gridded (0.5 degree)	1978-1987 Monthly data
	Source: http://nsidc.org/data/nsidc-0024.html Available at DNSC: full data set		
	Snow water equivalent	Global – over land Gridded (25 km)	1978-2003 Monthly data
	Source: http://nsidc.org/data/nsidc-0271.html Available at DNSC: northern hemisphere		
	Snow cover and sea ice extent	Northern hemisphere Gridded (25 km)	1966-2001 (snow cover) 1978-2001 (sea ice) Weekly data
	Source: http://nsidc.org/data/nsidc-0046.html Available at DNSC: full data set		

	Observation	Geographical coverage	Temporal coverage
Vegetation			
	NDVI	Global over land Gridded (8km)	1981-2003 Bi-monthly data
	Source: http://glcf.umiacs.umd.edu/data/gimms/ Available at DNSC: full data set		

2. Solar Activity

Solar activity varies on time-scales from hours to billions of years. Solar variability originates from the solar interior. One aspect of solar variability is linked to solar evolution driven by nuclear conditions in the core. This is a relatively slow process with changes on time-scales of the order of several million years and above for parameters such as mass, radius and luminosity. Figure 15 shows schematically the Sun's evolution its creation till its end as a white dwarf.

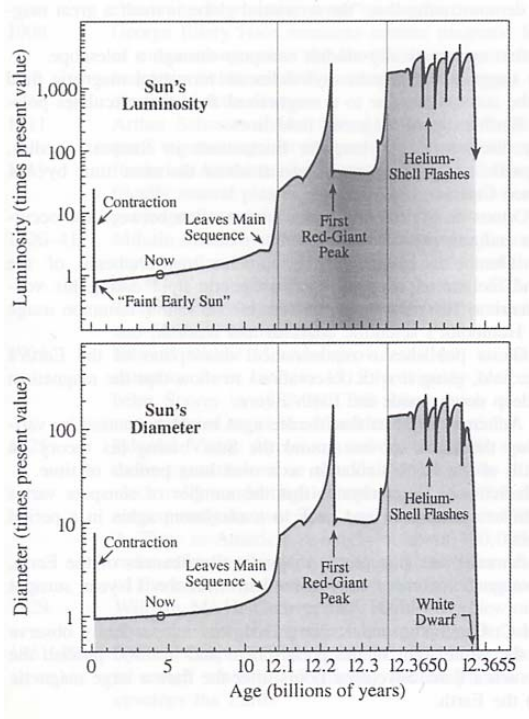

Figure 15: The Sun's evolution in terms of luminosity and diameter. At the moment it is approximately midway on its path on the main sequence.

The solar luminosity increases with 1% in 150 million years. For every 1% increase in the TSI, there should be a global increase in the Earth's surface temperature of 2 degrees C, so the Sun should have turned the heat up by about 60 degrees over 4.5 billion years. However, today the global T is 15°C and without the natural greenhouse effect -18°C.

Another aspect of solar variability is related to solar magnetic fields generated below the convective zone in the interior. The evolution of magnetic fields results in many manifestations, on time-scales in the range of hours to several hundred even thousand years, such as the well-known sunspot cycle and its longer-period modulations, solar wind structures, and coronal mass ejections. Fourier studies of solar activity give certain periods and frequencies. However, wavelet studies show that the periods and frequencies change with time. Certain frequencies come and go. A much more complex picture therefore appears, than variability on only the 11-year sunspot cycle.

A third aspect of solar variability deals with periodicities due to orbital conditions such as solar rotation, changes in Earths orbit, or inclination of rotation axis with respect to the ecliptic plane.

Here, we focus on the solar activity driven by the changes of the solar magnetic field. The solar magnetic activity often shows non-linear, transient and chaotic behavior. For that reason wavelet analysis methods are employed in order to compare the indicators with the mathematical concepts, such as the toroidal and poloidal magnetic fields. Wavelet analysis is a powerful tool both to find the dominant mode of variation and also to study how it varies with time, by decomposing a non-linear time series into time-frequency space. For details of the wavelet methods used here, see Liszka (2003), Lundstedt et al. (2005), and Lundstedt et al. (2006).

In Figure 16 the solar activity, as indicated by the group sunspot number and sunspot number, is given in an ampligram for the period 1610 to 2005. The variability is shown for fractions of the maximum wavelet coefficient magnitude. The large variation of the solar activity amplitude is clearly seen, including several minima such as Maunder minimum (1645-1715), Dalton minimum (1795-1823), and the most recent maximum (after 1940). The sunspot indicator shows the 11 year cyclicity for the whole period except during the Maunder minimum. In the lower panel only the weak signal, below 20%, of the WCM maximum is shown. It is interesting that even the very weak signal has structures.

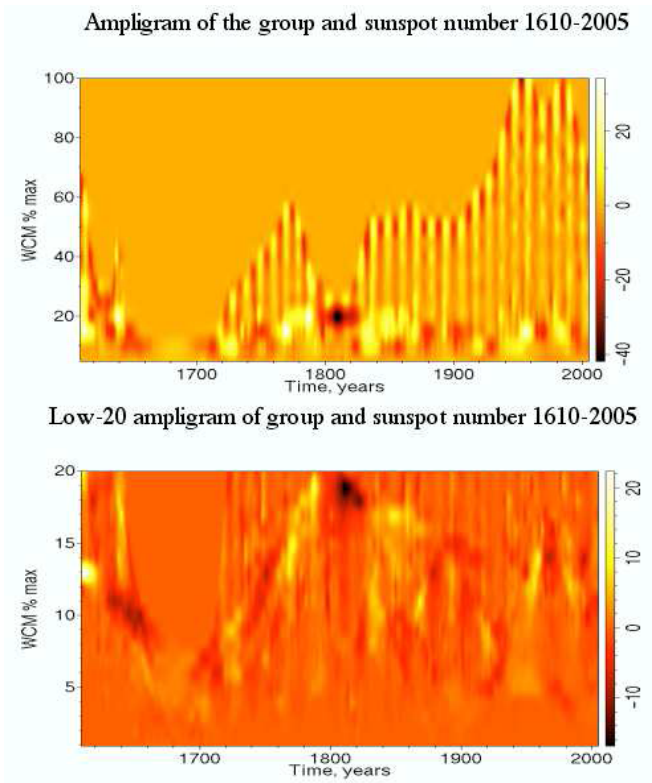

Figure 16: Ampligram of the group sunspot number 1610-1995 and the sunspot number 1995-2005. In the lower panel only the weak signal, below 20 % of WCM maximum. In the colour scale to the right, the zero represents the average value of the sunspot number.

In order to further study the cyclicity, revealing maximum and minimum, during the Maunder Minimum we carried out a Multi-Resolution Analysis of the annual ^{14}C production rate (Figure 17). The variation is studied at different resolutions. At level four in the detailed part the 22-year cycle is clearly present during the Maunder Minimum.

The 11-year cycle is also clearly seen at level three in the detailed part. At the lowest resolution (approximation level four) several peaks appear. The strongest occur around 1600 and about 1780. These are not seen in the group sunspot number. The found cyclicity for the solar indicator, ^{14}C production rate, during the Maunder minimum shows that this indicator is better than the sunspot number. The explanation for the difference is that during the Maunder minimum strong toroidal magnetic flux tubes (as indicated by the sunspot number) were absent but weak ephemeral magnetic fields (also indicated by the ^{14}C production rate) were present.

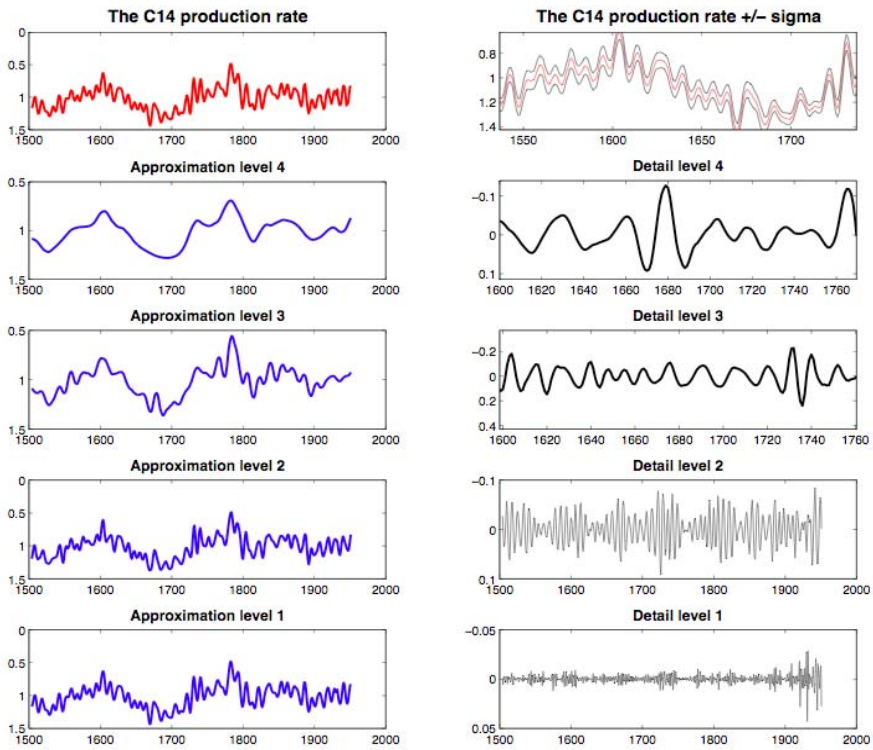

Figure 17: Multi resolution analysis of the ^{14}C production rate. The 22-year cycle is clearly present during the Maunder minimum (zoomed in period) at detail level 4. The 11-year cycle is clearly present during the Maunder Minimum (zoomed in period) at detail level 3.

During the latest solar cycle, the sunspot number has again shown to be a not so good indicator of the solar activity. On September 7, 2005, an X17 solar flare occurred and we have had as many geomagnetic storms and X-type solar flares in 2005 (i.e. close to sunspot minimum), as during Solar Max (2000). To improve the picture of the Sun's activity we need an indicator describing the activity of the whole Sun from below the solar surface, on the surface to the corona. Using the sunspot number we only describe the activity of largest flux tubes on the surface below about 35 degrees latitude.

For the use in climate analysis it is interesting to compare the most often used parameters such as sunspot number (Rz), solar irradiance (TSI), cosmic rays (CLIMAX), and UV. Figure 18 shows the wavelet coherence between Rz and TSI. In the top panel the wavelet

coherence is shown and for comparison Rz is shown in the bottom panel. For periods longer than 64 Carrington rotations (about 5 years) there is a significant correlation with no phase difference (right pointing arrows). At one year period (Period=13) the correlation is more patchy, and when there is a correlation the signals are basically out of phase and that the correlation mainly exists during the declining and minimum phases of Rz. It is clear that if Rz is used as a proxy for TSI care has to be taken to which process should be modelled if any temporal averaging is used. If we study periods in the range 8 days to 1.4 years there is a quite strong negative correlation which could be related to the sunspot blocking. For periods longer than 2.8 years, or even 5.6 years, the correlation is strongly positive probably due to the fact that bright regions and sunspots correlate on these time scales.

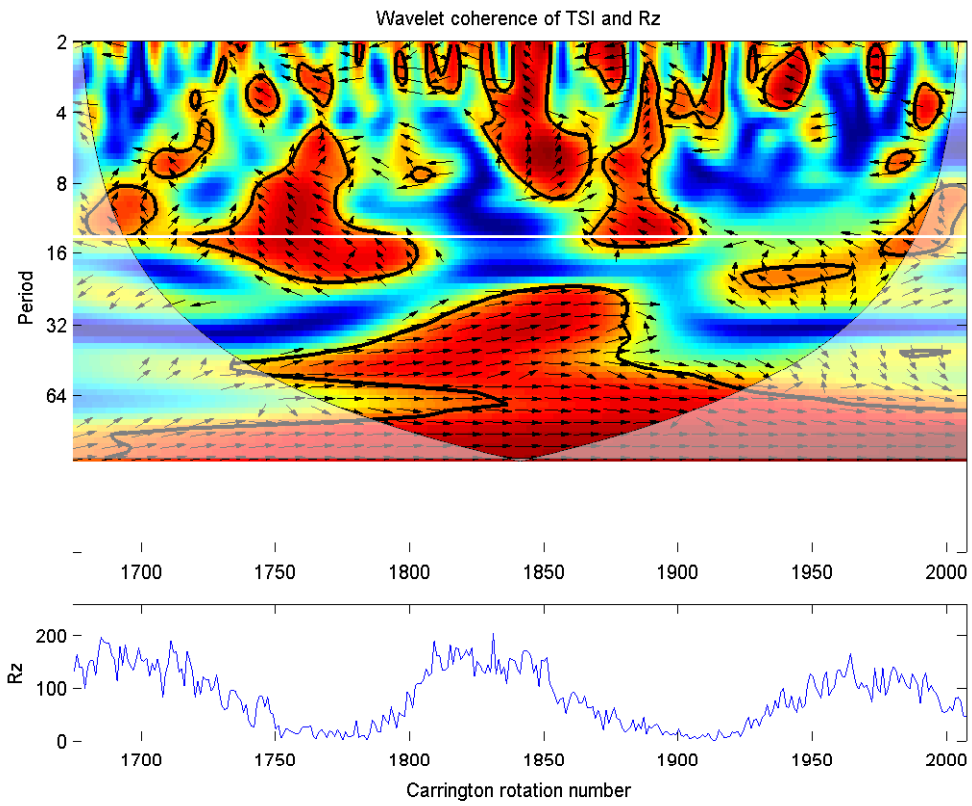

Figure 18: Wavelet coherence between TSI and Rz. Upper panel: Weak correlation is coloured blue and strong correlation red. The black heavy lines indicate a significant correlation at the 95% level. Arrows indicates any phase shift. An arrow pointing to the right means no phase shift, an arrow pointing down means that TSI leads Rz by 90 degrees, an arrow pointing up means that TSI lags Rz by 90 degrees, and an arrow pointing to the left means that they are 180 degrees out of phase. The period is given in units of Carrington rotations. The thick white line marks 1 year periodicity. Lower panel: The sunspot number Rz is shown for comparison.

Figure 19 shows a similar analysis for sunspot number and cosmic rays. A significant and strong anti-correlation is present at all times for periods longer than about 100 Carrington rotations (7 years) but for shorter periods the signals only occasionally correlate. Thus, on

long time scales Rz may serve as a good proxy for the cosmic ray flux, but not on shorter time scales.

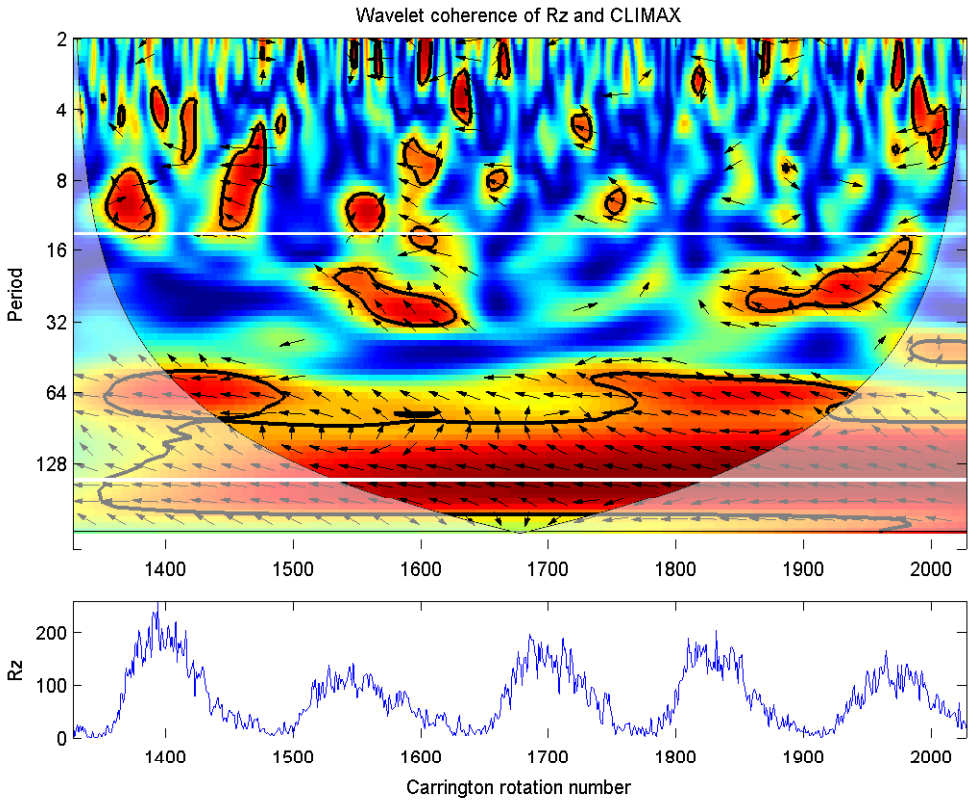

Figure 19: Wavelet coherence between Rz and CLIMAX. Upper panel: Weak correlation is coloured blue and strong correlation red. The black heavy lines indicate a significant correlation at the 95% level. Arrows indicates any phase shift. An arrow pointing to the right means no phase shift, an arrow pointing down means that Rz leads CLIMAX by 90 degrees, an arrow pointing up means that Rz lags CLIMAX by 90 degrees, and an arrow pointing to the left means that they are 180 degrees out of phase. The period is given in units of Carrington rotations. The two thick white lines mark 1 year and 11 year periodicities. Lower panel: The sunspot number Rz is shown for comparison.

When solar activity is discussed it is insufficient to speak in terms of sunspot numbers and 11-year cycles as there is wide range of processes taking place on different time scales. The prime cause of all solar variability is the changing solar magnet field. For example, sunspots are caused by strong magnetic flux penetrating the photosphere and thereby suppressing outgoing radiation leading to a lowering of TSI. However, sunspots appears in active regions where also bright features like plages appear giving a positive contribution to the TSI. On larger scales there is also a network of fields giving increased brightness with a positive contributing to the TSI. This complex response of the TSI to magnetic fields is partly seen in the TSI–Rz correlation in Figure 18. A similar correlation is seen between the F10.7 cm radio flux and TSI. Thus, any solar–climate study that uses Rz or F10.7 as a proxy for TSI must be carefully thought through. If monthly averages are used there will be a mixture of processes working on different temporal scales that will have opposite effects on TSI. We therefore suggest that a scale based approach

should be used when Rz or F10.7 is used as a proxy for TSI so that the solar–climate relation is studied on a scale-by-scale basis.

Rz and CLIMAX shows a simpler relation in the sense that they are anti-correlated on all scales, although the correlation is very weak for temporal variations shorter than 2.8 years (Figure 19). The weak correlation that is seen on time scales shorter than 2.8 years are only occasional covariation. A similar conclusion is reached if F10.7 is used. Thus, if Rz or F10.7 is used as a proxy for the cosmic ray flux one can only expect to find a strong Sun–climate correlation at time scales of several years and longer. A weak, or lack of, Sun–climate correlation on time scales from months to about 2–3 years using Rz as a proxy for cosmic rays can not be used to rule out a relation.

In solar–climate relations the description of climate is much more scientifically advanced than the solar part. If a Sun–climate relation breaks down one must look at the solar mechanism at work to rule out the possibility that the solar output parameter used is uncorrelated with the proposed physical mechanism.

3. Stratospheric Interactions

We focus in what follows on deriving the solar signal in stratospheric temperatures and zonal winds. To this end we apply a multiple regression technique to zonal mean data from the NCEP/NCAR reanalysis data set. Because our work, as previous studies, suggests that the solar influence on the lower atmosphere depends on dynamical coupling between different atmospheric layers we also consider some tropospheric signals, where these are linked, and consider how solar forcing influences the atmospheric polar modes of variability. We conclude by presenting a summary of the current understanding of how stratospheric ozone responds to changes in solar activity

3.1 Regression technique

Most of the analysis described below has been carried out using a multiple regression technique. The indices used in the regression include representations of some or all of the following features

- a constant, or individual constants for each month to represent the annual cycle;
- a linear trend representing long term climate change;
- a chlorine index;
- solar activity – mainly the 10.7cm solar radio flux;
- the QBO - zonal wind at 40hPa over Singapore;
- ENSO - the "cold tongue" index and
- volcanic aerosol – global average stratospheric aerosol loading as constructed by Sato et al (1993); a background level is assumed since 1996.

3.2 Temperature

Van Loon and Labitzke (1994), reviewing their work up to that date, concluded that a 10-12 year oscillation, in phase with solar activity, occurs over much of the Northern Hemisphere in both the stratosphere and troposphere. They found highest correlations in the summer stratosphere south of about 45ºN, associated with a corresponding periodicity in the temperature of the middle and upper troposphere in the tropics and sub-tropics and deduced that the oscillation is associated with variations in the tropical and sub-tropical circulation. In all their work, however, they used a single linear regression and thus were not been able to estimate the effects of different factors simultaneously influencing the temperature field. This could lead to misattribution of non-solar effects to the sun or, alternatively, to missing solar effects where these interact with the other influences. Most of their studies were also confined to discussions of correlation coefficients and so did not consider the magnitude of the implied solar signals.

By adopting the multiple regression approach the responses to all forcing indices supposed to influence temperature are derived simultaneously. Here we assess the solar contribution, along with the other factors outlined above, to variations in zonal mean temperature in the troposphere and lower stratosphere using the National Centers for Environmental Prediction – National Center for Atmospheric Research (NCEP/NCAR) Reanalysis dataset (http://www.cdc.noaa.gov/cdc/data.ncep.reanalysis.html). We use data only since 1979 as it is well documented (see e.g. Randel and Gaffen, 2000; Haigh 2003) that before that date the lack of satellite data makes the values in the stratosphere unreliable. The annual mean results are shown in Figure 20. There is a clear long-term cooling trend in stratospheric low to mid-

latitudes; the characteristic signal of the QBO is displayed in the equatorial stratosphere; ENSO shows a warming of the tropical troposphere a cooling above and a significant warming in the northern polar stratosphere while there is a strong response to the injection of volcanic aerosol – warming the stratosphere and cooling the troposphere. The solar signal shows a statistically significant warming in vertical bands in the mid-latitude troposphere in both hemispheres (discussed previously by Haigh 2003) and a bipolar structure in the lower stratosphere with preferential warming in the sub-tropics (previously noted in ERA-40 data by Crooks and Gray, 2005).

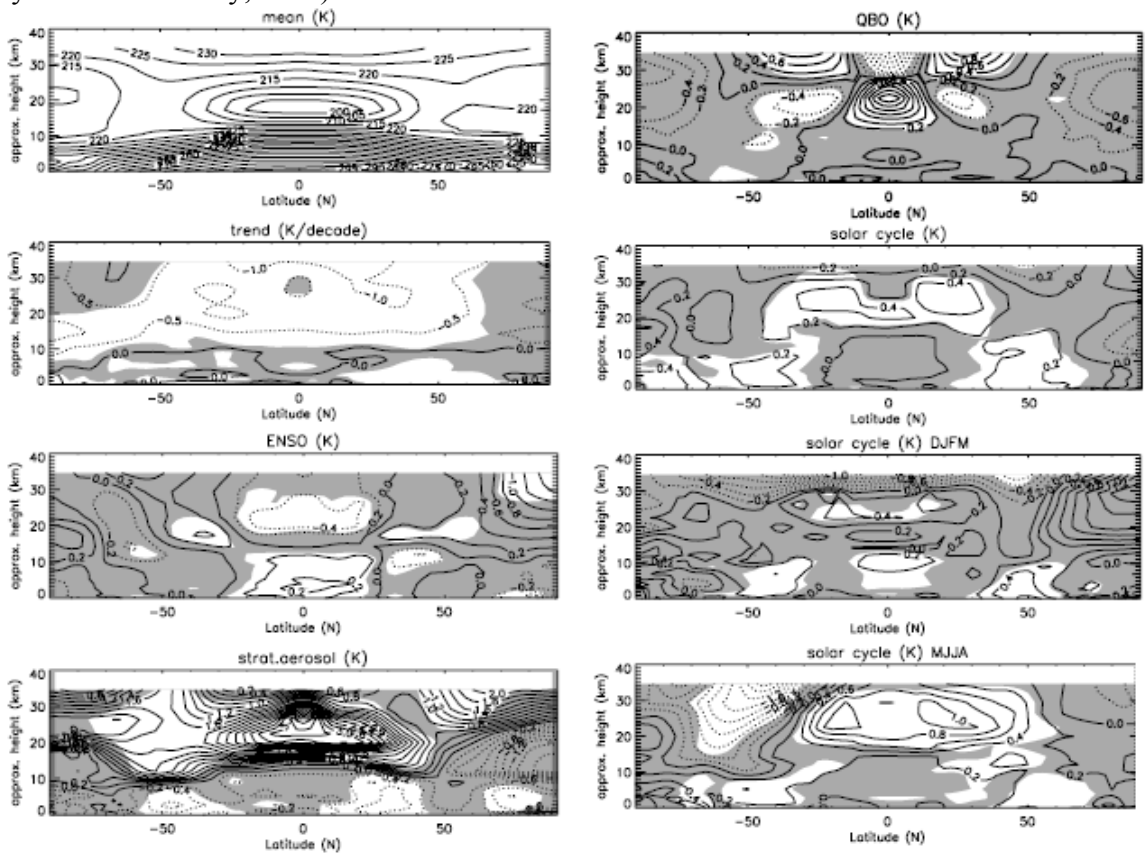

Figure 20: Signals in zonal mean temperature derived from NCEP/NCAR Reanalysis data 1979-2002. The component is identified in the title of each panel. The first six panels relate to the annual mean; the last two are the solar components derived from separate analyses of the DJFM and MJJA seasons. The contour interval is 5K for mean, 0.5 K decade^{-1} for trend, 0.2K all others. Shaded regions are not significant at the 5% level.

The last two panels in Figure 20 show the solar signals derived in separate regression analyses for the solstice seasons, December-March and May-August. Both show the same gross features seen in the annual mean results (warming bands in the mid-latitude troposphere, bipolar warming in the low to mid-latitude lower stratosphere) although the stratospheric response in much larger in MJJA. The suggestion of a cooling in the mid-to-high latitude middle stratosphere has also been seen in SSU/MSU satellite data (Keckhut et al, 2004). The patterns of response to higher solar activity in both the troposphere and stratosphere suggest that dynamical, as well as direct radiative, factors are taking effect.

3.3 Zonal wind

Associated with the temperature response to solar variability are changes in the zonal winds. These have also been analysed with data from the NCEP/NCAR Reanalysis and some of the results are shown in Figure 21. The annual mean signal shows the characteristic inverted horseshoe shape negative (easterly) anomaly in low latitudes, first identified as a solar signal in the modelling study of Haigh (1996), representing a weakening of the tropospheric jets. The seasonal data show very similar effects (though with somewhat different magnitudes) in the two winter hemispheres and the two summer hemispheres throughout the stratosphere and troposphere. In winter the sub-tropical jets are weaker when the sun is more active while in summer mid-latitude jets move polewards. In the stratosphere the summer easterly winds weaken poleward of 50º while the winter westerly polar jet moves equatorward.

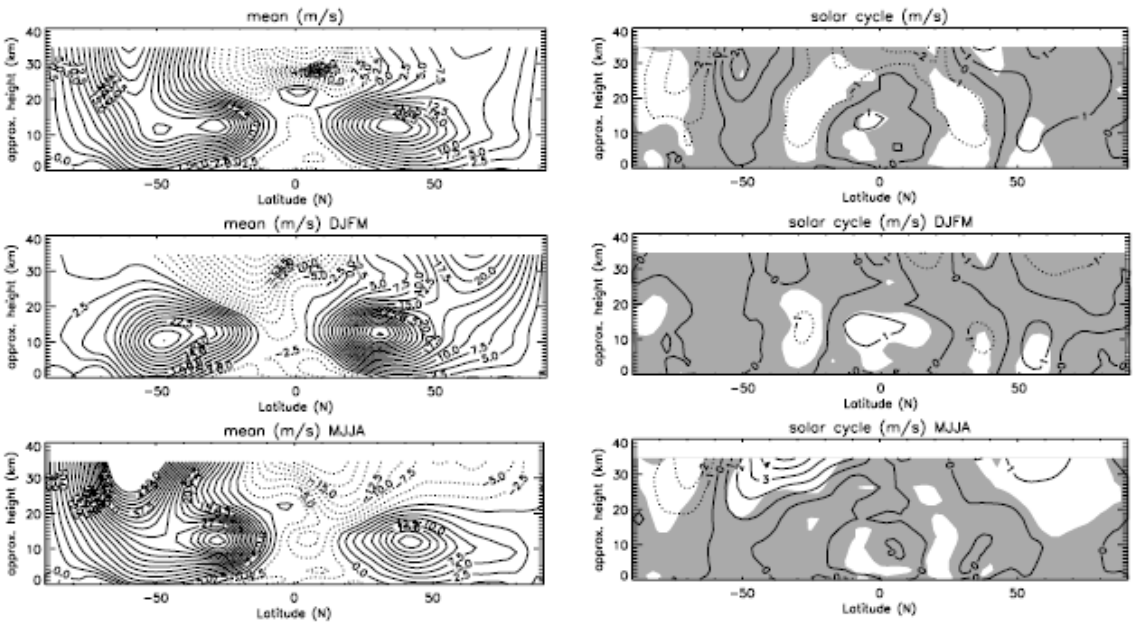

Figure 21: Signals in zonal mean zonal wind derived from NCEP/NCAR Reanalysis data 1979-2002. The top, middle and bottom rows contain analyses for the annual mean, DJFM and MJJA seasons respectively. The left hand column shows the mean values and the right the solar signal. The contour interval is 2.5 ms^{-1} for mean, 1 ms^{-1} for solar cycle. Shaded regions are not significant at the 5% level.

The changes in the zonal wind structure imply a redirection of vertically-propagating waves, which could then further impact the zonal winds if they are dissipated in different regions, as first proposed by Kodera (1995). To date numerical models of the global circulation of the middle atmosphere have had only limited success in reproducing the apparent solar signals and it will only be when a fuller understanding of these types of feedback effects is achieved that a more complete picture will emerge of solar effects on the middle and lower atmosphere.

3.4 Polar modes of variability

The atmosphere exhibits a number of characteristic modes of variability, that are important in determining the local climate in various regions, and it has been suggested that the impact of solar variability, as well as other climate forcing factors, may be to affect the frequency of occupation of certain phases of these modes. Studies of the polar annular modes have suggested that in both Northern (Hartley et al., 1998, Baldwin and Dunkerton, 1999, 2001)

and Southern (Thompson et al., 2005) high latitudes variations in the strength of the stratospheric polar vortex often precede similarly signed anomalies in the troposphere. Not all events follow this pattern (Black and McDaniel, 2004), and a chain of causality explaining the mechanisms involved has yet to be established, but the evidence suggests one route whereby any factor (and here, of course, we are specifically interested in solar variability) influencing stratospheric circulations might have an impact on surface climate.

Some authors (e.g. Kuroda & Kodera 1998; Castanheira & Graf 2003) have found evidence of modulation of the NAO by the state of the stratosphere and some (e.g. Kodera 2002; Boberg & Lundstedt 2002; Thejll et al 2003) of a solar signal in the polar modes. All of these studies, however, like Labitzke, have used single linear regression and often confined their discussions to correlation coefficients and so have not considered the magnitude of the implied solar signals in the context of other potential forcing factors.

Here we present a multiple regression analysis of factors potentially influencing the northern and southern annular modes, including the factors outlined above. We investigate levels from the surface to the middle stratosphere and we also conduct a similar analysis of the North Atlantic Oscillation (NAO) in surface pressure, which some authors see as a particular aspect of the NAM but which may alternatively give a more local picture representing synoptic scale variability in the position of the North Atlantic storm track.

The annular mode data used in this study (Mark Baldwin, Northwest Research Associates, USA, personal communication) are based on, at each pressure level, the first empirical orthogonal function (EOF) of 90-day low-pass filtered anomalies, poleward of 20º latitude in each hemisphere, of geopotential heights from the NCEP/NCAR reanalysis. Daily values of the annular mode from 1 January 1958 to 31 December 2001 are obtained by projection of the daily geopotential data onto the EOFs. For further details see Baldwin and Dunkerton (2001) regarding the NAM and Thompson et al. (2005) the SAM. We use monthly averages of the daily values, as we are more interested in the climatological response than in daily development, and we focus on three pressure levels: 1000hPa, 250hPa and 30hPa representing behaviour at the surface, the tropopause and the stratosphere respectively. In the stratosphere we restrict our analysis to data since 1979 because the NCEP reanalysis of the stratosphere is less reliable before this, as mentioned above. At other levels we retain all 44 years of data to provide statistical rigour.

The NAO data used are based on the monthly mean difference in sea level pressure between Gibraltar and South West Iceland as calculated by the University of East Anglia, UK, see http://www.cru.uea.ac.uk/~timo/projpages/nao_update.htm.

No indices representing inter-month variability (annual cycle etc.) are included in the regression analysis as the data are essentially de-seasonalised by the procedure of taking anomalies, as described above. The regression coefficients (β values) for the five varying indices are presented in Table 4. Values assessed to be statistically significant at the 80% confidence level and above are shown in bold type with levels indicated by different colours (see the caption to Table 4). Note that these are regression coefficients, not correlation coefficients; hence the confidence level indicates the importance of the parameters, not the actual size of the coefficients.

Looking first at the results for the NAO we find no significant trend over the period 1958-2001, nor any substantial influence of ENSO. There is a small response to the QBO showing positive NAO anomaly during the QBO-W, but this is not statistically significant. The responses shown to the solar and volcanic forcings, however, are clearly significant at the 95% level; with a positive NAO anomaly shown in response to both higher solar activity and the presence of stratospheric aerosol. While other authors have indicated a link between NAO

and solar variability we believe this is the first time that its magnitude has been estimated within a statistically robust framework, taking into account other potential influences.

	pressure (hPa)	Trend	Cl	ENSO	Vol	Sol	QBO
NAO		0.02		-0.09	**0.89**	**0.63**	0.24
NAM	**30**	0.07		-0.22	0.40	0.17	0.22
	250	0.02		**-0.49**	**0.46**	-0.02	0.05
	1000	**0.13**		**-0.53**	**0.53**	0.09	0.20
NAM (DJFM)	**30**	0.05		-0.38	0.67	0.24	0.73
	250	0.06		**-1.38**	0.53	0.64	0.39
	1000	**0.23**		-0.82	**1.08**	**0.81**	0.64
SAM	**30**		**0.71**	-0.30	**-0.71**	-0.27	0.31
	250		**0.61**	-0.26	**-0.65**	-0.09	-0.14
	1000		**1.01**	**-0.82**	**-0.65**	-0.04	0.13

Table 4: Regression coefficients for the five standard indices. The data covers the period 1958-2001, except for the 30hPa level for which only values since 1979 are used. Colours indicate the statistical significance levels of the values, derived using a Student's t-test, as follows: 99%, 95%, 90%, 80%, <80%.

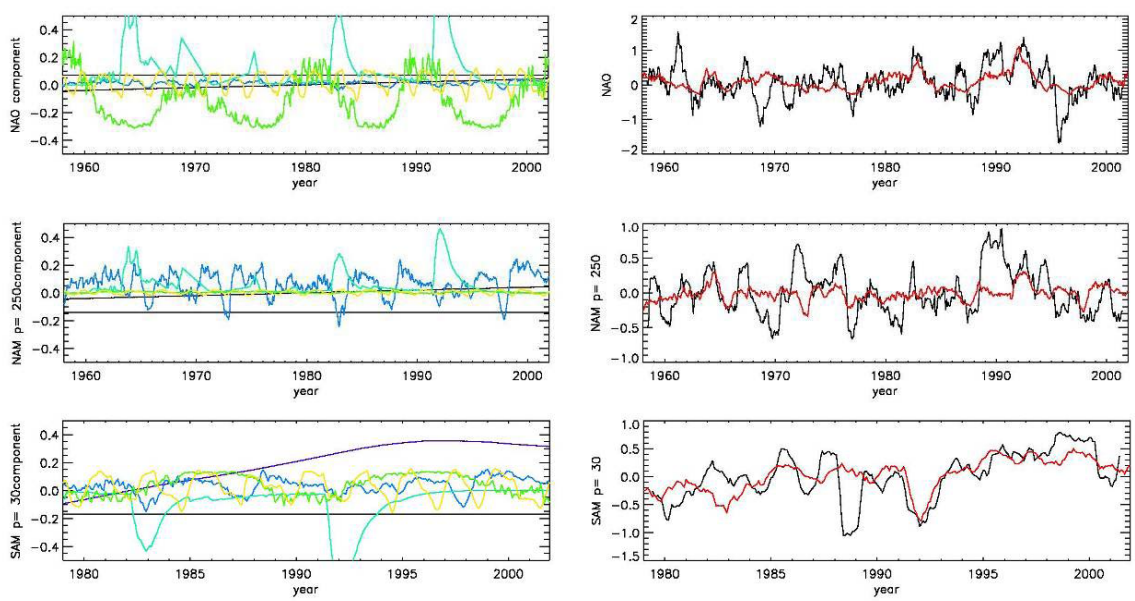

Figure 22: Results of the regression analysis of: Top: NAO; Middle: NAM at 250hPa; Bottom: SAM at 30hPa. The left-hand column shows the time series of the individual components deduced to be contributing to the data. The solar signal is in green, other components as follows: constant (black), linear trend (for NAO and NAM, black), chlorine (for SAM, purple), ENSO (blue), volcanic aerosol (cyan), QBO (yellow). The right-hand column shows the original time series of data in black and the reconstruction from the regression components (without noise component) in red, both smoothed by a 12-month running mean.

The volcanic signal is also seen at 1000hPa in the NAM, although somewhat weaker, but the solar signal has disappeared. If, however, the analysis is carried out using only winter months (average of December to March) there is again a large solar signal (the reduced significance level occurs as a result of the factor 12 decrease in the number of degrees of freedom). A strong ENSO signal is seen in NAM, in both all-month and winter analyses, with a positive ENSO phase being associated with a weaker Arctic circulation, as previously noted by Labitzke and van Loon (1999). No statistically significant solar or QBO signals are found in the stratosphere.

SAM shows a strong correlation with stratospheric chlorine at all levels, indicating a cooling and strengthening of the Antarctic tropospheric polar vortex and confirming the results of Thompson and Solomon (2002). It is also found to be associated with the negative phase of ENSO. No significant response is found to either the Sun or the QBO but a large signal is found of volcanic aerosol of opposite sign to that found in NAM.

3.5 A new index

Labitzke and van Loon (1999, LvL) found that the quasi-biennial oscillation modulates the solar signal. By grouping the data according to the phase of the QBO they showed that when it is easterly (QBO-E) the Arctic lower stratosphere is colder when the sun is more active, implying a stronger polar vortex and more positive NAM, but that the opposite holds during QBO-W. More recently Labitzke (2004) has extended this work and shown that introduction of the QBO also aids analysis of northern hemisphere summers, because of changes in global scale Brewer-Dobson circulation, and furthermore that the Antarctic polar vortex is influenced by the solar cycle, modulated by the QBO, in much the same way as the Arctic. This suggests that during QBO-E the SAM is also stronger when the sun is at maximum activity.

Apart from a solar signal in the NAO the responses, shown in Table 4, of the polar modes to solar variability and the QBO appear weak. However, perhaps this is due to the compensating effects described by LvL. To test this out in a statistically robust framework, which avoids the necessity of having to pre-sort data, we define a new regression index composed of the product of the original solar and QBO indices, as shown in Figure 23. Because the original indices were scaled to lie equally about zero their product represents a modulation such that a combination of high solar activity and QBO-W, or low solar activity and QBO-E, has positive values while solar max/QBO-E, or solar min/QBO-W, has negative.

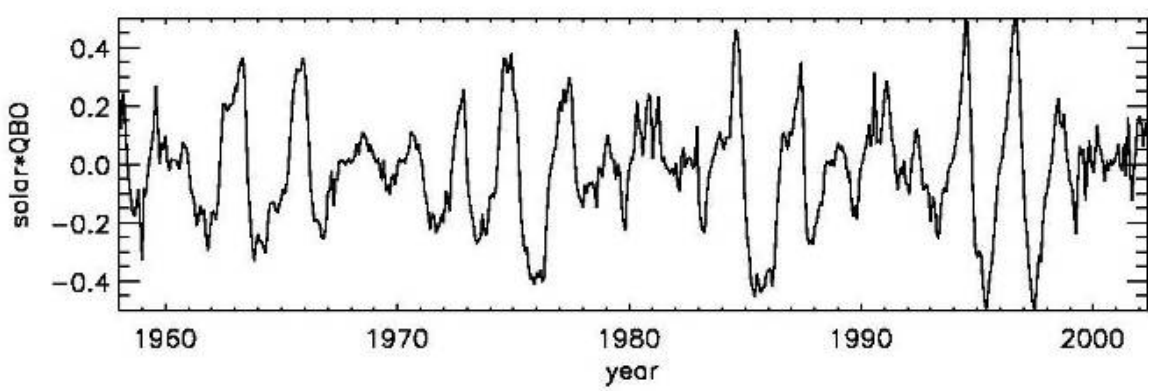

Figure 23: Composite index; this is the product of the independent solar and QBO indices scaled to lie within unit range

This index has been used in the regression analysis in place of the individual solar and QBO indices. An example of its application is shown in Figure 24 which presents, in the right-hand panel, the amplitude of this index for the zonal mean temperature data in DJFM. The left-hand panel shows the individual solar cycle and QBO signals from the original DJFM analysis for comparison.

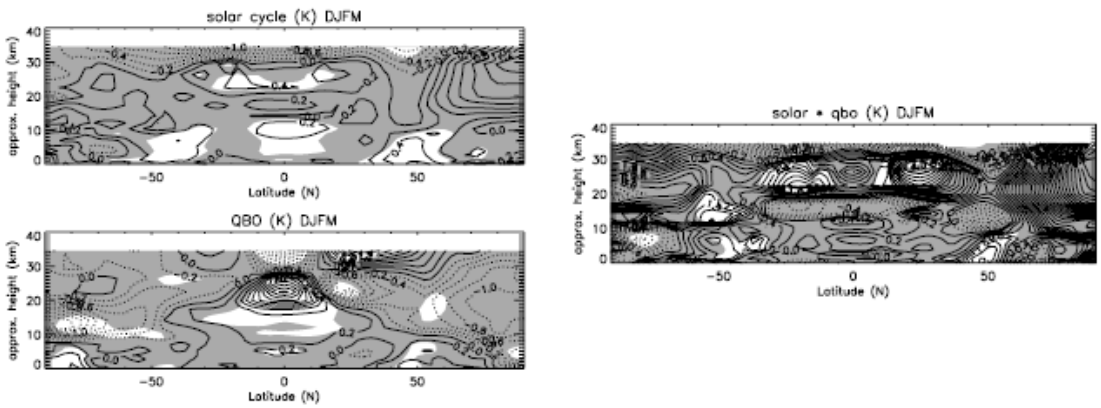

Figure 24: Signal in DJFM zonal mean temperature; left hand side shows results of regression using individual solar and QBO indices (as Figure 21); right hand side shows signal from compound index when this is used in the regression in place of the two original ones.

The regions of significance are still fairly restricted, although with the large internal variability and only 23 data points this is understandable, but it is clear that the signals are much larger than the responses derived for the solar cycle and QBO individually. In the winter polar stratosphere there is a substantial (exceeding 6K) positive response, i.e. the pole is warmer during solar min/QBOE and solar max/QBOW and colder during solar min/QBOW and solar max/QBOE, consistent with the LvL criterion. Signals exceed 2K in the sub-tropical lower stratosphere and 1.5K in the mid-latitude troposphere. This provides significant new evidence that in order to understand solar influences on the lower atmosphere it is necessary to consider dynamical coupling between the stratosphere and troposphere.

	pressure (hPa)	**Trend**	**Cl**	**ENSO**	**Vol**	**Sol*QBO**
NAO		0.03		-0.13	**0.85**	0.11
NAM	**30**	0.05		-0.25	0.40	-0.14
	250	0.02		**-0.47**	**0.45**	-0.16
	1000	**0.13**		**-0.52**	**0.50**	-0.27
NAM	**30**	0.02		-0.47	0.73	-0.13
(DJFM)	**250**	0.07		**-1.39**	0.38	**-0.91**
	1000	**0.24**		-0.85	0.96	**-1.16**
SAM	**30**		**0.78**	-0.27	**-0.76**	**-0.53**
	250		**0.61**	-0.17	**-0.71**	**-0.57**
	1000		**1.01**	**-0.71**	**-0.75**	**-0.89**

Table 5: As Table 4 for values derived using the compound solar*QBO index in place of the solar and QBO indices independently

The derived regression coefficients for the annular modes derived using the composite index are presented in Table 5. The first thing to note is that the values for the trend/chlorine, ENSO and volcanic signals are very similar to those in Table 4: this provides evidence of the independence of the indices and the robustness of these signals. The right-hand column of Table 5 shows all negative values (except for the NAO) consistent with the Labitzke criterion stated above. The signals in NAM (except at 30hPa) and in SAM are larger in magnitude than the individual solar and QBO signals in Table 4 and generally statistically more robust. This is particularly true of SAM for which a strong signal emerges at all levels where very little was shown for the individual indices.

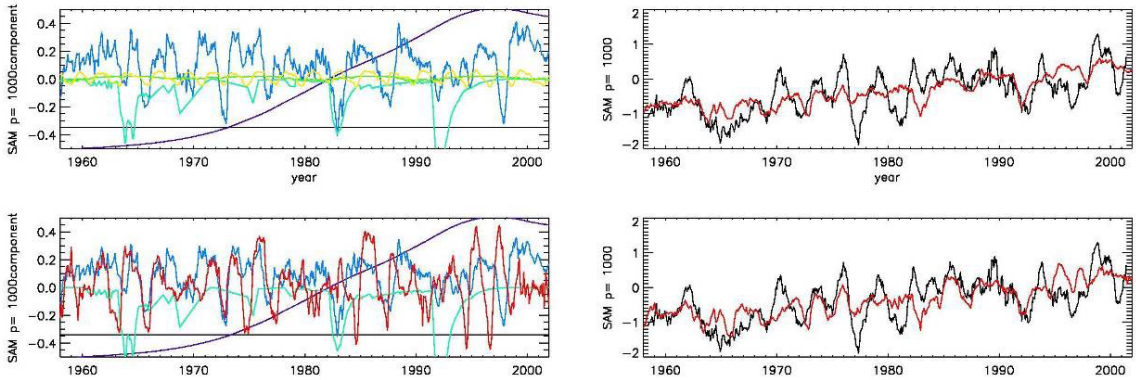

Figure 25: Results of the regression analysis of SAM at 1000hPa. The left-hand column shows the time series of the individual components deduced to be contributing to the data. The top row presents the results using the original indices (colours as in Figure 22 with the solar signal in green); the lower row shows the results using the compound (Solar x QBO) in place of the solar and QBO indices individually, with the compound index in red and other indices unchanged. The right-hand column shows the original time series of data in black and the reconstruction from the regression components (without noise component) in red, both smoothed by a 12-month running mean.

As an example the time series of the derived components of SAM at 1000hPa, and of the original and reconstructed data, are presented in Figure 25. The amplitude of the composite component is clear in the lower left-hand panel of this Figure and the right-hand panels show that the reconstructed time series is able to reproduce more of the variance in the original data than could be achieved with the original components.

3.6 Stratospheric ozone

Global satellite remote sensing records of ozone column amounts now exceed 25 years in length. Figure 26 (b) shows the time series of TOMS/SBUV ozone column data averaged over the 35ºS to 35ºN region from 1979 to 2003 inclusive. Eyeball comparison with the solar UV proxy portrayed in Figure 26(c) suggest a solar cycle signal but extraction of its magnitude has been complicated by the volcanic eruptions of El Chichon (April 1982) and Pinatubo (June 1991) which occurred near the ends of the 1980 and 1990 solar maxima. This is because volcanic aerosol provides the conditions for the destruction of ozone by anthropogenic chlorine compounds. Furthermore, ozone column amounts are dominated by the contribution from the lower stratosphere which is where the greatest concentration of volcanic aerosol resides. The passage of the most recent solar maximum without a coincidental major volcanic eruption has, however, provided additional evidence of a statistically significant solar cycle variation of nearly 3% (peak-to-peak), about 9 Dobson

Units, in the tropics. This is confirmed by independent analysis of ground-based ozone column data (1964-2005) by Fioletov (2006).

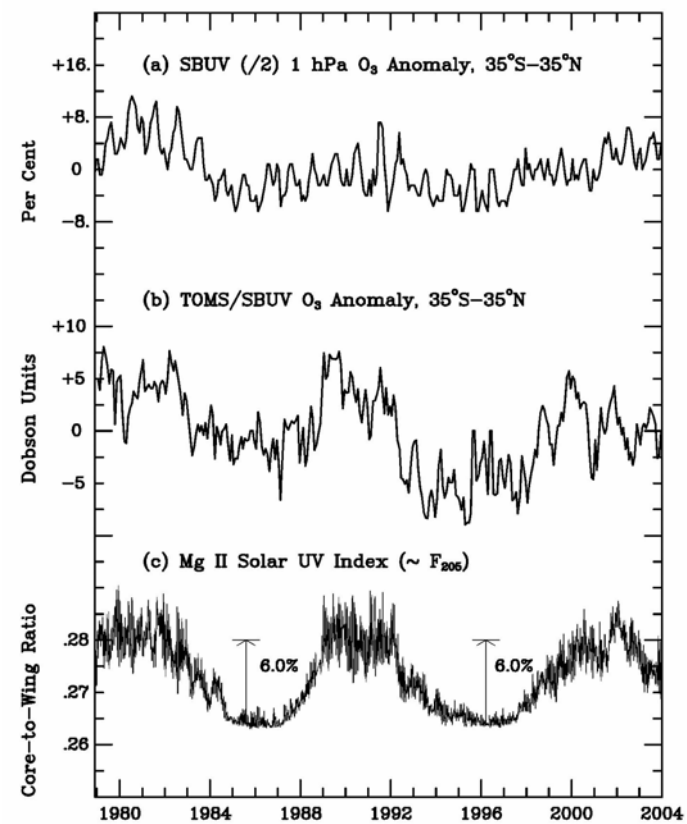

Figure 26: (a) Low latitude (area-weighted) ozone at 1 hPa from SBUV(/2) data; (b) Low latitude (area-weighted), deseasonalised ozone columns from TOMS/SBUV data; (c) Daily MgII 280nm core-to-wing ratio (as proxy for solar UV radiation). From the review by Hood (2004).

Volcanic aerosol is less likely to have an effect in the upper stratosphere and Figure 26(a), showing low latitude ozone concentrations near the stratopause, again suggests a solar cycle influence. Here, however, the problem is one of inter-calibration of the satellite instruments used at different times during the record. Figure 27 shows the solar signals derived in ozone profiles from two different satellite data sets. The overall structure is similar with largest increases (from solar min to solar max) in the upper stratosphere, very small (or possibly negative) responses in the tropical middle stratosphere and increases into the lower stratosphere. However, at any given point there can be sizeable differences between the results of the two analyses so the response of ozone profiles to solar variability remains very uncertain. No model results published to date have been able to reproduce the apparent minimum in the tropical middle stratosphere so, if it is real, it appears that there is a significant gap in our understanding. It has been suggested by Lee and Smith (2003), however, that this minimum may be an artifact introduced into the regression analysis by inappropriate handling of the QBO and volcanic signals. A solution to this problem will come only with acquisition of well-calibrated ozone data well past the next solar minimum.

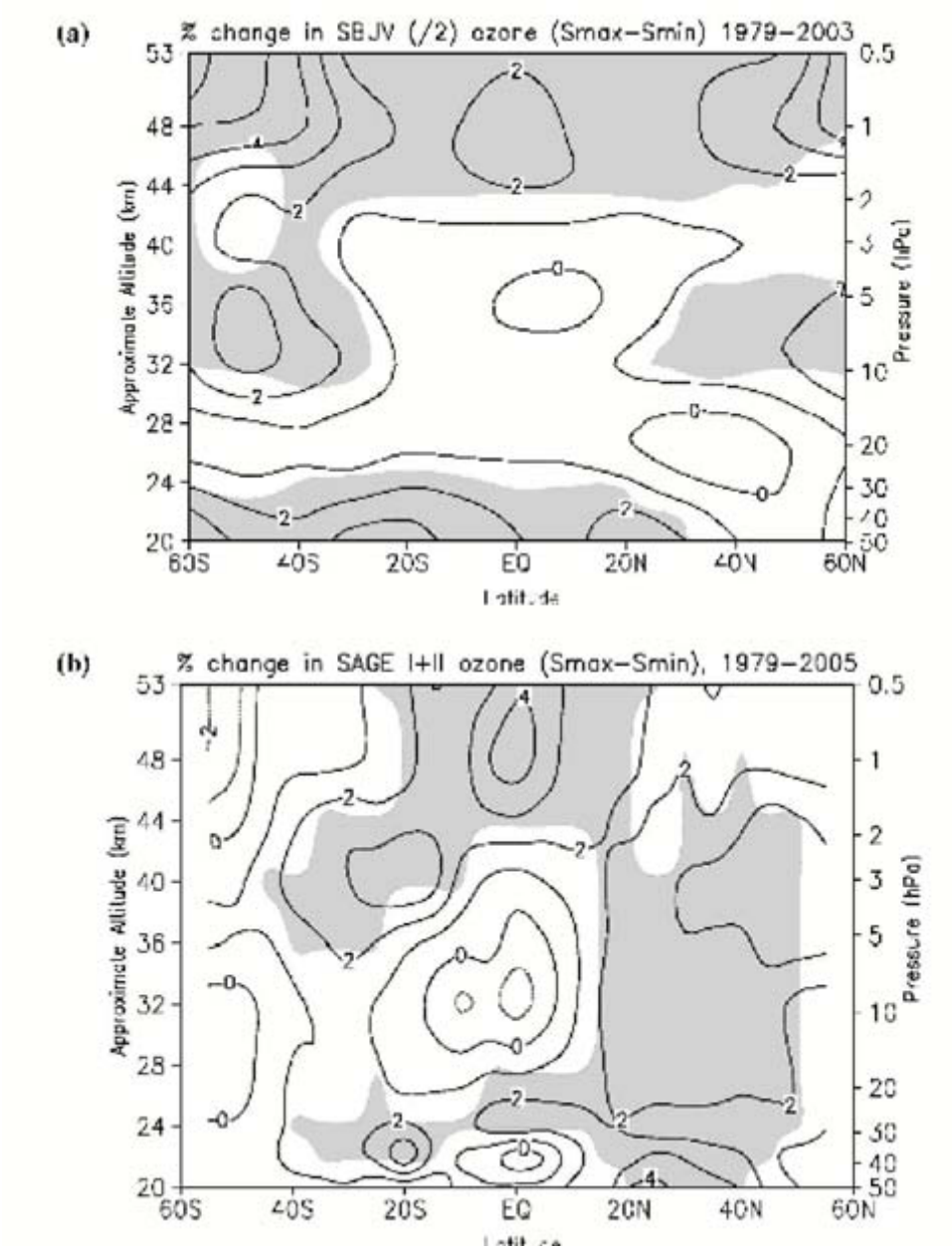

Figure 27: Annual mean solar regression coefficient of ozone concentration as a function of latitude and height using (a) SBUV/SBUV(2) data and (b) SAGE I/II data. The values are percent change in ozone for a 100 unit change in solar 10.7 cm radio flux. Shaded regions are statistically significant at the 5% confidence level. (Lon Hood, personal communication)

3.7 Summary

Our studies of the NCEP/NCAR Reanalysis dataset show signals in response to the solar cycle in zonal mean temperatures and winds throughout the troposphere and stratosphere and in all seasons. The clearest patterns to emerge are warming of around 0.5K (in solar max relative to solar min) in the low to mid-latitude lower stratosphere with largest values in the sub-tropics and northern hemisphere summer and vertical bands of warming, of a few 1/10ths K, in the mid-latitude troposphere. The winter polar stratospheric jet moves equatorward while the summer stratospheric easterlies weaken; in the troposphere the winter sub-tropical

jets weaken and the mid-latitude jets move poleward. There is a clear solar influence detected in the NAO, consistent with the strengthening of the winter westerlies near 50ºN, but no statistically significant signals of solar forcing are found in either the NAM or SAM.

Based on Labitzke and van Loon's findings concerning the combined influence of solar activity and the phase of the QBO on polar meteorology we have defined a new regression index, the product of the solar and QBO indices. When this is used is used in place of the two factors individually then several other features appear. Firstly, as expected, a strong signal in winter polar stratospheric temperatures, as identified by Labitzke and van Loon but we are now able to place these findings within a statistically robust framework and to assess the magnitudes of the effects in the presence of influences by other factors such as volcanic eruptions and ENSO. We also find that the magnitudes of the temperature signals in the tropical lower stratosphere and mid-latitude troposphere are considerable larger than derived using the solar and QBO indices separately.

A strong influence of the composite index is found throughout the atmosphere in the SAM which showed very little solar or QBO signals in the original analysis. The signal in winter NAM is also increased. Perhaps surprisingly our results for the polar modes show more significance in the troposphere than the stratosphere, but this may be due to the necessity of using a shorter time series at higher altitudes because of the unreliability of the reanalysis datasets in the stratosphere before the inclusion of satellite data.

The NAO behaves differently to the NAM (and SAM) in that the signal found for the combined solar*QBO index is in a different sense to that found in the other modes and also of smaller magnitude than that found for the single solar influence in the original analysis. We tentatively conclude that solar variability influences NAM and SAM through its impact in the polar stratosphere, modulated by the QBO, whereas the solar influence on the NAO is the result of a different process. Our previous work (Haigh 1999, Larkin et al 2000, Haigh et al 2005) suggests this may involve changes in the tropospheric Hadley circulation and storm tracks resulting from solar heating of the tropical lower stratosphere but the mechanisms whereby all these processes take place remain to be elucidated.

A signal in low latitude ozone column of about 3% peak-to-peak over the solar cycle is becoming better established as the lengths of the data series extend. However, substantial uncertainties still remain in the response of ozone vertical profiles to solar variability with reservations concerning both observational data analyses and model simulations.

4. Tropospheric Interactions and Surface Response

In the following we describe the most prominent results of our correlation study of between solar output/solar modulated parameters and the troposphere/surface. We first briefly review our method of analysis

4.1 Method of analysis

In the correlation study we focused on 5 external forcing parameters that are modulated by solar variability and have the potential to influence Earth's lower atmosphere below 50km:

- Total Solar Irradiance (TSI) 1978 – 2005 (Fröhlich and Lean, 2002).
- the Ultra-Violet (UV) 1978 – 2005 (Deland and Cebula, 1993;Viereck and Puga, 1999). Prior to 1978, it is possible to use the 10.7 cm radio flux, obtained from ground stations, to produce an index for the Extreme Ultra-Violet (EUV – wavelengths ~20-30nm) component of solar radiation (Tobiska 2001).
- Galactic Cosmic Rays (GCR), are represented by the monthly averaged hourly neutron counts from the ground station at Climax (39N, 106W, 3400m, Geomagnetic vertical cut-off = 3.03 GeV) that has monitored GCR continuously from 1953 to present.
- the direct input from the Solar Wind (SW) is represented by the product between the solar wind speed, v_{sw}, and the southward component of the Interplanetary Magnetic Field (IMF), B_z. Only the southern polarity is included since this is the most efficient configuration for transferring energy directly from the solar wind to the Earth's magnetosphere. 1963 to present.
- the total Hemispheric Power Input (HPI) indicates the amount of energy deposited over an entire hemisphere in the upper atmosphere by precipitating particles measured inside the magnetosphere. The precipitating particles have various sources, foremost directly from the solar wind and from the tail of the Earth's magnetosphere during magnetic (sub-)storms. The particles mainly dump their energy at high latitudes at ionospheric heights. The HPI parameter is given as total energy deposited during a satellite pass and is derived from the high latitude precipitating flux that has been continuously monitored by the NOAA/TIROS and DMSP satellites over the period 1978-2003 (Foster et al., 1986; Fullerrowell and Evans, 1987).

The five parameters are plotted in Figure 28.

As it was noted in the Introduction there is little difference in the phase between the various solar modulated forcing parameters over a solar cycle. As a result, it is difficult to determine the solar modulated process responsible for any significant response found in the climate data at time scales where the effects of the solar cycle dominate. During the study it was suggested to represent the forcing parameters in Fourier series and to remove the solar cycle signal by suppressing the lowest frequency components, hoping thus to remove the correlation between the forcing parameters and using the uncorrelated high frequency parameters to study correlations with climate observations. Figure 29 shows the correlation between GCR and EUV as a function of cut-off frequency. The correlation

drops off sharply at the frequency corresponding to the 11-year solar cycle, but then finds a constant level of about 0.4. GCR and EUV thus never become entirely uncorrelated even at high frequencies. For comparison the correlation of GCR and EUV with tropospheric temperature is shown. The two curves follow each other closely and the frequency cut-off does not aid in distinguishing between the influences of the two forcing parameters.

In an attempt to tackle the problem of the dominating solar cycle, the effects of the solar cycle were removed from the data using two techniques;

1) via multiple-regression where the solar cycle is represented by the sunspot number. In general, we made three sets of correlations for each pair of solar-climate parameters: with raw data; removing linear trends (also internal modes of variability from the climate data, see below); removing the solar cycle. Representing the solar cycle by the sunspot number was an arbitrary choice. Any parameter representing the overall activity of the Sun would be usable.
2) by selecting narrow periods around solar max and solar min where the effects of the solar cycle are almost stationary.

This allowed for a comparison of fluctuations in the data at higher frequencies than the solar cycle. A cursory glance at the solar modulated forcing parameters in Figure 28 indicates that the amplitudes of fluctuations around the solar cycle are much larger under solar maximum than solar minimum conditions. These fluctuations, which are generally independent for each forcing parameter, e.g., Forbush decreases, ground level events, solar flares etc., provide a possible means to distinguish between the different processes. However, the solar processes are highly variable at time-scales of hours to days. This makes the task of identifying a solar signal in the climate data more involved since, at these timescales, fluctuations in local weather phenomena and internal climate variations are often large and can mask the solar effect being explored. This is likely to have a strong impact on the data analysis. So there is a trade-off between the need to resolve short term fluctuations, possibly driven by solar variability, above the internal noise of the climate system. The data used in the following analysis is therefore limited to monthly averages, which reduces the climatic noise, but also allows for an analysis of high frequency fluctuations around the solar cycle.

The effect of the solar cycle on these five parameters is clearly visible from the correlation coefficients, (Table 6), with sunspot number (SSN). Also indicated are the correlation coefficients between the five solar modulated parameters before removal of the solar cycle (above the diagonal, bold face), after removal of the solar cycle (below the diagonal, normal type), and between each solar modulated parameter before and after removal of the solar cycle (diagonal, italics).
Note that SW and in particular HPI, display the weakest correlation with both SSN and the other parameters.

	TSI	UV	EUV	SW	HPI	GCR	SSN
TSI	*0.70*	**0.80**	**0.79**	**0.31**	**0.09**	**-0.63**	**0.72**
UV	0.59	*0.30*	**0.98**	**0.48**	**0.17**	**-0.79**	**0.77**
EUV	0.50	0.77	*0.27*	**0.50**	**0.19**	**-0.85**	**0.96**
SW	-0.02	-0.06	0.07	*0.87*	**0.59**	**-0.54**	**0.46**
HPI	-0.03	0.04	0.14	0.60	*0.99*	**-0.44**	**0.15**
GCR	-0.21	-0.44	-0.42	-0.29	-0.53	*0.61*	**-0.79**

Table 6: Correlation coefficients between the solar modulated forcing parameters. Above the diagonal (bold face) is given the correlations for the observed parameters. Below the diagonal (normal type) the same coefficients after removal of linear trend and the solar cycle from the parameters are shown. The diagonal shows the correlations for each parameter before and after removal of the solar cycle and linear trend.

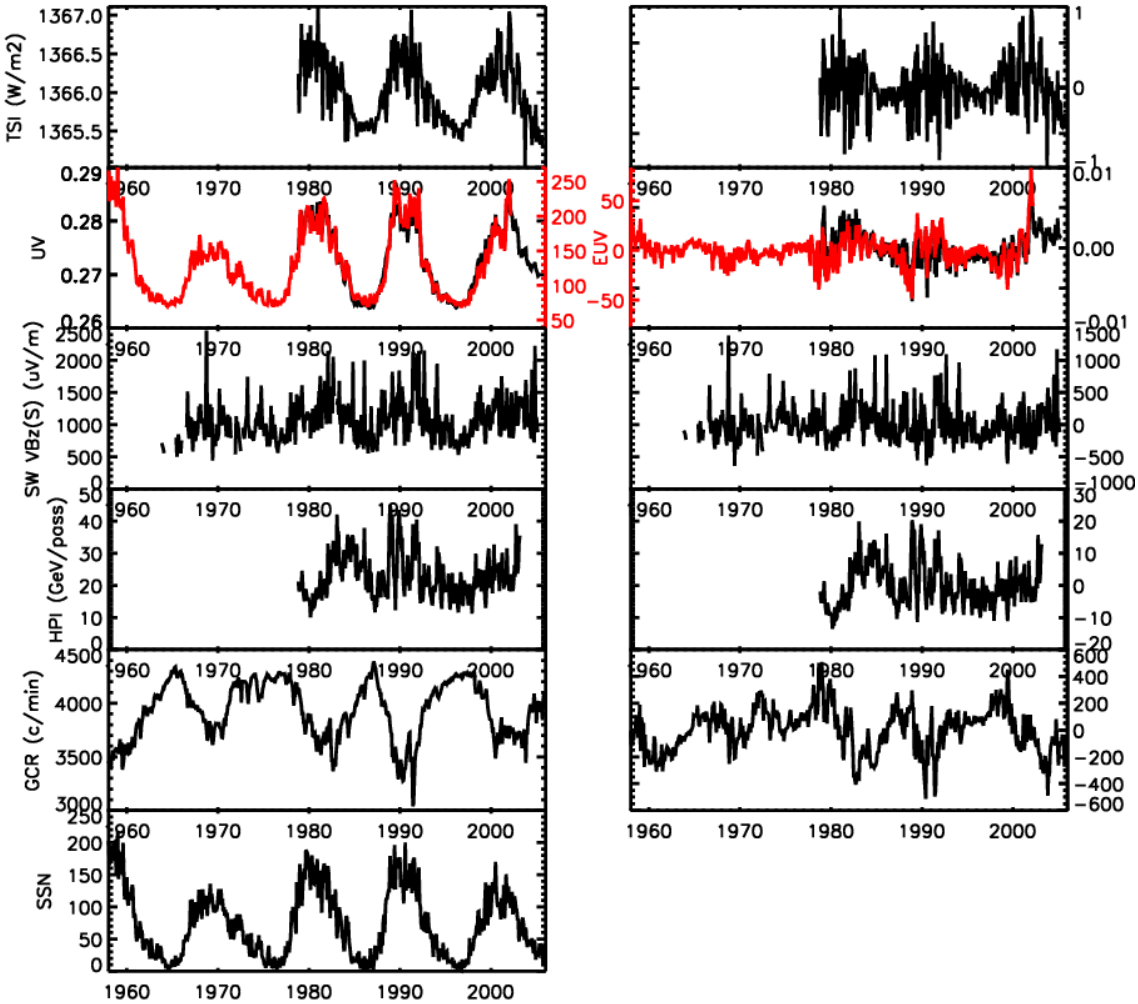

Figure 28: The five Solar Modulated Forcing Parameters over the periods where data is available. From the top a) total solar irradiance (TSI), b) solar ultraviolet radiation (UV) and the 10.7 cm proxy for extreme ultraviolet proxy (EUV - red), c) the solar wind (SW) v_swBz component for southward IMF, d), the total hemispheric power input from precipitating particles (HPI) and e) Galactic cosmic rays from the Climax station (GCR). The lowest panel (f) shows the solar activity cycle as represented by the sunspot number (SSN). To the right is shown the same parameters after removal of mean, linear trend and the solar cycle.

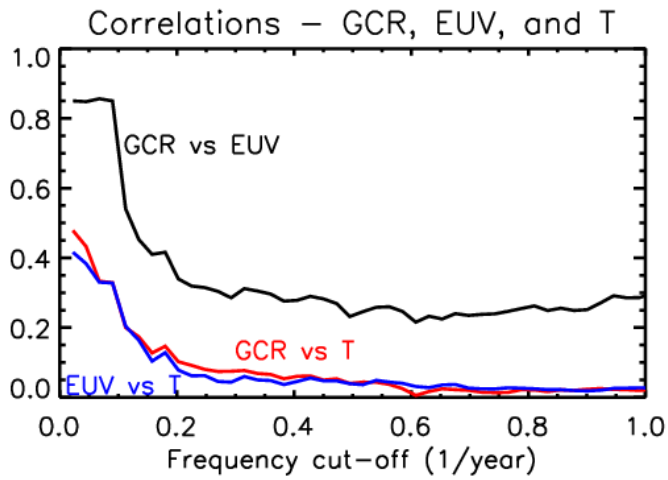

Figure 29: Correlations between GCR, EUV and Tropospheric temperature vs. cut-off frequency. The correlation between GCR and EUV drops off sharply at 1/(11 years) to a constant level after 2/(11 years).

Another important consideration is the effect of internal climate variability at decadal time scales and the impact from volcanoes. Since these processes can have a strong impact on many climate parameters in the troposphere and at the surface, they could mask, or artificially enhance, a possible solar cycle signal with an average length around 11 years. To reduce this problem, temporal indices describing the variability from El Nino Southern Oscillation (ENSO), North Atlantic Oscillation (NAO) and Volcanic Stratospheric Aerosol have also been included in the multiple regression analysis.

The multi-regression procedure inherently assumes that the observations are linearly dependent on the 3 internal climate modes and solar modulated parameters, and that the indices themselves are independent, i.e., orthogonal. Table 7 reports the correlations between each of the indices, none of which are significantly different from the null hypothesis of no correlation, thus confirming the assumption of linear independence for monthly averages during the period 1963-2005. However, the validity of assuming a linear response is not so clear. It is well known that the nature of the climate response to El Nino was quite different during the major event of 1983 to that of 1998; this lack of stationarity needs to be borne in mind when interpreting the results. It is also possible that sensitivity to solar variability may depend on the current internal state of the climate system. A solar modulated mechanism may only be active during certain periods of the observations investigated. An attempt to address this problem is partially explored in the section comparing the solar induced response of tropospheric temperatures under solar min and solar max conditions.

	NAO	Volc.	TSI	UV	EUV	SW	HPI	GCR	SSN
Nino3	0.00	0.22	-0.05	-0.13	0.01	0.05	-0.08	-0.02	0.00
NAO		0.09	0.16	0.10	0.09	0.05	0.09	-0.05	0.09
Volc.			0.06	0.02	-0.08	0.15	0.22	-0.02	-0.09

Table 7: Correlation coefficients between solar modulated forcing parameters and the internal modes of variability.

When estimating the significance of any statistical quantity, it is important to take into account any serial- (or auto-) correlations that might be present. This is especially the case when dealing with climate data where persistence is a strong feature. In the present work significance of the correlation coefficient is found by using the so called random phase test (Ebisuzaki, 1997). This requires that the probability of obtaining a correlation coefficient, r, between a specific climate parameter and solar modulated parameter by chance is found from an ensemble of Monte Carlo simulations. Each member of the ensemble consists of an artificial time series. These are generated by Fourier transforming the time series of the climate parameter in question, randomizing the phases, and then Fourier transforming back to generate a random time series which possesses the same power spectrum as the original climate parameter time series. For each random time series the correlation coefficient with the solar modulated parameters is found. This is repeated 10000 times for each ensemble, generating a probability distribution from which the significance of the original correlation coefficient can be estimated. Estimating significance by randomizing the Fourier phases in this manner is the strictest test available which accounts for any auto-correlations that are present.

4.2 Tropospheric Response

The troposphere is the inner layer of the atmosphere defined by a steady decrease of temperature with increasing altitude. Nearly all clouds and most weather phenomena felt at the surface are created in this region. In the correlation study we analysed temperature, vertical circulation, low clouds, ozone, and aerosols. Here we extract the results for temperature and low clouds. In the Summary we include results for all the parameters.

Temperature

Reliable measurements of atmospheric temperatures at other levels than ground have been collected from balloon radiosonde measurements since 1958, beginning with observations from a few stations reaching thousands of stations at the present time. The Hadley Centre of Climate Prediction and Research has compiled the radiosonde temperature measurements into a gridded data set from 1958 to present. The data are available as monthly temperature anomalies at 9 pressure levels [850, 700, 500, 300, 200, 150, 100, 50, 30hPa] on a 5-degree latitude and 10-degree longitude grid. For the analysis in this section the internal modes of variability have been subtracted from the temperature data by multi-linear-regression and the temperature data been recomputed as latitude zones containing monthly means of the anomalies

Global averages

The global average of the temperature in the troposphere is here defined as the average of the lowest 4 levels from the balloon radiosonde measurements (850 hPa – 300 hPa). Below, in Figure 30, we show the correlation between global tropospheric temperature anomalies and EUV radiation and galactic cosmic rays. In the top panels are shown the raw data giving correlations of 0.33 with EUV and –0.31 with GCR. In the temperature the effect of particularly the El Niño is clearly seen. In the middle panels the internal climate modulators, NINO3, NAO, and VAI have been removed from the temperature together with a linear trend by linear regression. A linear trend has also been removed from the GCR and EUV curves. The correlation coefficient grows somewhat to 0.42 and –0.47. The improved correlation is clearly seen by visual inspection. However, since all the external parameters are strongly modulated by the solar cycle, it is not at all obvious how to distinguish coincidental correlation from actual physical influence. In the bottom panel we have therefore removed the solar cycle, represented by the monthly sunspot number, from both the temperature and the external parameters. The correlation drops significantly, most dramatically for the EUV-temperature correlation. In Table 8 we give the correlations for all 5 external parameter for raw data, with NINO3, NAO, VAI, and a linear trend removed, and with the solar cycle removed. The numbers in parentheses are the same correlation coefficients but after a 3 months box average has been applied. Particularly, TSI, EUV, and GCR show strong correlations. However, these correlations drop significantly after removal of the solar cycle. Only the GCR correlation survives to some extent.

One must bear in mind that the correlations for the various parameters are not calculated over the same time period. TSI and HPI are only available from November 1978. In Table 9 we show the correlations if we limit the analysis for all the parameters to this

period. The correlations for UV, SW, GCR, and SSN drop. In fact, only the correlations for UV and SSN are above the 95% significance level after removal of the internal modes of variability. After removal of the solar cycle none of the parameters show any correlation.

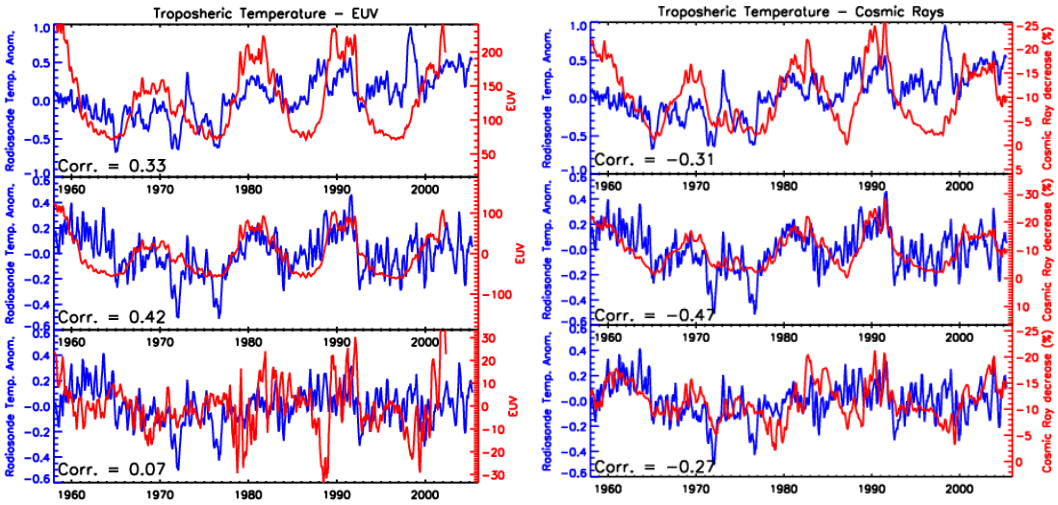

Figure 30: Left) correlation between 10.7 cm EUV proxy and global mean temperature anomalies for the troposphere. Top panel: observations. Middle panel: after removal of nino3, NAO, volcanic aerosols, and a linear trend. Bottom: after removal of the solar cycle. Right) the same for galactic cosmic rays.

	TSI	EUV	SW	HPI	GCR	SSN
Observ.	0.13 (0.16)	**0.33 (0.35)**	**0.20 (0.31)**	-0.08 (-0.07)	**-0.31 (-0.33)**	**0.25 (0.27)**
Niño, etc.	0.31 **(0.44)**	***0.42 (0.50)***	0.19 **(0.35)**	0.07 (0.14)	***-0.47 (-0.57)***	***0.40 (0.48)***
Solar cycle	0.05 (0.00)	0.07 (0.07)	-0.02 (0.02)	-0.01 (0.03)	**-0.27 (-0.33)**	

Table 8: the correlations coefficients for the 5 external parameters with tropospheric temperature. Given are the correlations for raw observation, after removal of the internal climate parameters, and after removal of the solar cycle. Numbers in bold face are above the 95% significance level. Numbers in bold italics are above the 99% significance level.

	TSI	UV	SW	HPI	GCR	SSN
Observ.	0.13 (0.16)	0.18 (0.21)	0.06 (0.08)	-0.08 (-0.07)	-0.16 (-0.18)	0.12 (0.14)
Niño, etc.	0.31 (0.44)	**0.39 (0.50)**	-0.13 (-0.23)	0.07 (0.14)	-0.22 (-0.27)	***0.42 (0.54)***
Solar cycle	0.05 (0.00)	0.04 (0.03)	-0.06 (-0.06)	-0.02 (0.03)	-0.05 (-0.04)	

Table 9: same as Table 8, but limited to the period November 1978-present.

Zonal averages

The various external parameters may influence different parts of the globe differently, both geographically and at different altitudes. Below we analyse the correlations with zonal averages of temperature anomalies given by balloon radiosonde measurements at nine different altitude levels (850 hPa – 30 hPa).

In Figure 31 we illustrate the analysis for the GCR parameter. For the raw observations (top, left) a clear correlation is seen in the troposphere, particularly strong in the tropical region, but without much signal in the stratosphere. After removal of the internal climate

parameters (top right) the region of strong correlation extends into the stratosphere. However, after removal of the solar cycle (bottom, left) most of the correlations disappear. The correlation with the solar cycle (bottom, right) displays very much the same pattern as the GCR correlation before removal of the solar cycle. The zonal correlations with GCR are made for the full time period 1958-present. Limiting the analysis period to 1978-present will reduce the correlations corresponding to what is seen in Table 9.

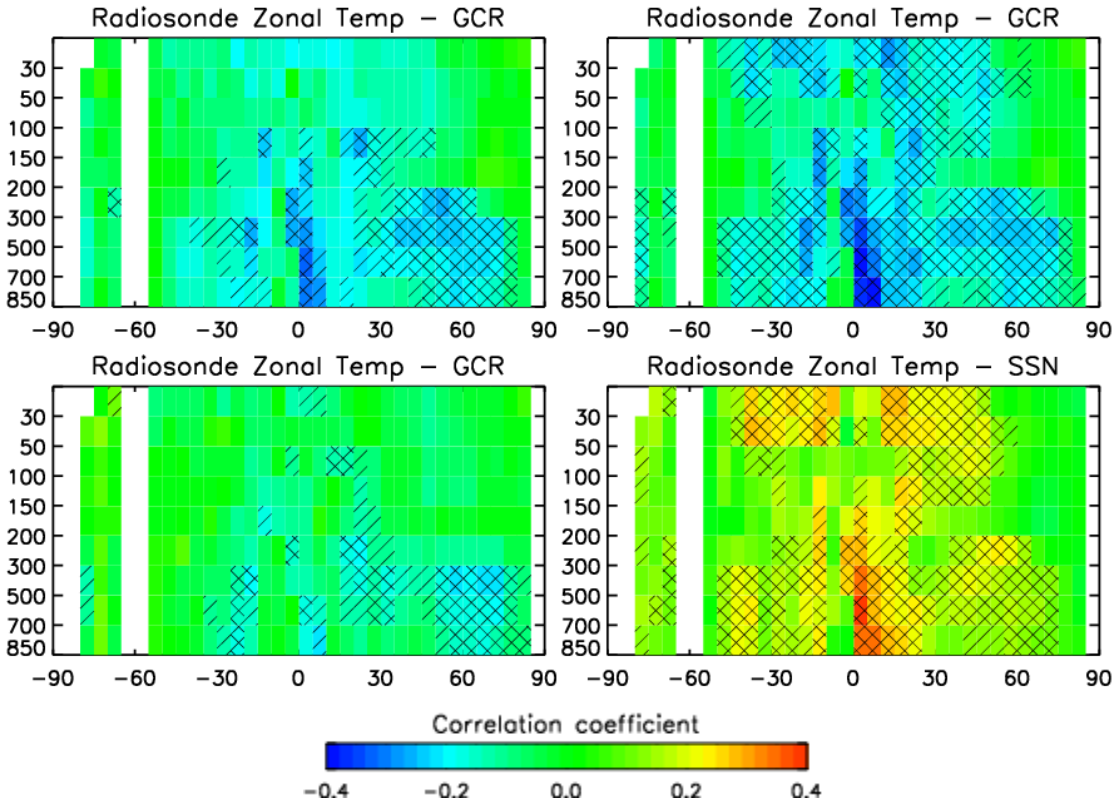

Figure 31: zonal correlations between GCR and radiosonde temperatures. Top left: raw observations. Top right: after removal of nino3, NAO, VAI, and linear trend by linear regression. Bottom left: after removal of the solar cycle. Bottom right: zonal correlation between sunspot number and radiosonde temperatures. Hatched areas have correlations above the 90% significance level, cross hatched above 95%.

Figure 32 shows the zonal temperature correlations with the external parameters after removal of the solar parameters. None of the parameters displays correlations comparable to those between temperature and sunspot number, though GCR and EUV do show some areas with significant correlations.

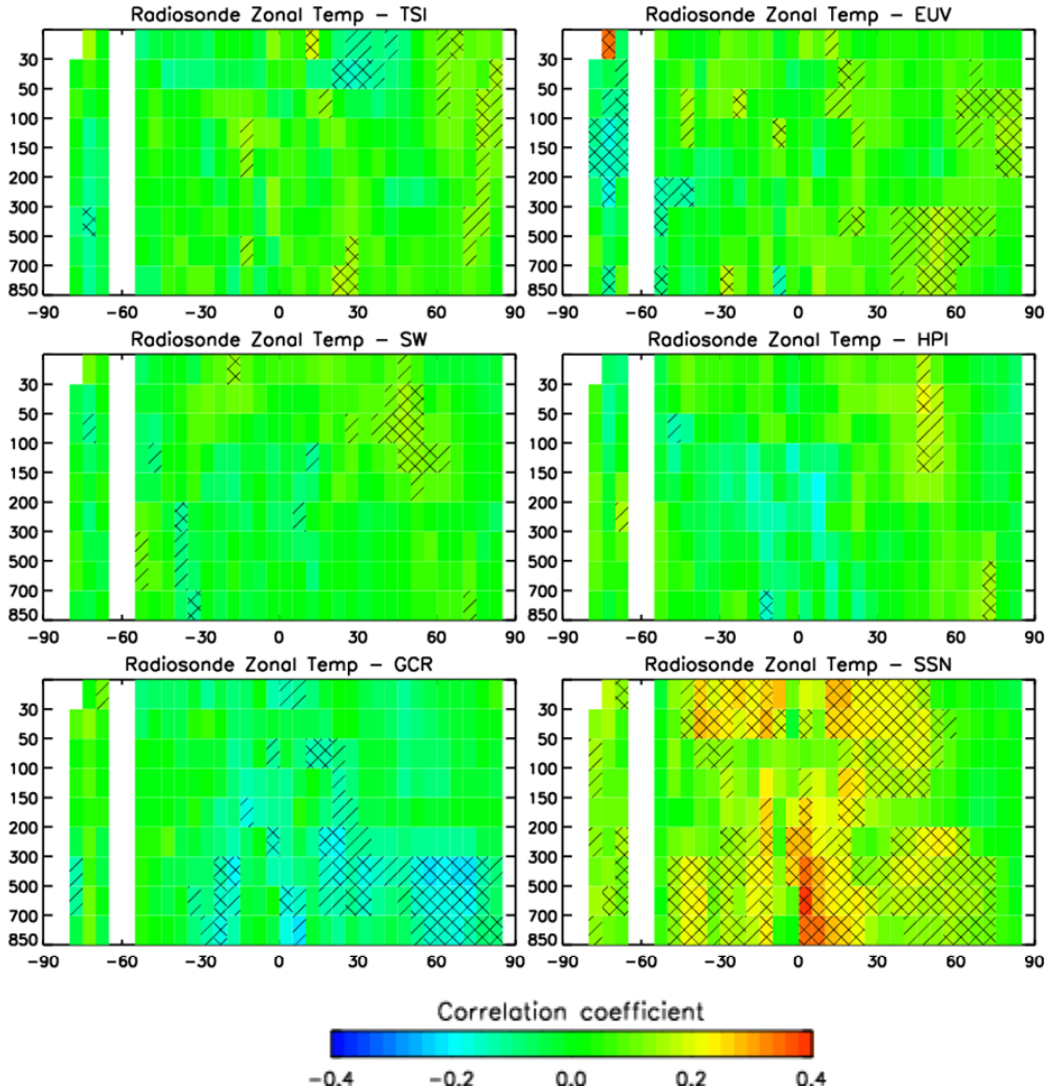

Figure 32: zonal correlations between the 5 external parameters plus the sunspot number and radiosonde temperature anomalies. The correlations are calculated after removal of the solar cycle. From top TSI and EUV, SW and HPI, GCR and SSN. Hatched areas have correlations coefficients above the 90% significance level, cross hatched above 95%.

MSU temperatures

Since the radiosonde temperature data are only collected over land, we use the MSU satellite measurements of temperature to show the geographical distribution of correlations between tropospheric temperatures and the solar modulated forcing parameter (Figure 33). Most notably, UV displays a band of positive correlation in the tropics, and HPI a band of negative correlations in the same region. GCR displays some negative correlations in the temperate and polar zones, while SSN various patches of mainly positive correlations. It should be noted that the MSU measurements only cover the period 1978-present.

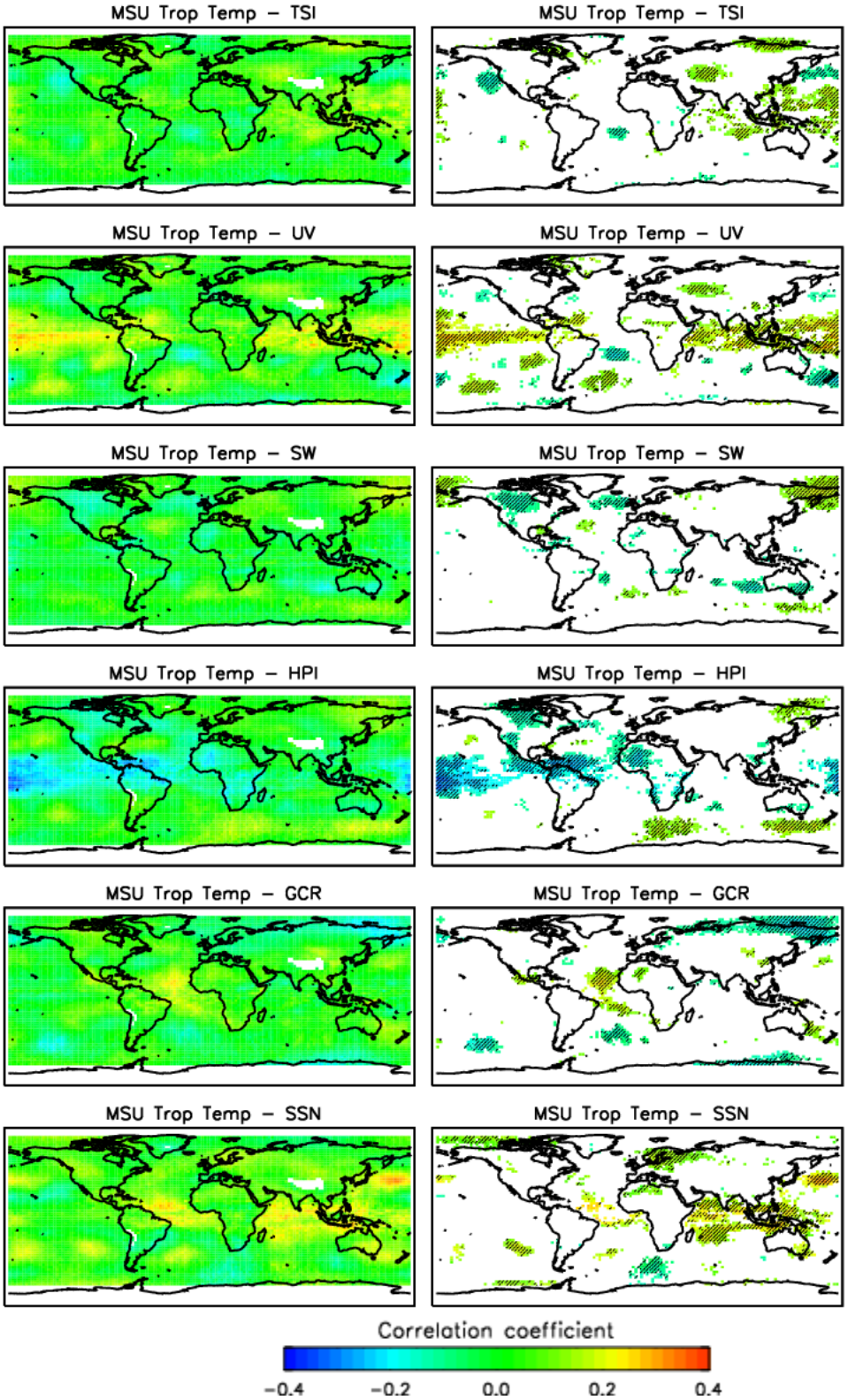

Figure 33: correlations between the 5 external parameters plus the sunspot number and tropospheric temperatures measured from satellite. The correlations are given after the removal of the internal parameters and the solar activity. To the right are shown only the areas with correlations coefficients above the 90% significance level, hatched areas are above 95% significance.

Solar max/min

The previous section describes how the solar parameters are correlated with tropospheric temperatures over the past 45 years. In this section the correlation between the Hadley radiosonde temperatures and the 5 solar modulated parameters are investigated during periods of solar minimum and solar maximum. The aim is to analyze the short term fluctuations and identify any differences in the correlation properties over these respective periods:
Solar Max: 1966-1973, 1978-1983, 1988-1993, 1998-2002
Solar min: 1963-1966, 1973-1978, 1983-1988, 1993-1998

Figures 34-38 show the correlations during solar max and min periods for the 5 solar parameters with HADAT zonal anomalies covering three different time periods: 1963-1978, 1978-2002 and 1963-2002 (where available).

GCR: Over equatorial regions during the solar max of 1968-1971 a negative correlation is found in the troposphere up until 150 hPa, which switches to a positive correlation above 150 hPa in the stratosphere. There is little or no significant correlation outside of 30º in either hemisphere. From 1978 onwards a significant correlation pattern is found in the troposphere which is negative under solar max conditions and positive under solar min conditions. This correlation pattern persists throughout the whole period of available observations, and is largely restricted to ±30º latitude up until 100 hPa. Under solar max conditions there is an additional significant negative correlation around 60ºN near the surface. The change in sign of the correlation between solar min and solar appears to be robust. However, it is an unusual feature since it suggests that if the temperatures are really responding to GCR then the nature of the response can be quite different during different phases of the solar cycle.

UV: The patterns are less clear here than for GCR. Prior to 1978 under solar max conditions there are a few areas of both positive and negative correlation in the northern hemisphere. During solar min conditions there is little correlation. From 1978 onwards a similar correlation pattern to that seen with GCR, although much weaker and with a reverse in sign, is found in the troposphere under solar max/min conditions.

SW: Little significant correlation is found under solar max conditions. There is a negative signal in the mid-upper troposphere between the years 1978-2002, but this disappears when including all periods under solar max conditions from 1968-2002. Solar min conditions show a significant negative correlation for the period 1978-2002 in the upper troposphere/stratosphere around 60ºS. However, when both periods are combined virtually all significant correlations disappear.

TSI: In this period the correlation signal under solar min conditions is fairly weak, with the strongest significant correlation in the upper troposphere at high latitudes in the northern hemisphere. During solar max there is a significant band of a weak positive correlation throughout the troposphere mostly around equatorial regions but also at higher latitudes.

HPI: During solar max conditions some significant positive correlation appears in the stratosphere between 30ºS-30ºN and little elsewhere. However, under solar min conditions there is a significant negative signal throughout the troposphere around the equator.

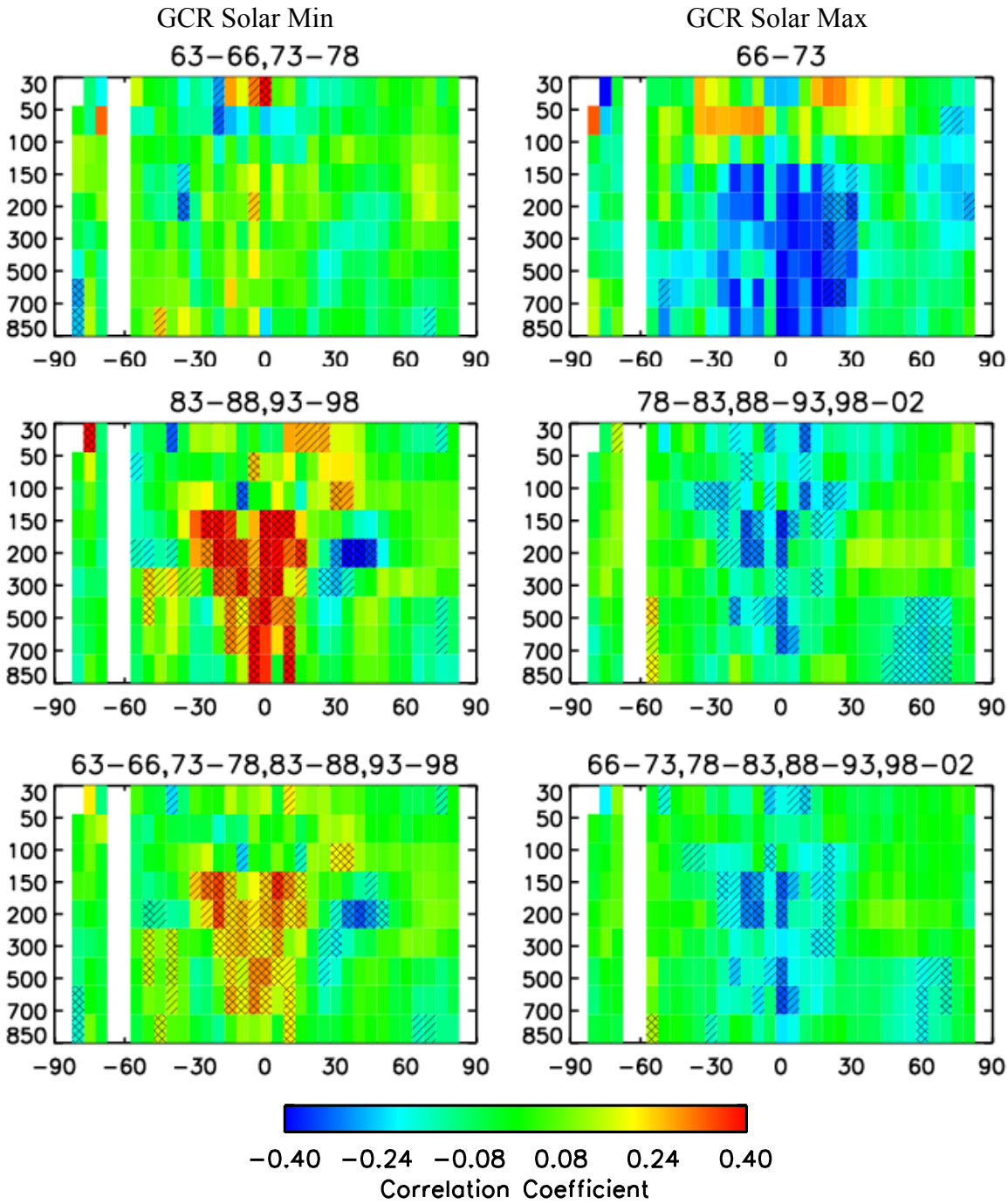

Figure 34: Plot of correlation coefficients of GCR signal with Hadley zonal anomalies. 3 different time periods are shown. Correlations with significances higher than 0.9 and 0.95 are hatched and cross hatched, respectively.

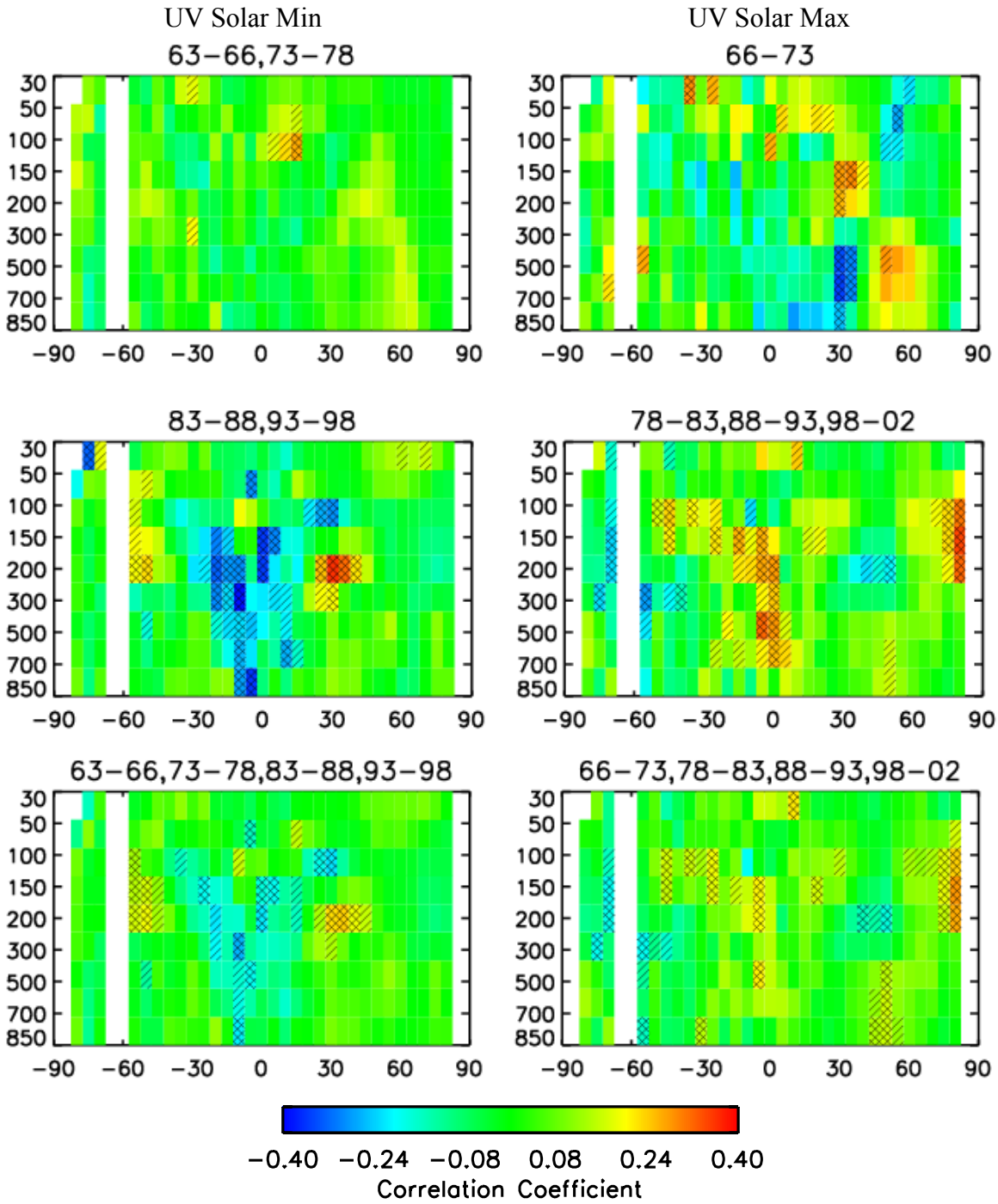

Figure 35: Plot of correlation coefficients of UV signal with Hadley zonal anomalies. 3 different time periods are shown. Correlations with significances higher than 0.9 and 0.95 are hatched and cross hatched, respectively

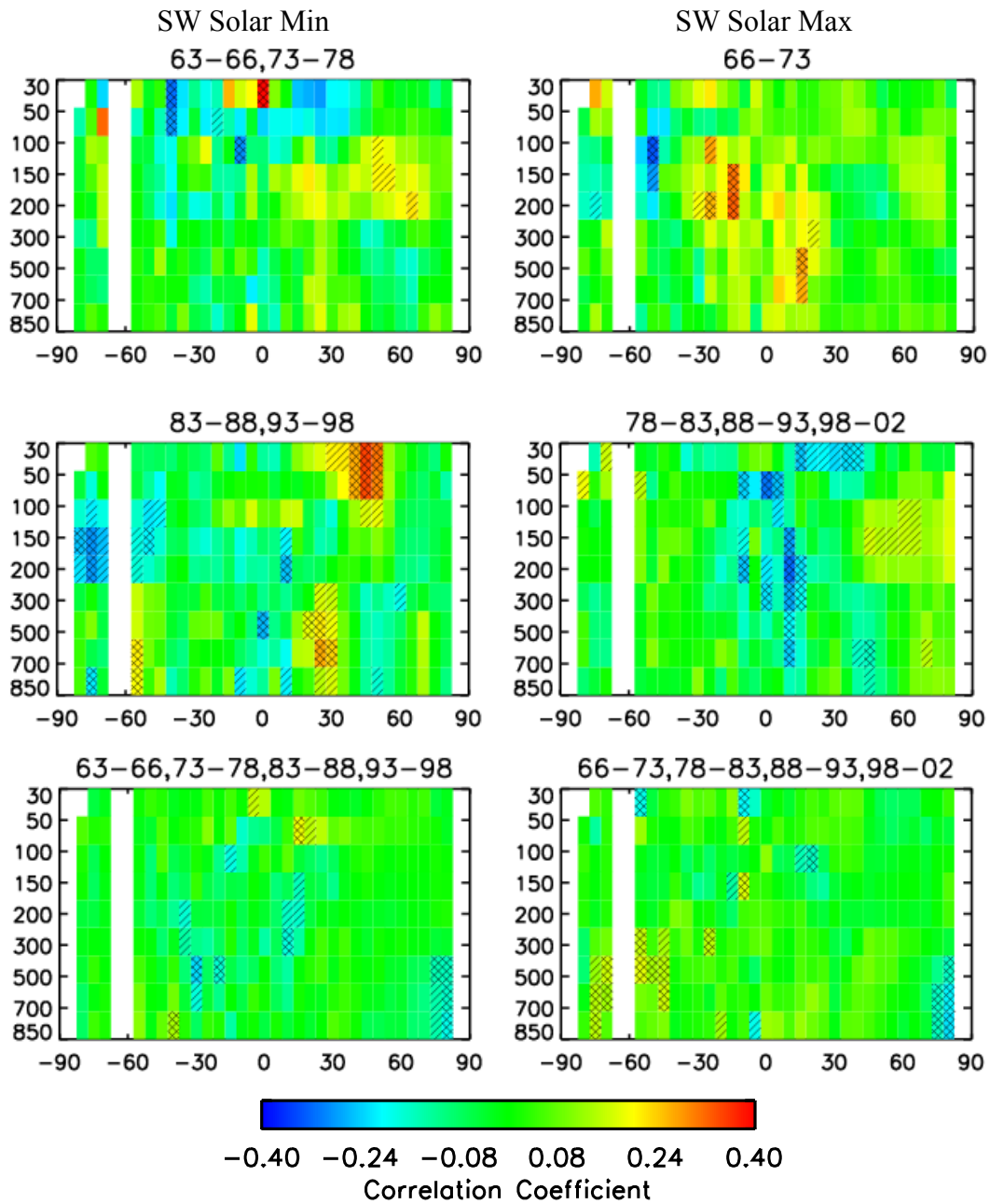

Figure 36: Plot of correlation coefficients of SW signal with Hadley zonal anomalies from 1978-2002. Correlations with significances higher than 0.9 and 0.95 are hatched and cross hatched, respectively

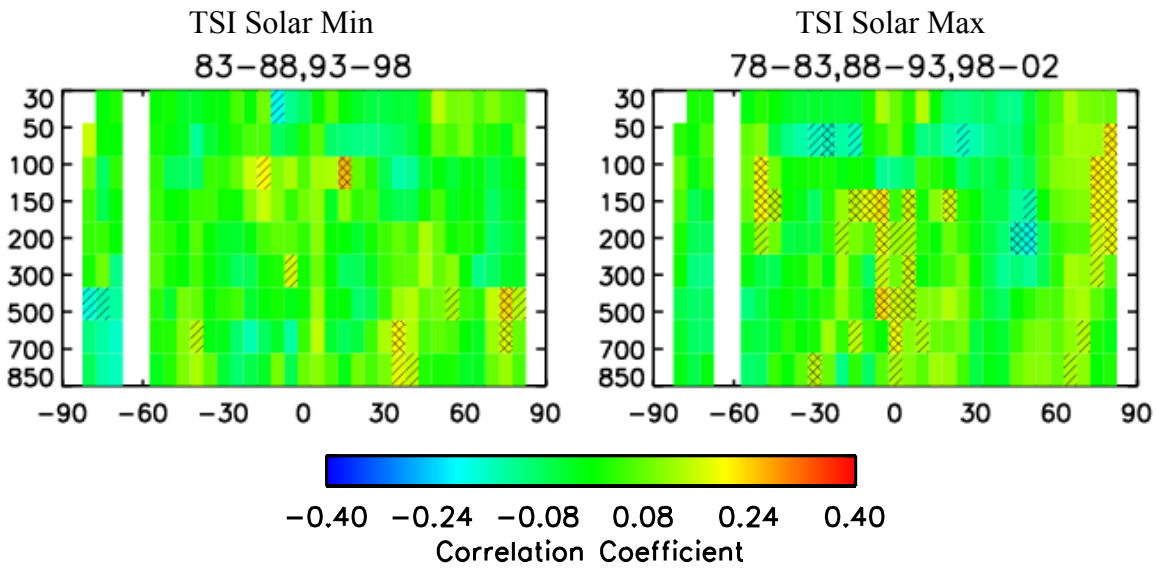

Figure 37: Plot of correlation coefficients of HPI signal with Hadley zonal anomalies from 1978-2002. Correlations with significances higher than 0.9 and 0.95 are hatched and cross hatched, respectively

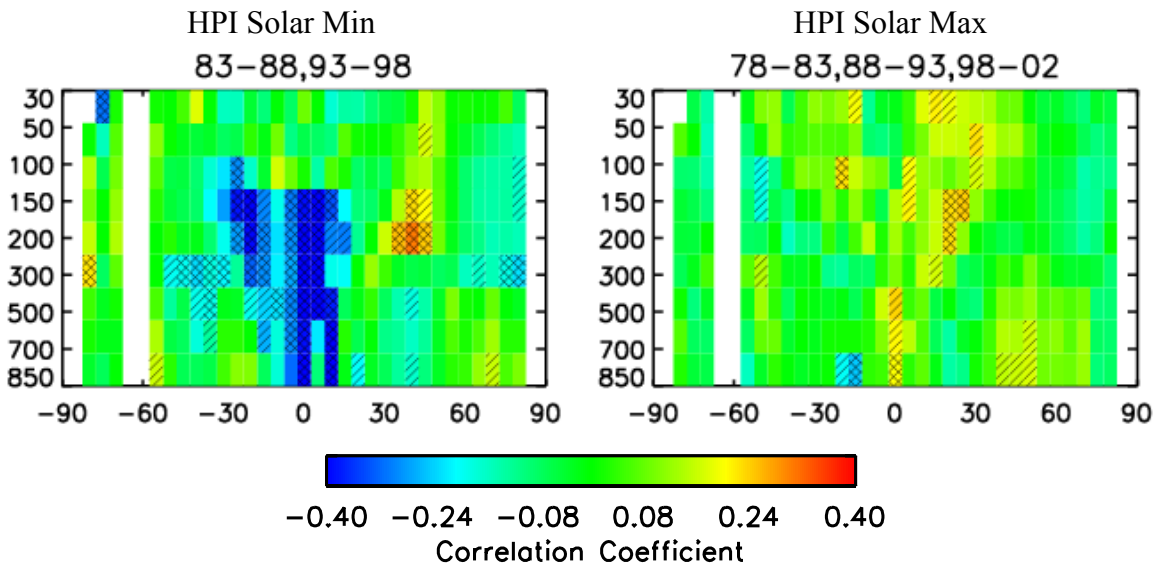

Figure 38: Plot of correlation coefficients of HPI signal with Hadley zonal anomalies from 1978-2002. Correlations with significances higher than 0.9 and 0.95 are hatched and cross hatched, respectively

Low clouds

Low clouds are taken from the ISCCP cloud data sets which have recently been updated to provide a systematic view of global cloud behaviour over the period July 1983 – December 2005. ISCCP initially divides the clouds into three types based on altitude, low, middle, or high, using either infrared or a combination of infrared and visual observations. The analysis here is restricted to low clouds derived from infrared observations only.

Previous work has suggested that a problem with the continuous calibration exists at the end of 1994 and beginning of 1995. The problem is most easily noticed in the high cloud cover as demonstrated in Figure 39. A clear drop of more than 1% in global high cloud coverage is seen at the end of 1994. At the end of 2001 the high cloud coverage comes back up to the level pre-1995. Comparison with an independent data set of low cloud provided by the SSM/I microwave instrument aboard the DMSP satellites suggest that there is an offset between these two data sets. Following the procedure of Marsh and Svensmark (2003) the ISCCP low cloud data has been adjusted to account for this offset at every grid point after 1994. Below the analysis from both the original and adjusted data is presented.

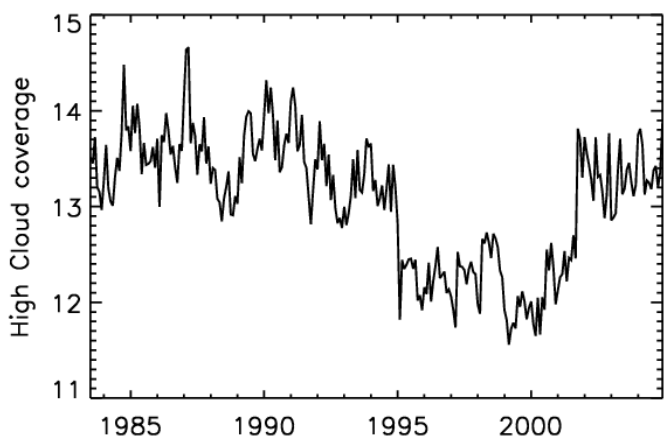

Figure 39: Global high cloud coverage with annual cycle removed.

	TSI	UV	SW	HPI	GCR	SSN
Observ.	-0.40(-0.46)	**-0.58(-0.62)**	-0.24(-0.37)	-0.08(-0.11)	0.40(0.43)	-0.36(-0.40)
Niño, etc.	**-0.41(-0.50)**	***-0.50(-0.57)***	-0.24**(-0.42)**	**-0.31(-0.43)**	***0.52(0.61)***	-0.42(-0.50)
Solar cycle	**-0.21**(-0.24)	***-0.50(-0.60)***	-0.07(-0.17)	-0.18(-0.27)	**0.35(0.41)**	

Table 10: the correlations coefficients for the 5 external parameters and the sunspot number with low cloud coverage. Given are the correlations for raw observation, after removal of the internal mode of variability, and after removal of the solar cycle. Numbers in bold face are above the 95% significance level, numbers in bold italics above the 99% significance level.

	TSI	UV	SW	HPI	GCR	SSN
Observ.	**-0.54(-0.67)**	**-0.61(-0.71)**	**-0.34*(-0.57)***	-0.30**(-0.40)**	**0.62(0.72)**	-0.57(-0.68)
Niño, etc.	-0.49**(-0.63)**	**-0.57(-0.68)**	-0.27**(-0.49)**	-0.28**(-0.39)**	***0.59(0.71)***	**-0.54(-0.67)**
Solar cycle	**-0.23**(-0.26)	***-0.41(-0.47)***	-0.03(-0.13)	-0.10(-0.17)	***0.32*(0.39)**	

Table 11: same as Table 10, but after adjustment with the SSM/I DMSP cloud data.

Tables 10 and 11 report the correlation coefficients between all 5 solar modulated parameters and low clouds (original and adjusted respectively). A key feature is that the strongest significant correlations are found with UV and GCR, both with and without the inclusion of the solar cycle. For the original observed data in Table 10 UV displays the strongest correlation, however, after filtering out internal climate modes GCR becomes slightly stronger. For the adjusted data in Table 11 correlation coefficients with GCR are actually slightly stronger than UV for both the observed and filtered data. The strong correlation with SSN indicates that a large fraction of these strong correlations are due to the solar cycle, however, a significant correlation still exists in UV and GCR once the solar cycle is removed. This displays the most consistent feature since both in the original and adjusted data it is the UV that possesses the strongest significant correlation.

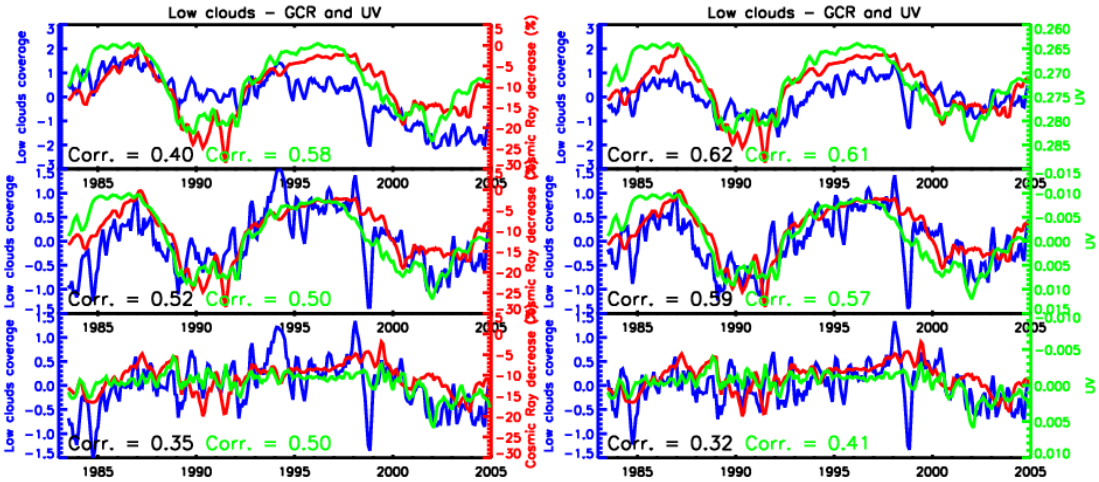

Figure 40: Correlation between GCR (red) and UV (green) and coverage of low clouds (blue). Left: ISCCP data for coverage of low altitude clouds. From top: annual cycle removed, trend and internal modes removed, solar cycle removed. Right: same as left, but after adjustment with the SSM/I DMSP cloud data.

Figure 40 shows a plot of UV (green) and GCR (red) together with the original (left) and adjusted (right) globally averaged low cloud data (blue). The correlation over nearly two and a half solar cycles is quite striking, particularly once the internal climate modes have been filtered out. The spatial distribution of correlation coefficients once the solar cycle has been removed (Figure 41) indicate that the strongest significant correlations are found at mid to high latitudes for both UV (negative) and GCR (positive). However, there also exist regions of positive (UV) and negative (GCR) correlation around the equator, particularly for GCR, which are washed out when taking the global average

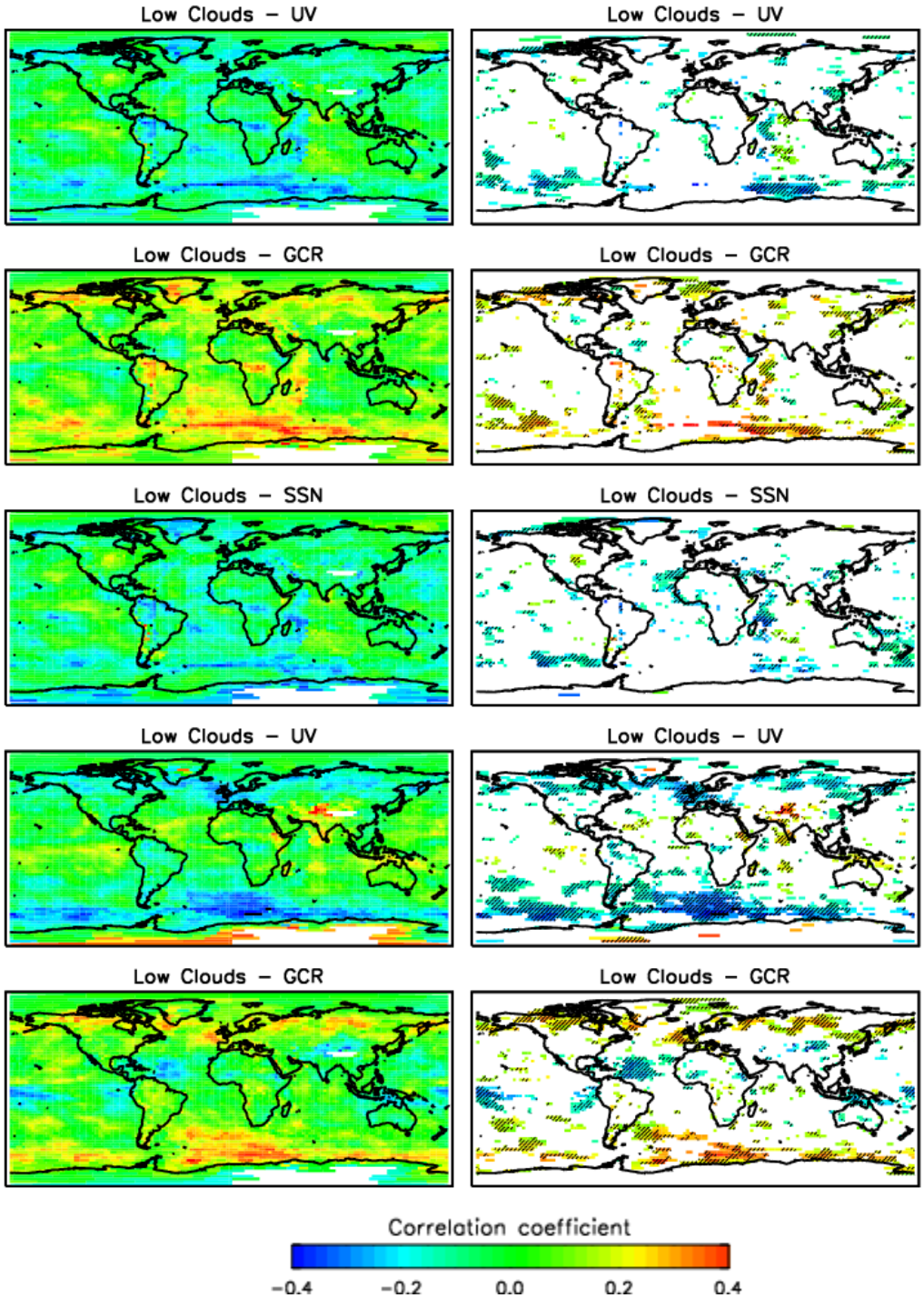

Figure 41: correlations between the UV and GCR plus the sunspot number and coverage of low clouds. The top two rows show the correlations with UV and GCR before the solar cycle is removed; third row shows the correlation with sunspot number; two bottom rows show the UV and GCR correlations after the solar cycle is removed. Some strong contrasts, for example in the Indian Ocean east of Africa are the effect of the foot point of the observing geo-stationary satellites. To the right are shown only the areas with correlations above the 90% significance level, hatched areas are above 95% significance.

4.3 Surface Response

The surface response to the solar parameters is investigated in this section. Focus is on how vegetation, snow, precipitation and surface pressure and temperature correlate with the solar parameters. Time series for selected areas are also shown.

Vegetation

NDVI is calculated from the visible (VIS) and near-infrared (NIR) light reflected by vegetation and expressed by: (NIR - VIS)/(NIR + VIS). Chlorophyll in healthy vegetation absorbs most of the visible light (for use in photosynthesis) and reflects a large portion of the near-infrared light. The NDVI value for healthy vegetation is thus close to 1. Unhealthy or sparse vegetation reflects more visible light and less near-infrared light and has a NDVI value closer to zero.

The NDVI index used in the analysis is computed from band measurements from the NOAA AVHR instrument. The data set is available from July 1981 to September 1994.
In Figure 43 we show the correlations between NDVI and the solar modulated forcing parameters. Only the correlations with more than 90% significance are shown. Basically very little is seen, except for a relatively strong correlation over central Europe for almost all the solar parameters. Due to the short period of availability of the NDVI index (1981-1994) the removal of the solar cycle does not make a large difference for this parameter. In Figure 42 we show the correlation between NDVI and UV and GCR over central Europe before and after removal of the solar cycle.

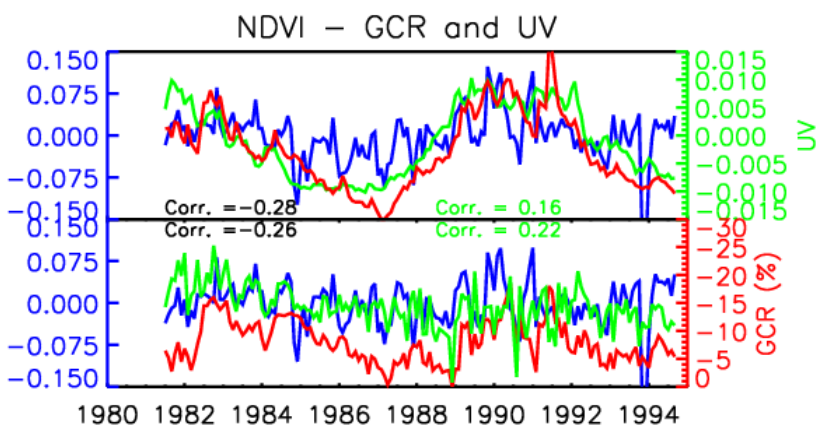

Figure 42: Correlation between NDVI and GCR and UV in central Europe (40-60° N, 0-50° E), before removal of the solar cycle (top) and after (bottom).

.

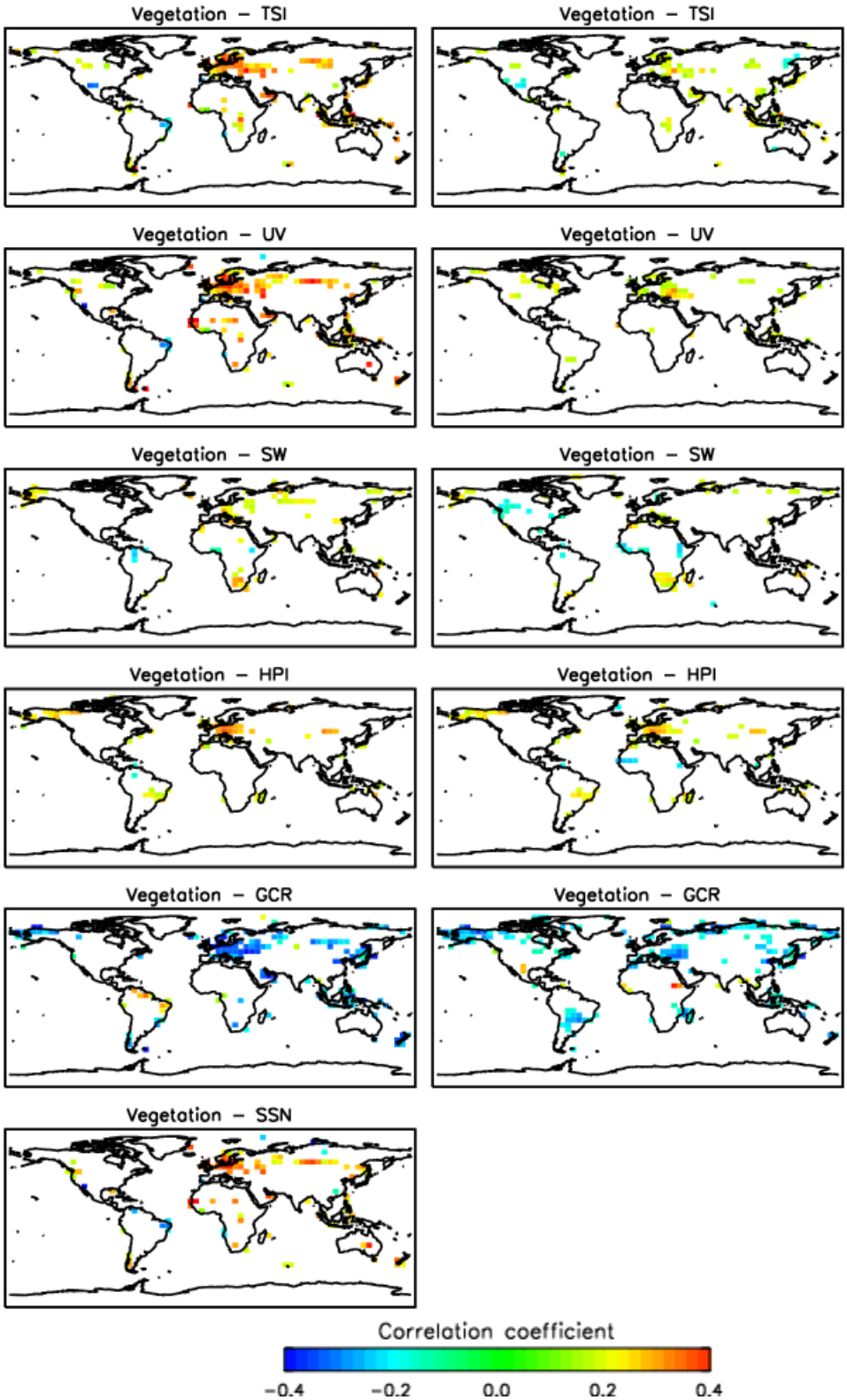

Figure 43: Correlations between the 5 external parameters plus the sunspot number and the normalized differenced vegetation index. The correlations are given after the removal of the internal parameters and linear trend (left column) and the solar activity (right column). Only the areas with correlation coefficients above the 90% significance level have been shown.

Snow

The snow data is monthly data from the Nimbus-7 SMMR Derived Global Snow Depth data set which is available from October 1978 – August 1987. The data is on a half-degree 720 by 360 lat/lon grid. Figure 46 shows the areas with correlations with significance above the 90% level. TSI seem to be somewhat negatively correlated and GCR somewhat positively correlated with snow depth. In Figure 44 we show the time series for snow depth for the areas with a significant positive GCR-correlation in North America together with the time series for GCR. Similarly, in Figure 45 we show the time series for snow depth for the areas with a significant negative TSI-correlation in Asia together with the time series for TSI.

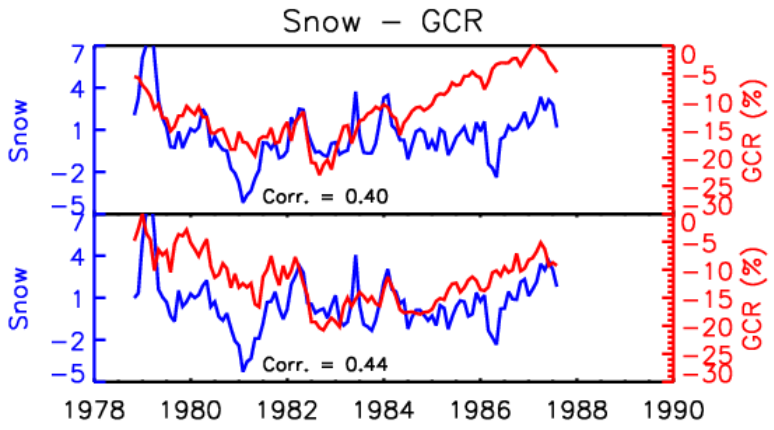

Figure 44: Correlation between snow depth and GCR in the areas of North America where the correlation is (significantly) positive (see Figure 46), before removal of the solar cycle (top) and after (bottom).

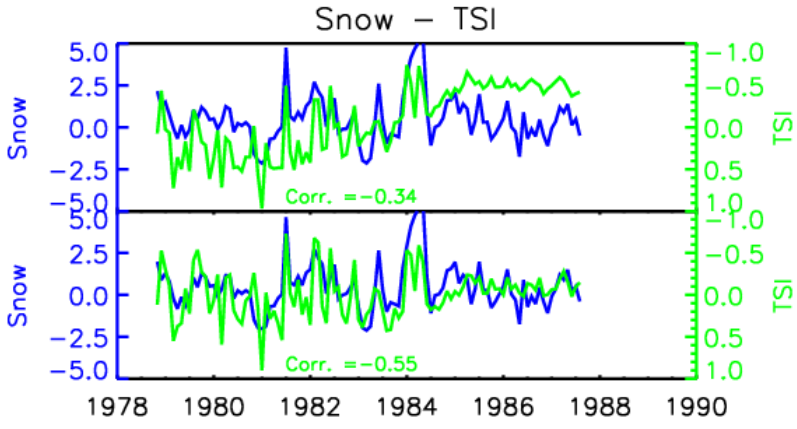

Figure 45: Correlation between snow depth and TSI in the areas of Asia where the correlation is (significantly) negative (see Figure 46), before removal of the solar cycle (top) and after (bottom).

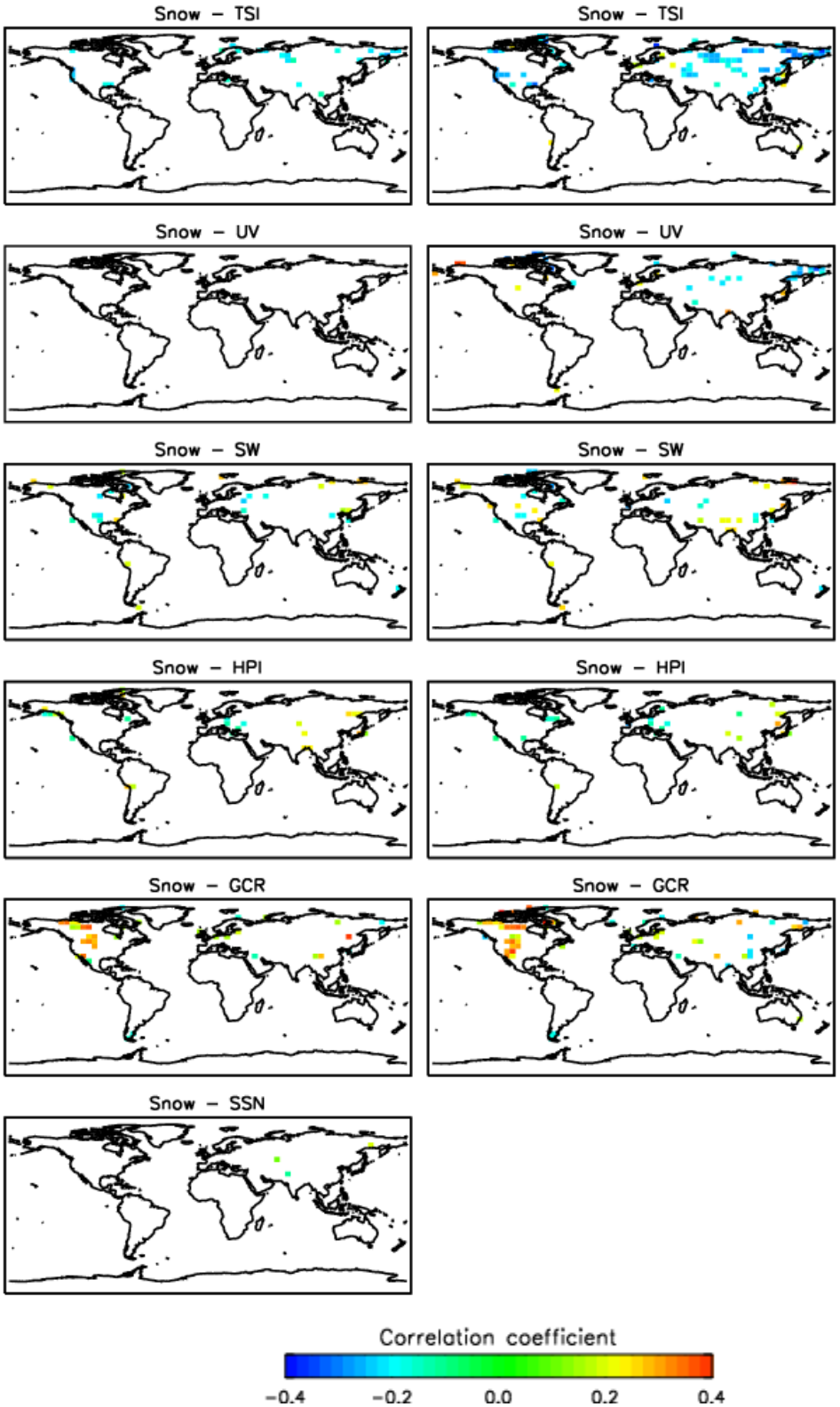

Figure 46: Correlations between the 5 external parameters plus the sunspot number and snow depth. The correlations are given after the removal of the internal parameters and linear trend (left column) and the solar activity (right column). Only areas with correlations above the 90% significance level have been plotted.

Sea Ice

The Sea Ice Extent is monthly data from the DMSP SSM/I instrument delivered by NCDC. The Sea Ice data are available from July 1987 – July 2005 on a 2.5° lat/lon grid. Figure 49 shows the areas with correlations with significance above the 90% level. GCR seems to be strongly correlated with sea ice close to the North Pole and close to Antarctica, as does sunspot number. However, as can be seen in Figures 47 and 48, where we show the mean sea ice cover on the northern and southern hemisphere as derived from the SSM/I data, the strong correlation arises from an anomalous drop in the sea ice extent around 1991. This drop of nearly 10% of the sea ice cover must be suspected to be due to erroneous data.

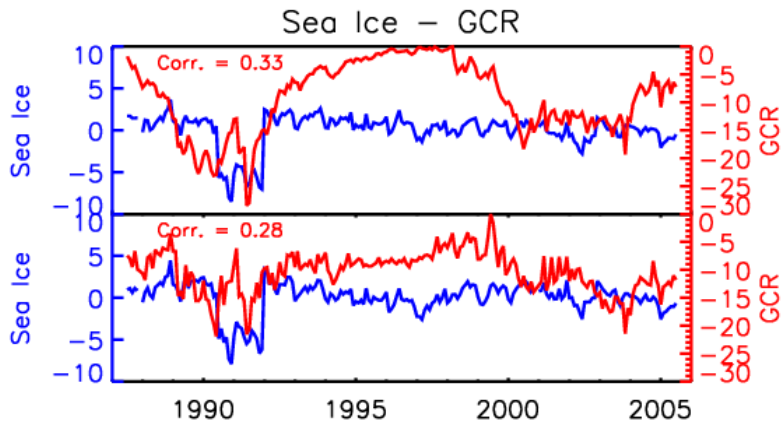

Figure 47: Sea Ice extent in the northern hemisphere above 45° after the removal of linear trend and internal modes of variability (top panel) and the solar cycle (bottom). The drop in sea ice cover around 1991 must be suspected to be due to erroneous data.

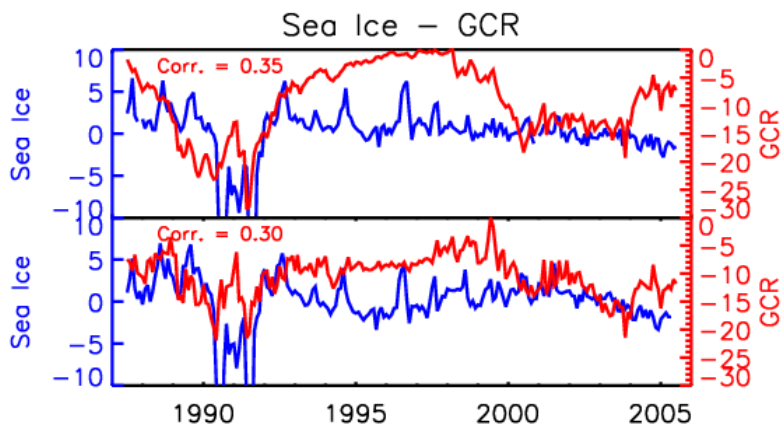

Figure 48: Equivalent to Figure 47, but for the southern hemisphere.

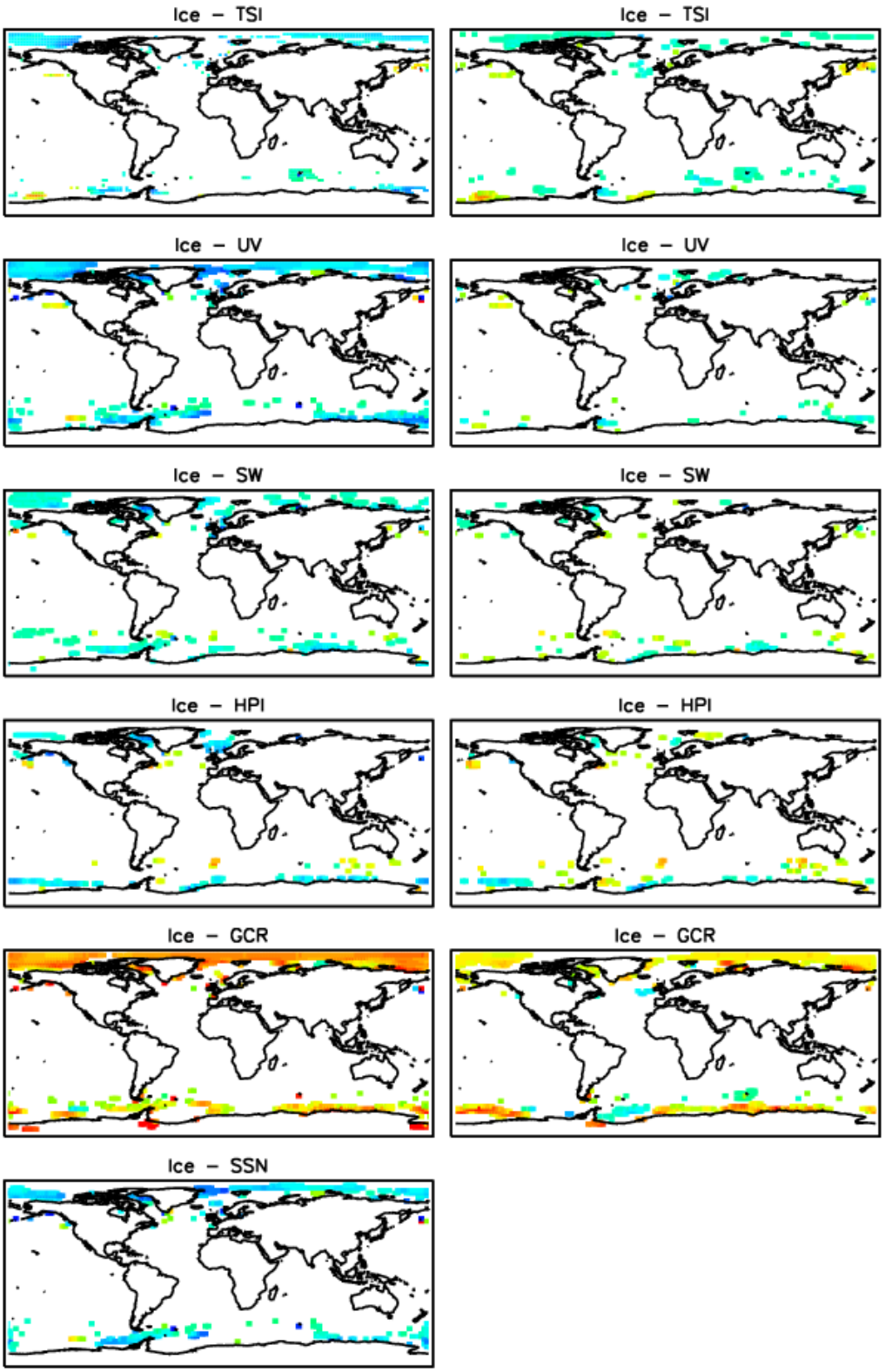

Figure 49: Correlations between the 5 external parameters plus the sunspot number and sea ice cover. The correlations are given after the removal of the internal parameters and linear trend (left column) and the solar activity (right column). Only the areas with correlation above the 90% significance level have been plotted

Precipitation

Precipitation is monthly surface data in mm from the Climate Research Unit in Norwich (CRU) and available on a 5.0 x 5.0 degree grid from 1900 – 1998. Figure 50 shows the correlation between rainfall and the solar modulated forcing parameters, with only correlations with significance above 90% shown.

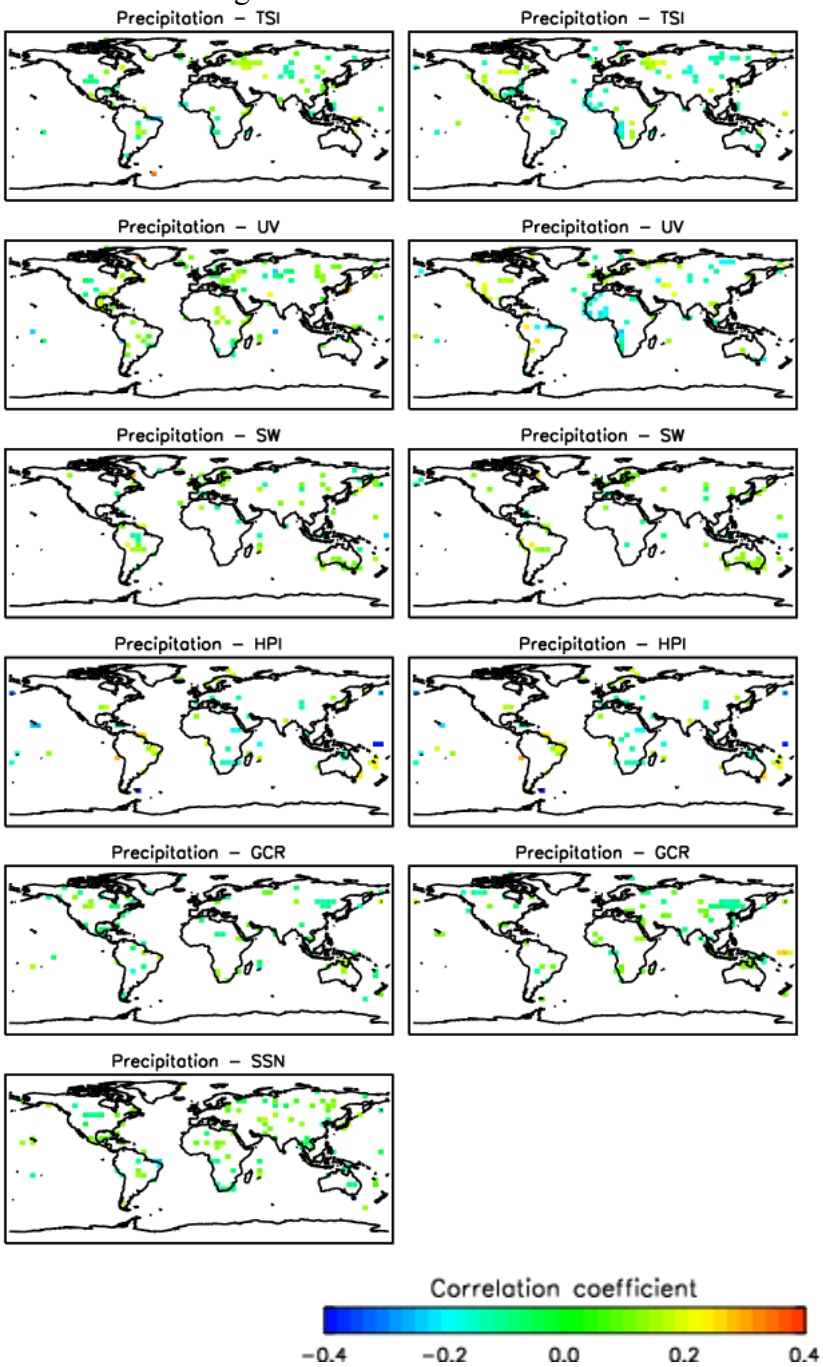

Figure 50: Correlations between the 5 external parameters plus the sunspot number and precipitation. The correlations are given after the removal of the internal parameters and linear trend (left column) and the solar activity (right column). Only the areas with correlation above the 90% significance level have been plotted.

Surface Pressure

The surface pressure is available only for the Northern Hemisphere provided by CRU. This dataset contains monthly mean-sea-level pressure data on a 5° latitude by 10° longitude grid. Figure 53 shows the correlations between surface pressure and the 5 solar modulated forcing parameters. An equivalent pattern is seen in the pictures for TSI, UV, SW, and HPI: a patch of negative correlation in the North Sea/North Atlantic, balanced by positive correlations in the polar regions and further south in the
Atlantic. The same pattern is not seen for GCR or SSN. In Figures 51 and 52 we give example of the time series for the surface pressure in selected areas, the North Atlantic and the tropic Pacific where the correlations with TSI and UV differ significantly from 0.

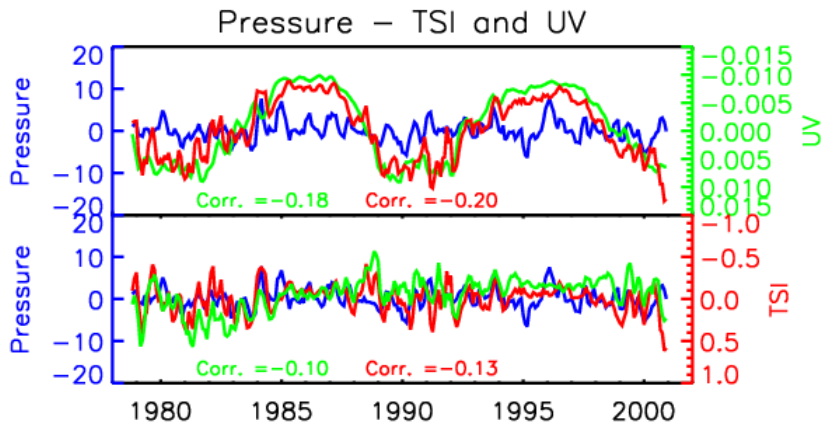

Figure 51: Correlation between surface pressure and TSI and UV in the North Atlantic before removal of the solar cycle (top) and after (bottom).

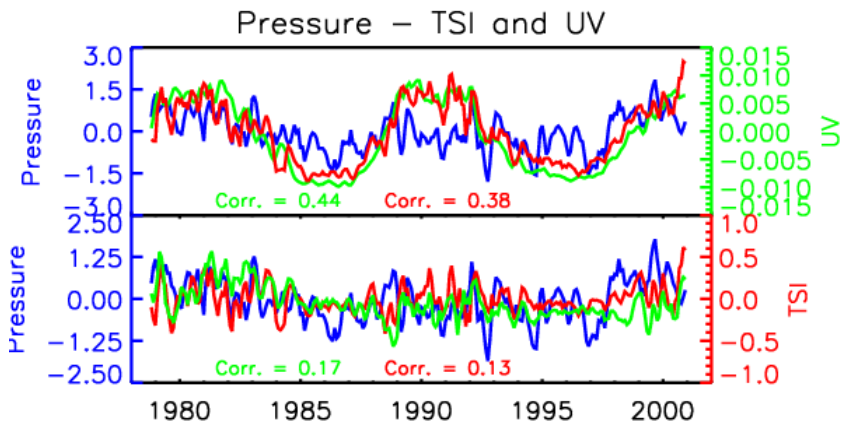

Figure 52: Correlation between surface pressure and TSI and UV in area of the tropic Pacific where the correlation is significantly positive before removal of the solar cycle (top) and after (bottom).

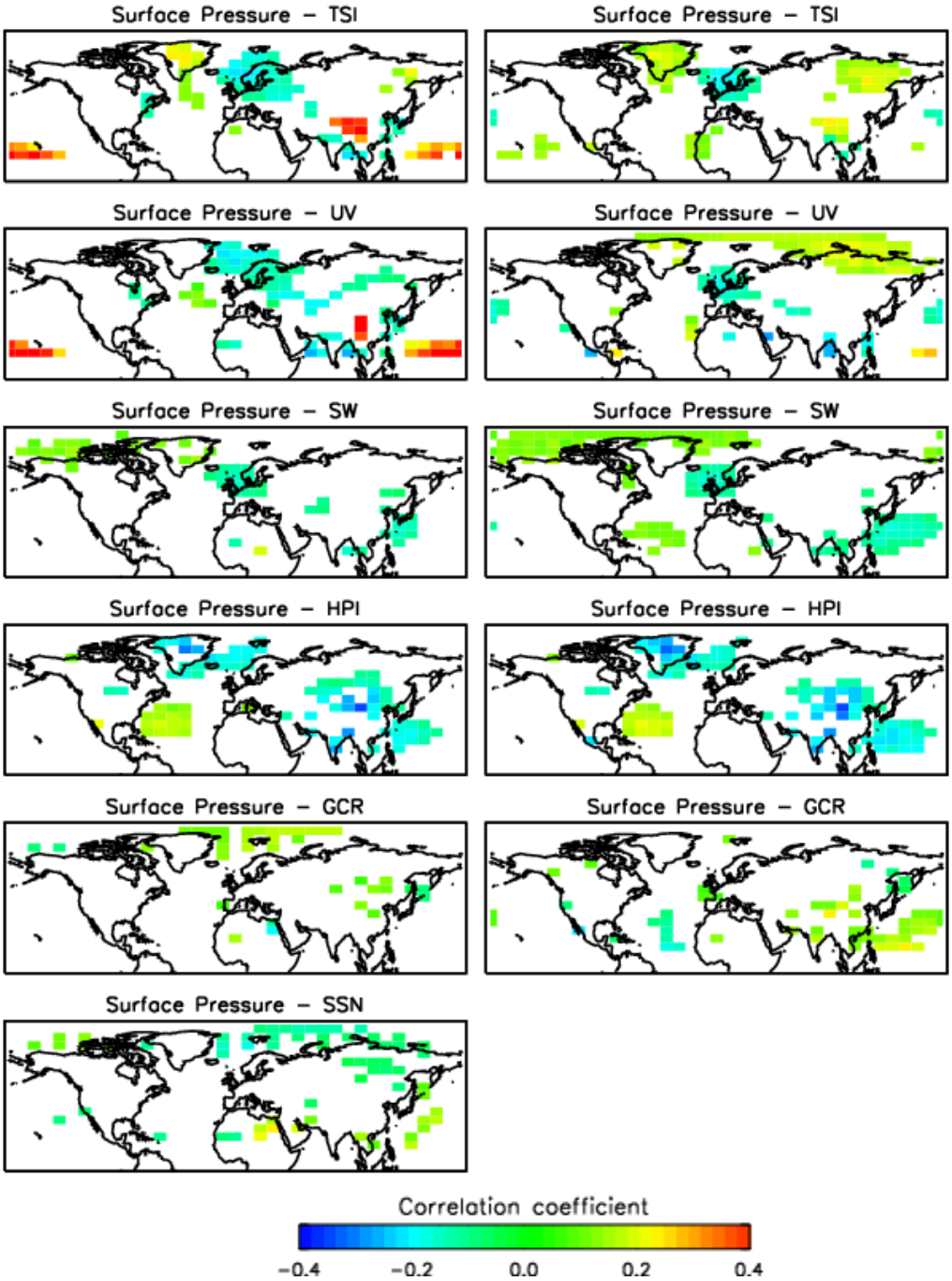

Figure 53 Correlations between the 5 external parameters plus the sunspot number and surface pressure. The correlations are given after the removal of the internal parameters and linear trend (left column) and the solar activity (right column). Only areas with correlations coefficient above the 90% significance level have been plotted.

Surface Temperature

Surface temperature is monthly anomaly data from the Climate Research Unit (air temperature over land) and Hadley Centre (sea surface temperature) and available on a 5.0 x 5.0 degree grid from 1870 – present. Figure 56 shows the correlation between temperature and the solar modulated forcing parameters, with only correlations with significance above 90% shown. Scattered areas of correlations are observed for all parameters. For GCR these correlations are predominantly negative, whereas there are mixed positive and negative correlations for the other parameters.
In Figures 54 and 55 we present the time series for the global mean surface temperature and global mean sea surface temperature together with the time series for GCR and UV.
In Tables 12 and 13 we give the correlation coefficients for the mean global surface and mean global sea surface temperatures with the 5 external parameters and the sun spot number. EUV and GCR show significant correlations with the surface temperatures, but only for GCR does the correlation survive the removal of the solar cycle.

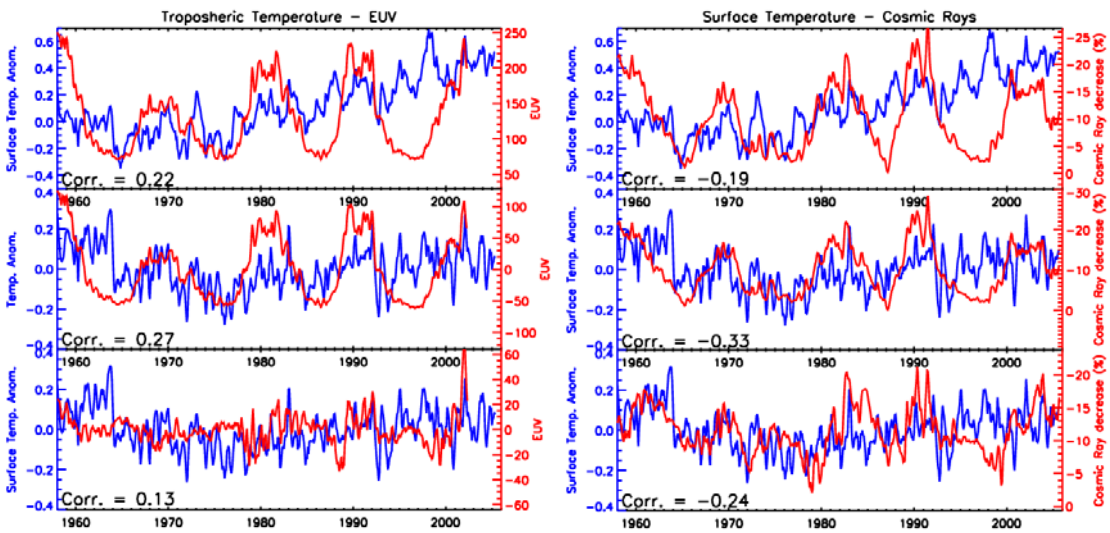

Figure 54: Left) correlation between 10.7 cm EUV proxy and global mean surface temperature anomalies. Top panel: observations. Middle panel: after removal of nino3, NAO, volcanic aerosols, and a linear trend. Bottom: after removal of the solar cycle. Right) the same for galactic cosmic rays.

	TSI	EUV	SW	HPI	GCR	SSN
Observ.	-0.06 (-0.08)	0.22 (0.23)	0.13 (0.19)	-0.11 (-0.12)	-0.19 (-0.20)	0.11 (0.12)
Niño, etc.	**0.21 (0.27)**	***0.27 (0.31)***	0.04 (0.07)	0.00 (0.02)	***-0.33 (-0.38)***	**0.23 (0.27)**
Solar cycle	0.08 (0.07)	0.13 (0.15)	-0.07 (-0.11)	-0.04 (-0.04)	**-0.24 (-0.29)**	

Table 12: The correlations coefficients for the 5 external parameters with surface temperature. Given are the correlations for raw observation, after removal of the internal climate parameters, and after removal of the solar cycle. Numbers in bold face are above the 95% significance level. Numbers in bold italics are above the 99% significance level.

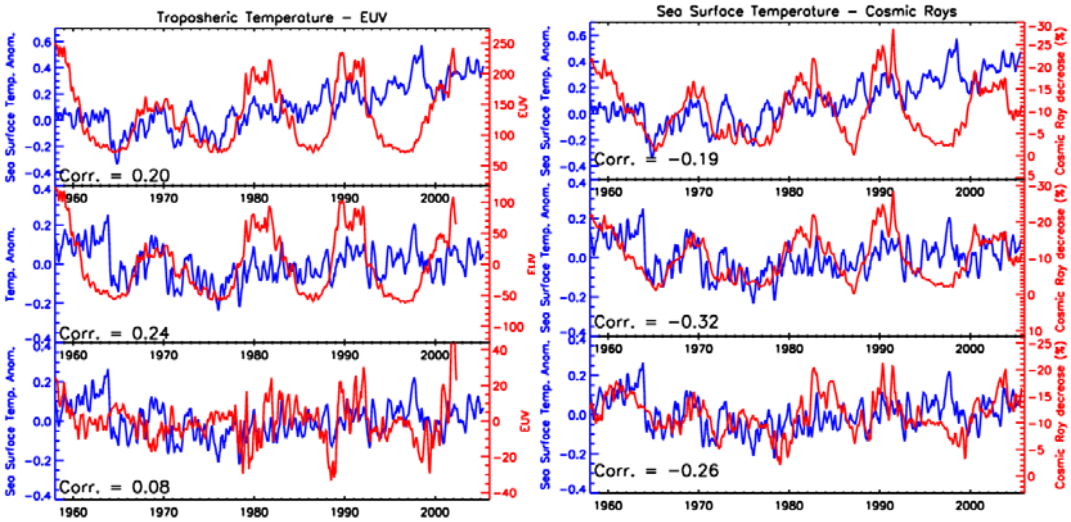

Figure 55: Same as Figure 54, but for sea surface temperatures.

	TSI	EUV	SW	HPI	GCR	SSN
Observ.	-0.17 (-0.20)	0.20 (0.21)	0.12 (0.16)	-0.16 (-0.19)	-0.19 (-0.20)	0.10 (0.12)
Niño, etc.	0.08 (0.09)	0.24 (0.27)	0.04 (0.06)	-0.03 (0.04)	**-0.32 (-0.36)**	0.21 (0.27)
Solar cycle	0.01 (-0.05)	0.08 (0.09)	-0.05 (-0.12)	-0.06 (-0.07)	**-0.26 (-0.30)**	

Table 13: Same as Table 12, but for Sea Surface temperatures.

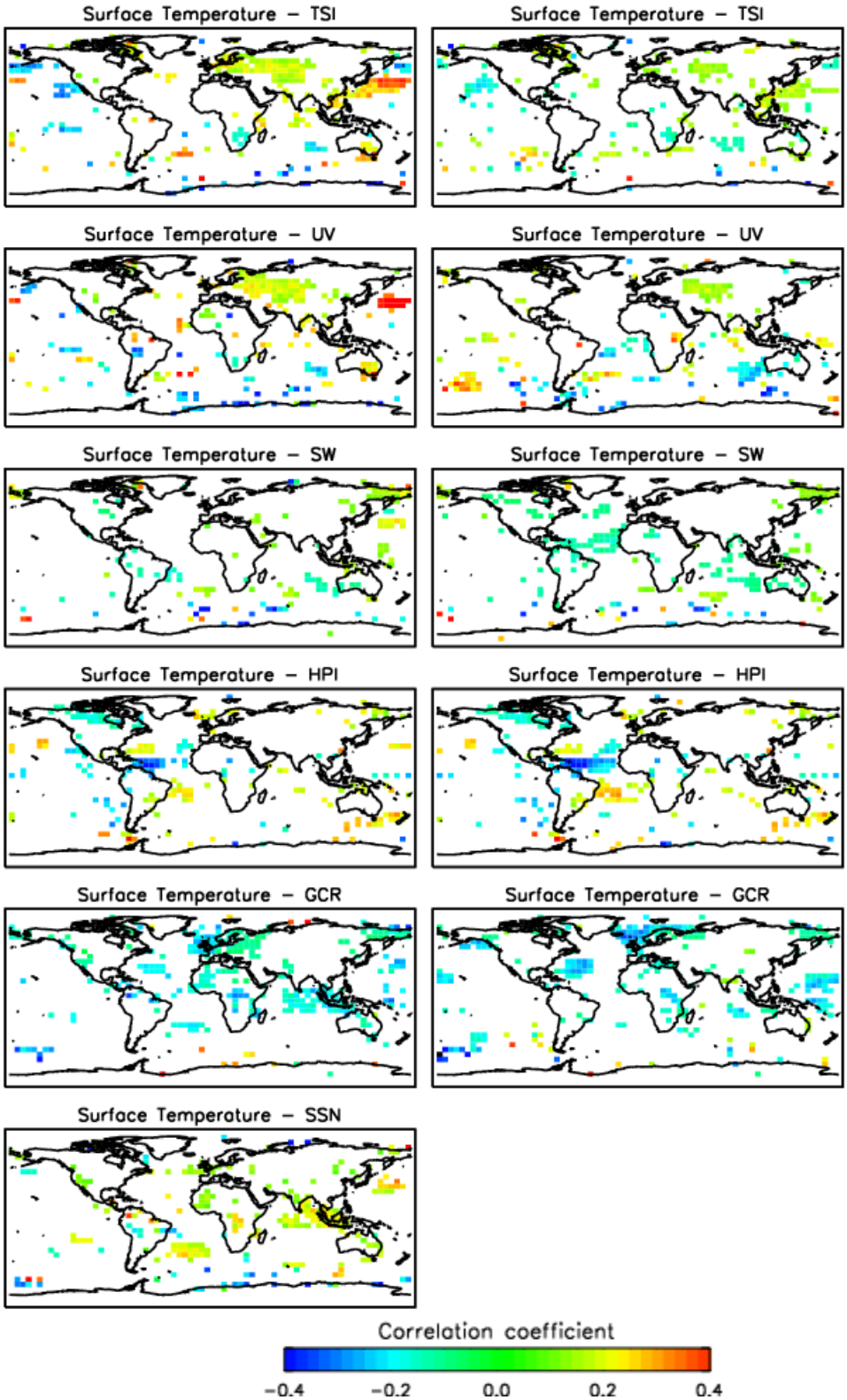

Figure 56: Correlations between the 5 external parameters plus the sunspot number and surface temperature. The correlations are given after the removal of the internal parameters and linear trend (left column) and the solar activity (right column). Only the areas with correlation above the 90% significance level have been plotted

4.4 Summary

No single solar modulated parameter consistently dominated the response found in each of the climate parameters investigated in this report. The clear majority of solar modulated variability in the various climate parameters could be explained by effects related to the solar cycle. However, some significant differences in the strength, sign and spatial distribution of the correlation became apparent once the effects of the solar cycle had been removed.

The main highlights from the correlation study, once the solar cycle had been accounted for, can be summarised for each of the solar modulated parameters as follows:

TSI

- Zonally averaged temperature under solar min conditions showed some significant positive correlation in the equatorial troposphere.
- No significant correlation was found in any of the other climate parameters.

UV

- Zonally averaged temperatures displayed significant positive correlation coefficients that were comparable to those found with GCR, but then disappeared after removal of the solar cycle.
- Zonally averaged temperatures under solar max/min conditions show a negative/positive correlation in the troposphere, similar, but weaker than, the feature found with GCR.
- Low clouds displayed negative bands of correlations at mid to high latitudes. These bands were *strengthened* by removal of the solar cycle leading to additional positive bands of correlation to appear in the tropics.
- Ozone displayed limit areas that were correlated with UV but these were significantly stronger than with the other solar modulated parameters.
- Aerosols displayed a significant positive correlation in the southern hemisphere.

SW

- Zonally averaged temperature under solar min conditions showed some significant positive correlation in the stratosphere.
- No significant correlation was found in any of the other climate parameters.

HPI

- Zonally averaged temperature under solar min conditions showed some significant negative correlation in the equatorial troposphere.
- Aerosols displayed a significant positive correlation at the equator.
- No significant correlation was found in any of the other climate parameters.

GCR

- Zonally averaged temperatures displayed a significant negative correlation. GCR was the only parameter displaying a significant correlation for global averages

after removal of the solar cycle. However, when limiting the analysis to data after 1978 this correlation disappeared.

- Zonally averaged temperatures under solar max/min conditions show a negative/positive correlation in the troposphere. A similar, but weaker, feature was found with UV, but did not appear with any of the other solar modulated parameters.
- Low clouds displayed negative(positive) bands of correlations at mid to high latitudes similar to UV. The response with UV and GCR was generally very similar and it was difficult to distinguish between these two parameters. However, after removal of the solar cycle the globally averaged correlations were definitely weaker for GCR.
- Aerosols displayed a significant correlation in the southern hemisphere which could not be distinguished from the signal found with UV.

Two final features of note are:

1) That the vertical circulation displayed significant latitudinal bands of positive and negative correlation with all solar modulated forcing parameters after the solar cycle had been removed. However, the latitudinal position of these bands was different for each parameter.
2) Virtually no significant correlation was found in any of the surface climate parameters.

5. Mechanisms

Though a solar signal is evident in many climate parameters, and though it is obvious that the Sun drives Earth's climate, the exact physical mechanisms by which solar variations manifest themselves in the climate system is yet poorly understood. One reason is that it is difficult, if not impossible, to separate each solar driver, e.g., TSI, UV, modulation of cosmic rays, and pinpoint it to a single climate response. Table 14 gives a summary of the most often cited mechanisms.

Forcing factor	**Generic mechanism**
Total solar irradiance (variations due to orbital variations or to variable solar emission).	Radiative forcing of climate. Direct impact on sea surface temperatures and hydrological cycle.
Solar UV irradiance	Heating the upper and middle atmosphere, dynamical coupling down to troposphere. Middle and lower atmosphere chemistry and composition; impacts temperature structure and radiative forcing.
Solar energetic particles	Ionisation of upper and middle atmosphere; impact on composition and temperatures. Magnetosphere – ionosphere – thermosphere coupling.
Galactic cosmic rays	Ionisation of lower atmosphere; impact on electric field. Impact on condensation nuclei.

Table 14: Summary of routes through which solar variability may influence the climate of the lower atmosphere.

A key concept in the area of climate change is that of "Radiative Forcing". This is loosely defined[1] as the instantaneous net radiative imbalance at the top of the atmosphere introduced by some perturbing factor. The latter could be a change in atmospheric composition or incoming solar irradiance or of the Earth's albedo. Radiative forcing is a useful concept as it gives a top level indication of the potential impact of the perturbing factor on the equilibrated global mean surface temperature of the Earth. Because of this it is used extensively to indicate the relative impacts of various anthropogenic and natural factors on climate. Figure 57 shows radiative forcings since 1750 as set out in the Fourth Assessment Report of the Intergovernmental Panel on Climate Change (IPCC, 2007).

[1] More precisely radiative forcing is defined as the change in net radiative flux at the tropopause after allowing for stratospheric temperatures to readjust to radiative equilibrium but with surface and tropospheric temperatures held fixed.

The solar contribution is perceived to be very small, but the ascribed "Level of Scientific Understanding" is low. In this context it should be noted that:

1. Larger or smaller values would be found if the start date had been, say, 1800 or 1700.
2. While the contribution over the 255 year period is small the IPCC does find a detectable influence of solar irradiance increase on the warming of the first half of the 20th century.
3. The solar RF value is based on the very low secular trend in solar irradiance since the Maunder Minimum suggested by Wang et al (2005) whereas other reconstructions of total solar irradiance (e.g. Solanki and Krivova, 2004) show a larger long term increase.
4. This value takes no account of either direct or indirect feedback factors on solar radiative forcing (such as due to changes in ozone or to cloud cover) nor can it be used to interpret geographical distributions of any solar impact.

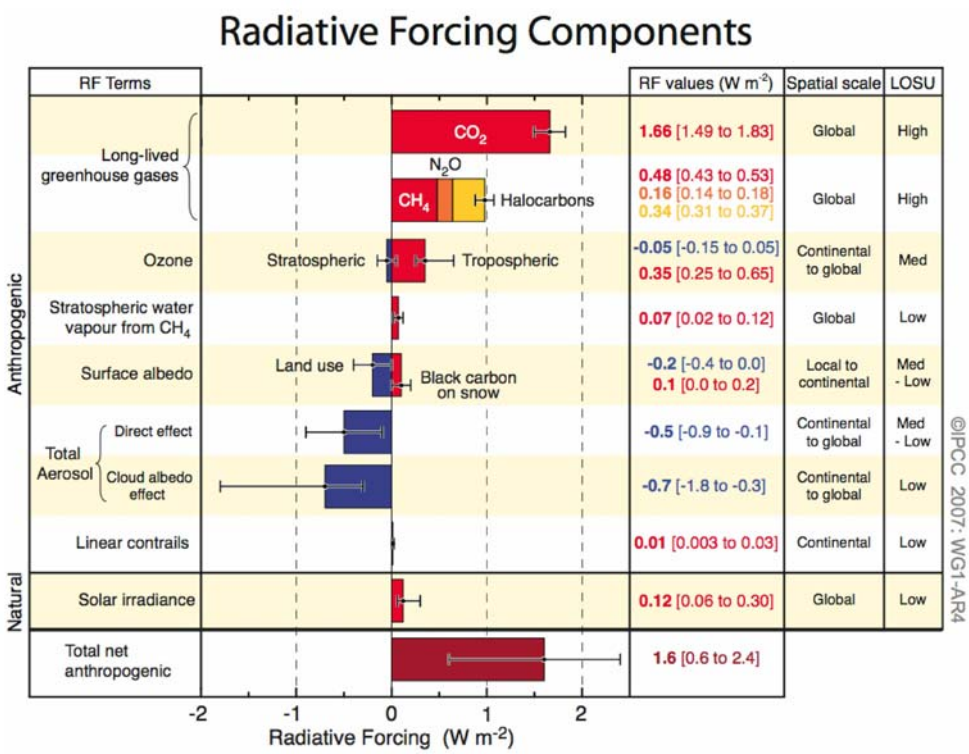

Figure 57: Components of radiative forcing 1750-2005 as determined by IPCC (2007).

Below we outline the physical mechanisms responsible for the solar signals in the atmosphere with an emphasis on UV, TSI, and cosmic rays.

5.1 Solar signals through the stratosphere and troposphere

A number of analyses now indicate a statistically significant signal of solar cycle variability in a range of meteorological parameters throughout the stratosphere and

troposphere. Early work indicating correlations between solar activity and lower atmospheric temperatures was presented by Labitzke and van Loon (1995), see Figure 58.

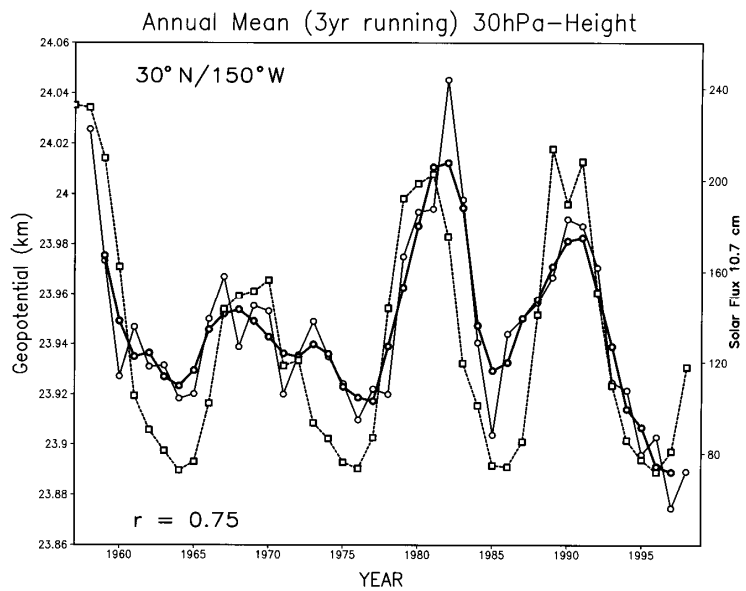

Figure 58: Circles and thin line: annual mean geopotential height of the 30hPa surface (which represents the mean temperature of the atmosphere below about 22 km) over the sub-tropical Pacific Ocean. Circles and thick line: 3-year running mean of the same parameter. Squares and thin line: Solar 10.7cm flux as an indicator of solar activity. (Labitzke and van Loon, 1995)

More recently the availability of reanalysed datasets from the US National Centre for Environmental Prediction (NCEP) and the European Centre for Medium Range Weather Forecasts (ECWWF) has provided global data over a forty year period for climate studies. These have allowed some rigorous analysis of solar signals, such as those shown in zonal wind and temperature in Figures 59 and 60.

Temperatures show not the uniform warming that might be expected when the Sun is more active but statistically significant warmer regions in the low latitude upper and lower stratosphere, and in the subtropics to mid-latitudes extending throughout the lower stratosphere and troposphere.
The corresponding zonal wind fields indicate that the mid-latitude tropospheric jets are weaker and displaced slightly towards the poles at maxima of the solar 11-year cycle relative to the minima.

The influence on surface winds at high latitudes can also be seen in terms of the polar modes of variability. Boberg and Lundstedt (2002) have shown a correlation between the North Atlantic Oscillation and the electric field strength of the solar wind. In a different study of the Northern Annular Mode we also found that it varied with solar activity but that the combined influence of the Sun and the quasi-biennial oscillation in tropical stratospheric winds provided a better indicator of the strength of the circumpolar circulation in both northern and southern hemispheres (see Table 15).

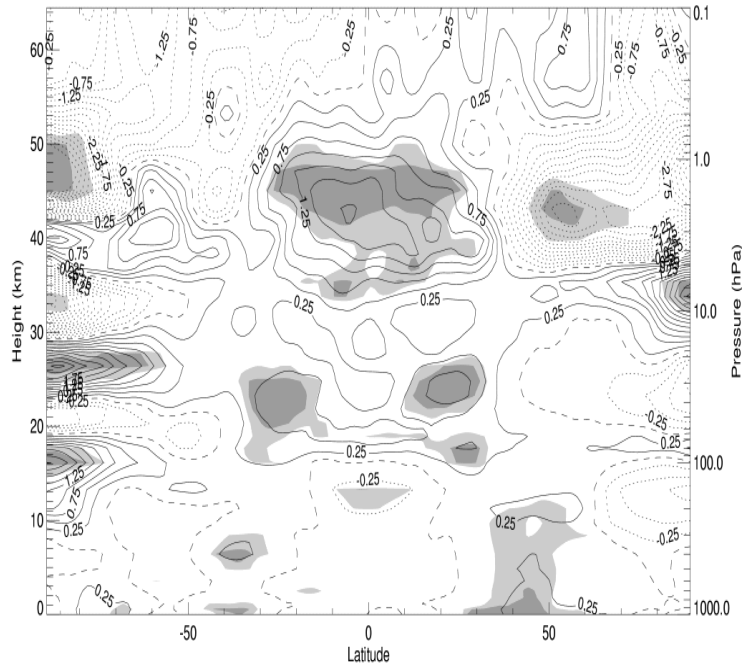

Figure 59: Solar cycle signal in zonal mean, annual mean temperatures, calculated using a multiple regression analysis of data from the ERA-40 reanalysis dataset of the ECMWF. Light/dark shading indicates statistical significance at the 5%/1% level. (Crooks and Gray, 2005).

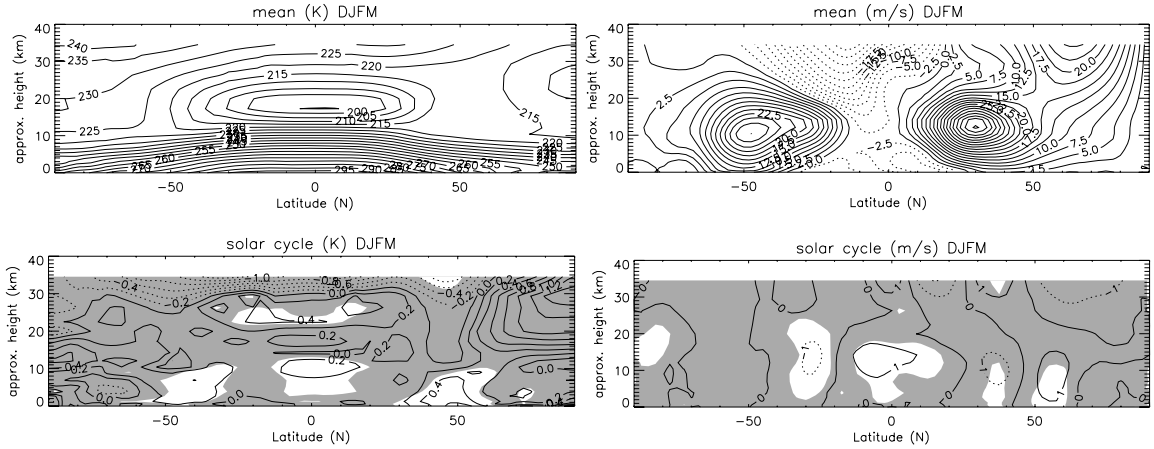

Figure 60: Signals in December-March zonal mean temperature (left) and zonal wind (right) derived from NCEP/NCAR Reanalysis data 1979-2002. The top row shows the climatological averages and the bottom row the solar cycle signal. Shaded areas are not significant at the 5% level.

As well as signals in temperature zonal wind studies have indicated a solar signal in the mean overturning circulation of the atmosphere. Figure 61 shows an analysis of zonal mean vertical velocities from the NCEP reanalysis dataset. The results show weaker ascent in the inter-tropical convergence zone, weaker descent in the sub-tropics and a poleward shift of the descending branches.

	Trend	Cl	ENSO	Vol	Sol	QBO	Sol*QBO
NAM (DJFM)	**0.23**		-0.82	**1.08**	**0.81**	0.64	
	0.24		-0.85	0.96			**-1.16**
SAM		**1.01**	**-0.82**	**-0.65**	-0.04	0.13	
		1.01	**-0.71**	**-0.75**			**-0.89**

Table 15: Multiple regression analysis of the Northern Annular Mode at the surface in winter and of the Southern Annular Mode at the surface. Columns show regression coefficients for linear trend (N.H. only), stratospheric chlorine (S.H. only), El Niño-Southern oscillation (ENSO), volcanic (stratospheric) aerosol loading, solar variability (10.7cm index) and the quasi-biennial oscillation (QBO). The column labelled Sol*QBO indicates that an index composed of a product of the solar and QBO indices was used in place of those two factors individually. The data cover the period 1958-2001. Colours indicate the statistical significance levels of the values, derived using a Student's t-test, as follows: 99%, 95%, 90%, 80%, <80%. (Haigh and Roscoe, 2006)

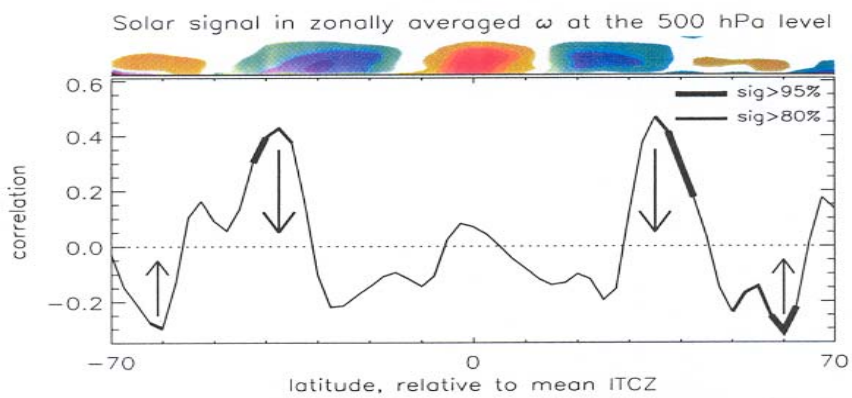

Figure 61: Zonally-averaged pressure velocity in the middle troposphere from the NCEP reanalysis dataset. Colours indicate the climatological mean with red indicating ascent and blue descent. The line indicates the correlation between solar activity and vertical velocity with positive (negative) values indicating relative descent (ascent) at solar maximum relative to solar minimum. (Gleisner and Thejll, 2003).

5.2 Solar variability and stratospheric ozone

The influence of solar variability on stratospheric ozone is important because this will impact both the temperature of the stratosphere (with implications for stratosphere-troposphere coupling – see below) and radiative forcing of the troposphere. However, the 11-year cycle in ozone remains poorly characterised. Figure 62 shows a summary from the recent World Meteorological Organisation assessment. The results from the satellite data appear to show a minimum in the profile near 30km which is not seen in any of the model simulations. It remains to be seen if this disparity is due to some process being omitted from the theoretical assessments or to some inadequacy with the data analysis (possibly due to the relatively short data period and influence of other factors such as the QBO and volcanic eruptions).

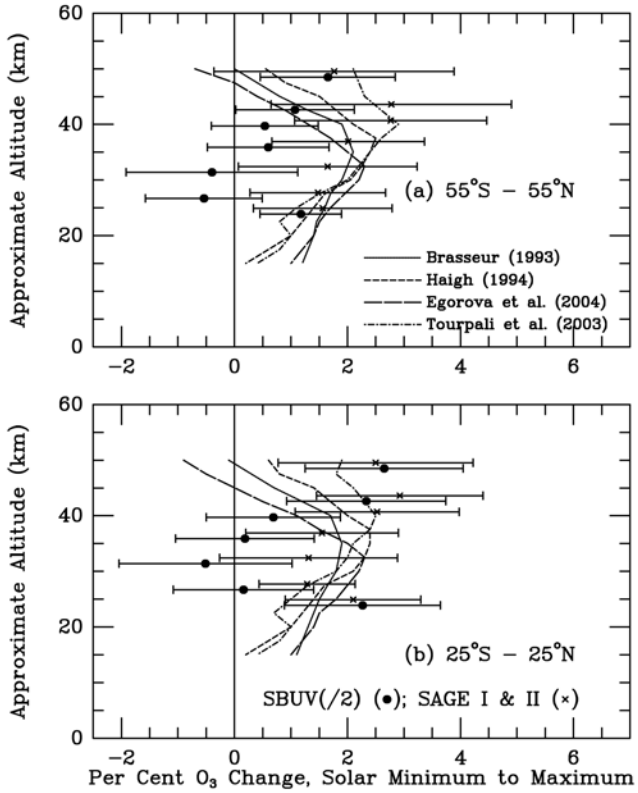

Figure 62: Solar cycle variation in ozone as a function of altitude as estimated from satellite data (spots and crosses with error bars) and various photochemical models for (a) quasi-global and (b) tropical latitudes. (WMO, 2007)

The importance of the ozone change in determining the radiative forcing is illustrated in Figure 63. The left hand panel shows how the solar spectral irradiance is modified as it travels down through the atmosphere by ozone absorption bands mainly in the ultraviolet but also the visible regions of the spectrum.

The right hand panel shows the difference in irradiance between peaks of the 11-year solar cycle. Because of the additional ozone at solar maximum the amount of radiation reaching the lower atmosphere is considerably reduced so that, for the low solar zenith angles pertaining at this latitude and time of year, the spectrally-integrated solar energy is actually less at solar maximum than minimum.

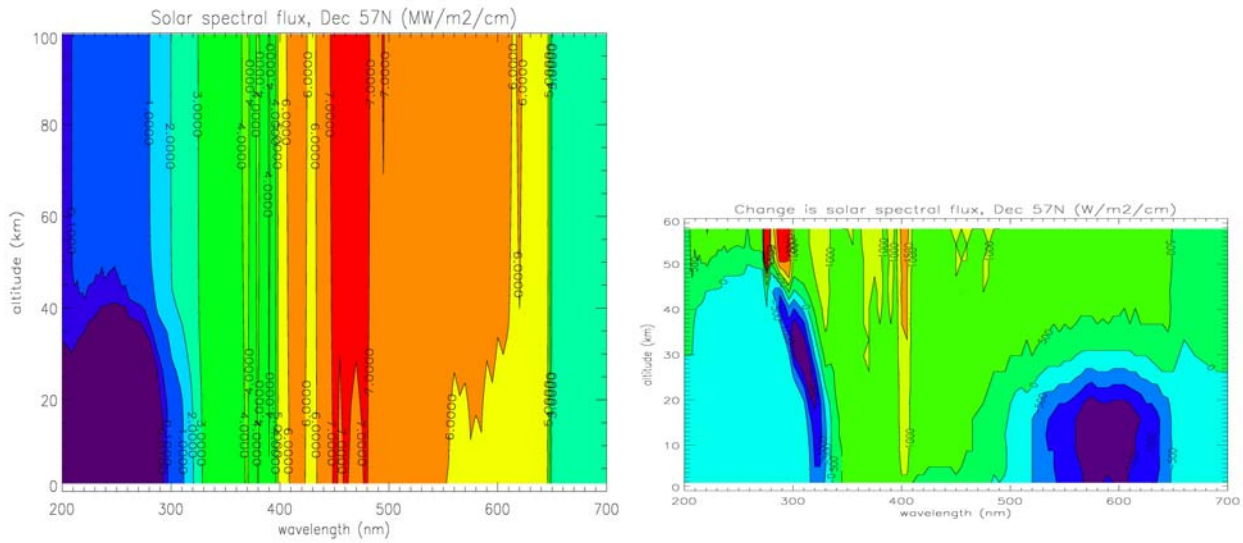

Figure 63: Left: Solar irradiance as a function of wavelength and altitude for December at 57°N, contour interval 1 MW m^{-2} cm^{-1}. Right: Difference in solar spectral irradiance between solar max and solar min, contour interval 500 W m^{-2} cm^{-1}, the zero contour is marked by the blue-green boundary. (After Haigh, 1994)

5.3 Evidence for stratosphere-troposphere coupling

There is some observational evidence that variations in the strength of the polar vortex in the upper stratosphere may subsequently influence surface climate. Figure 64 shows an apparent downward propagation of anomalies in the strength of the NH winter polar vortex. A study of polar temperature trends by Thompson and Solomon (2005) also suggests a downward influence and modelling experiments by Gillett et al (2004) demonstrate that depletion of stratospheric ozone over the South Pole can affect the troposphere after about one month. None of these studies is specifically concerned with a solar influence but the accumulating evidence suggests that any factor influencing the strength of the polar stratospheric jet may be able to influence surface climate.

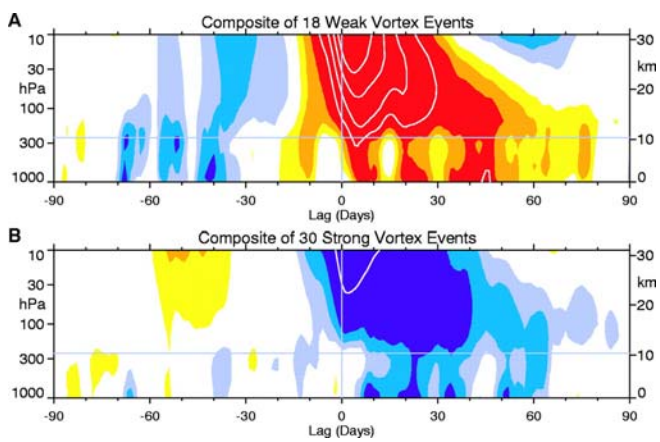

Figure 64: Time-height section of geopotential height anomalies. Plots show a composite of events characterized by a weak (top panel) or strong (bottom panel) polar vortex at 10 hPa on day zero. (Baldwin and Dunkerton, 2001)

The original modelling study of Haigh (1996) showed, using an atmospheric GCM with fixed sea surface temperatures, that changes in solar UV produced a weakening and poleward shift of the mid-latitude jets, reproduced on the right-hand side of Figure 65. These changes are similar in sense, though of a somewhat smaller magnitude to those found in the NCEP data analysis shown in Figure 62, and reproduced on the left-hand side of Figure 65.

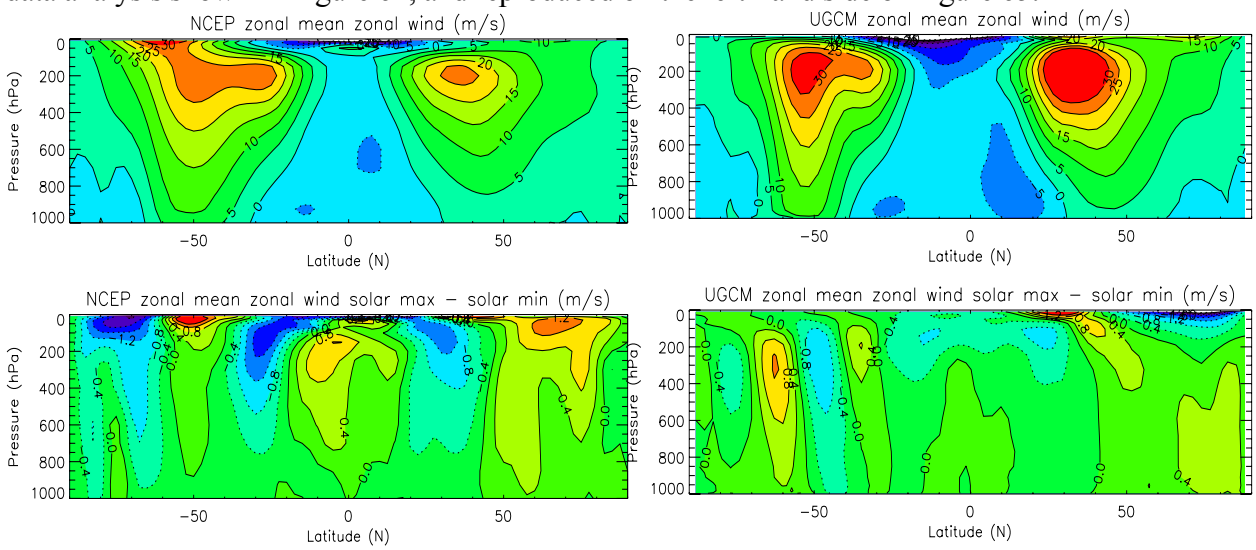

Figure 65: Top: zonal mean zonal wind, u, as a function of latitude and pressure. Bottom: difference in u between solar max and solar min. Left column: from NCEP data (similar to Fig. 59). Right column: from a GCM experiment in which solar UV radiation has been increased to represent the difference between solar min and solar max (Haigh et al, 2005; Haigh, 1996)

The Haigh (1996) model also showed a weakening and broadening of the tropical Hadley cells (mean meridional overturning) at solar maximum. This experiment was repeated using an entirely different model by Larkin et al (2000) with similar results in all seasons, see Figure 66. These changes are consistent with the vertical velocity signals shown in Figure 62.

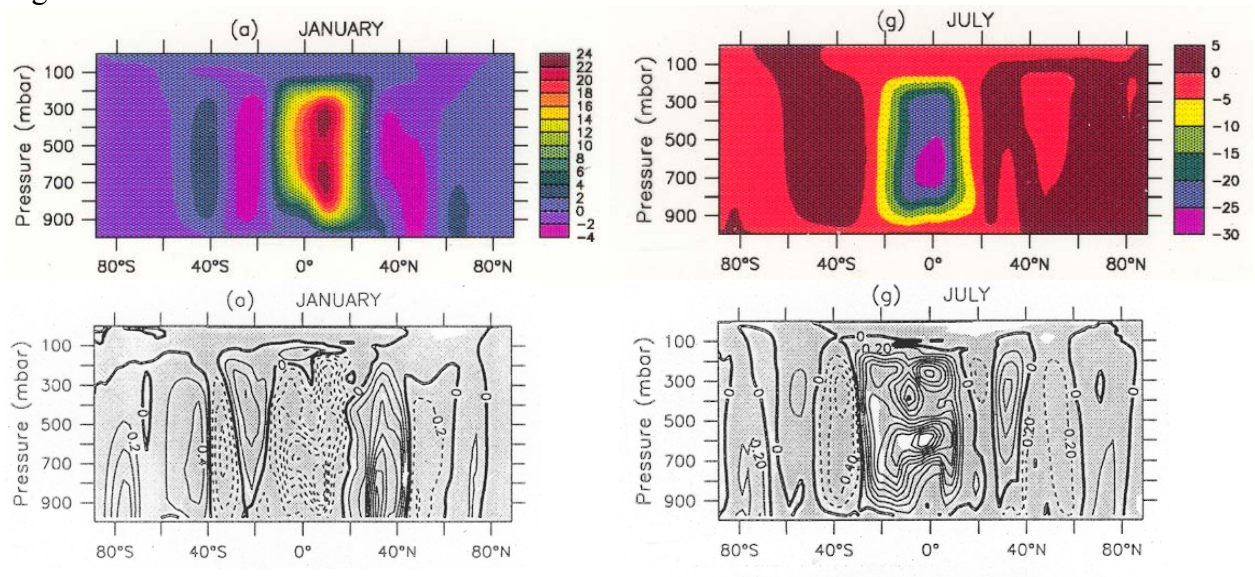

Figure 66: Top: Mean meridional circulation, *MMC*, as a function of latitude and pressure; positive (negative) values indicate a clockwise (anti-clockwise) circulation. Bottom: difference in *MMC* between solar max and solar min; solid (dashed) contours indicate increases (decreases). Left column: January. Right column: July (Larkin et al, 2000)

5.4 Mechanisms of stratosphere-troposphere coupling

While some of the similarities between the observational analyses of solar influence and modelling studies of UV effects are intriguing they do not explain the mechanisms whereby the influence takes place. In a series of papers Kodera has argued that changes in the winter polar stratospheric brought about by anomalous solar heating may influence the passage of upward propagating planetary waves and thus their deposition of momentum and hence the strength of the mean overturning of the stratosphere (aka the Brewer-Dobson circulation) (see Figure 67)

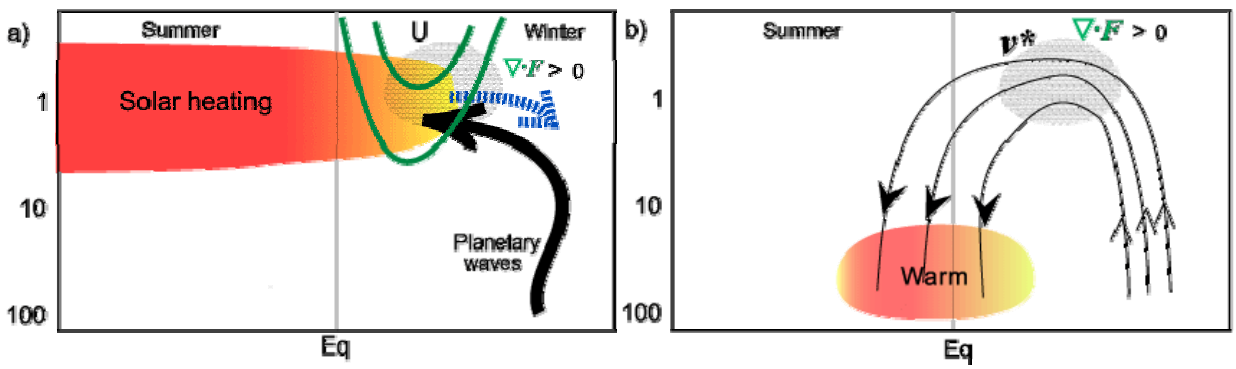

Figure 67: Cartoon to illustrate proposed mechanism whereby solar heating around the stratopause may influence the atmosphere below. The solar heating anomalies change the strength of the polar stratospheric jet (U); this influences the path of upward propagating planetary waves which deposit their zonal momentum on the poleward side of the jet. The effect of this is to weaken the Brewer-Dobson circulation and thus to warm the tropical lower stratosphere (Kodera and Kuroda, 2002)

An alternative (or additional?) perspective is provide by the work of Gray and co-workers who have demonstrated using rocketsonde and satellite data that zonal wind anomalies in the tropical upper stratosphere are correlated with subsequent temperature anomalies in the polar lower stratosphere. They also demonstrated this effect in a mechanistic model of the middle atmosphere (see Figure 68).

The Kodera and Gray studies provide evidence and mechanisms whereby solar perturbations to the upper stratosphere may affect the lower stratosphere, in both cases enhancing any direct solar heating in this region. However, they do not explain the apparent subsequent propagation downwards into the troposphere. To investigate this we have carried out some studies using a simplified general circulation model which includes a full representation of atmospheric dynamics but only highly-parameterised representations of radiative and cloud processes. In these experiments the radiative equilibrium temperature, T_e, of the stratosphere was perturbed, while the tropospheric values unaffected and the impact on the modelled climate investigated. For example, in Run U5 T_e was increased by a uniform 5K throughout the stratosphere while in Run E5 it was increased by 5K in the equatorial stratosphere decreasing to 0K at the poles. Note

that these experiments are not intended to simulate solar effects but to investigate possible mechanisms for stratosphere-troposphere coupling.

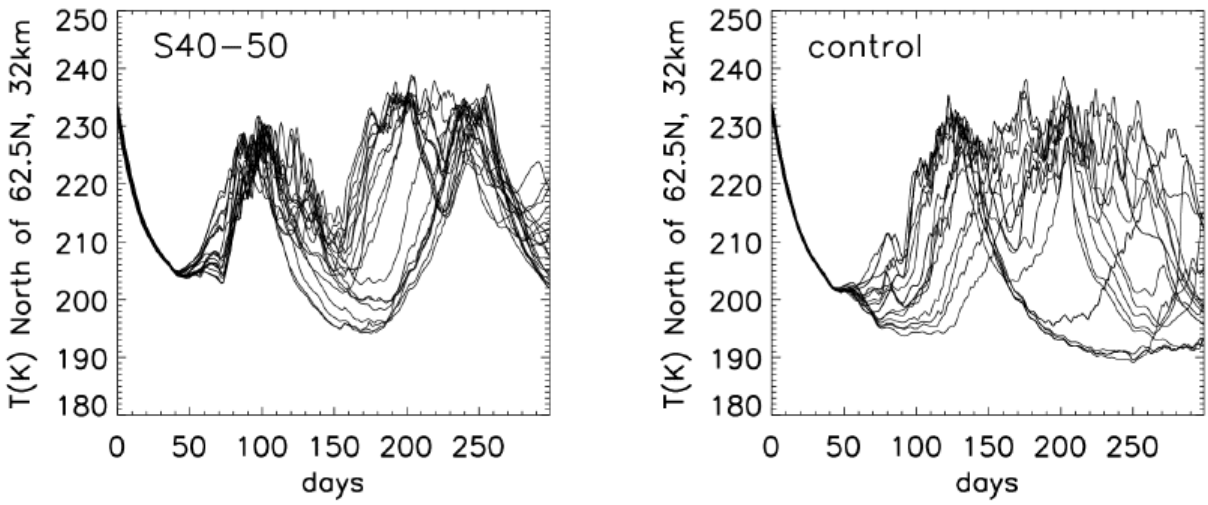

Figure 68: Temperature of the NH polar lower stratosphere evolving through the winter as calculated in a stratosphere-mesosphere mechanistic model. Each panel shows the results from twenty different simulations in each of which the initial conditions were slightly altered. Right: control situation; Left: anomalous westerly momentum applied in the winter sub-tropics near the stratopause. (Gray, 2005)

Figure 69 shows the resulting zonal wind fields: in the perturbed runs, despite the heating anomaly having been prescribed only in the stratosphere, changes to the wind field are seen through the depth of the troposphere. In both cases the mid-latitude jet is weakened but, while the jet shifts poleward in the E5 case, in moves strongly equatorward in the U5 case. Thus the results of the E5 run, which plausibly has a more solar-like heating perturbation, shows qualitatively similar response in winds to that seen in the data analysis and full GCM studies (see Figure 65).

Further understanding of the processes involved has been gained by diagnosis of the vertically integrated budget of zonal momentum. It is clear from Figure 70 that the major response is in the flux of momentum due to the zonally asymmetric eddies (i.e. synoptic-scale weather systems). Current studies are investigating this further using an ensemble of spin-up runs in which the perturbation is switched on at day zero and the evolution of all the fields observed.

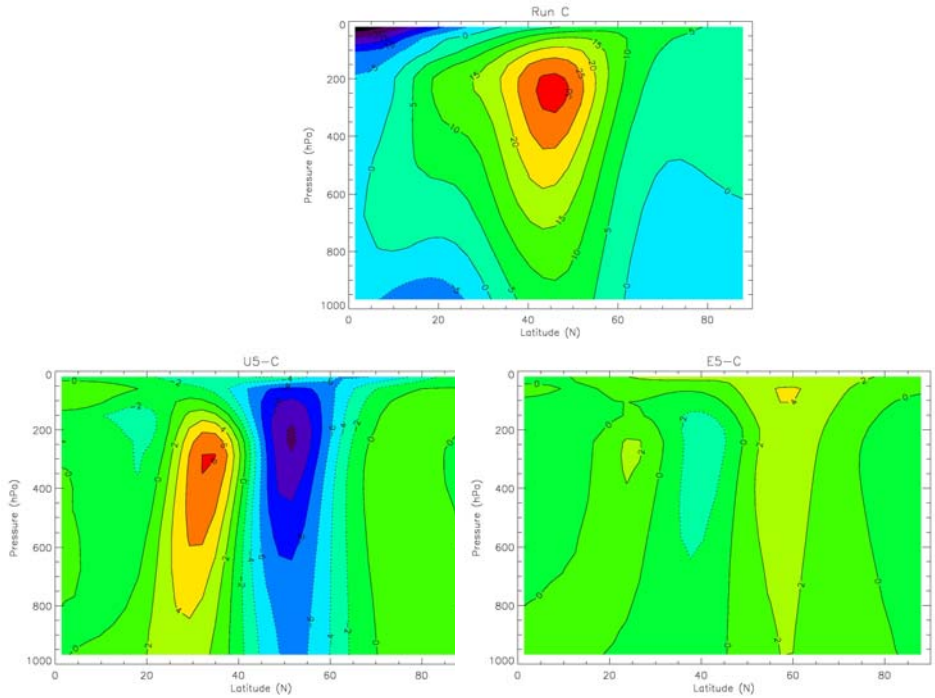

Figure 69: Results from a simplified global circulation model showing how anomalous heating of the stratosphere (only) can influence the jets through the depth of the troposphere. Top: zonal mean zonal wind in one hemisphere as a function of latitude and pressure from the control run; bottom left: difference between uniform stratospheric heating case and the control; bottom right: difference between equatorial stratospheric heating case and the control (Haigh et al, 2005)

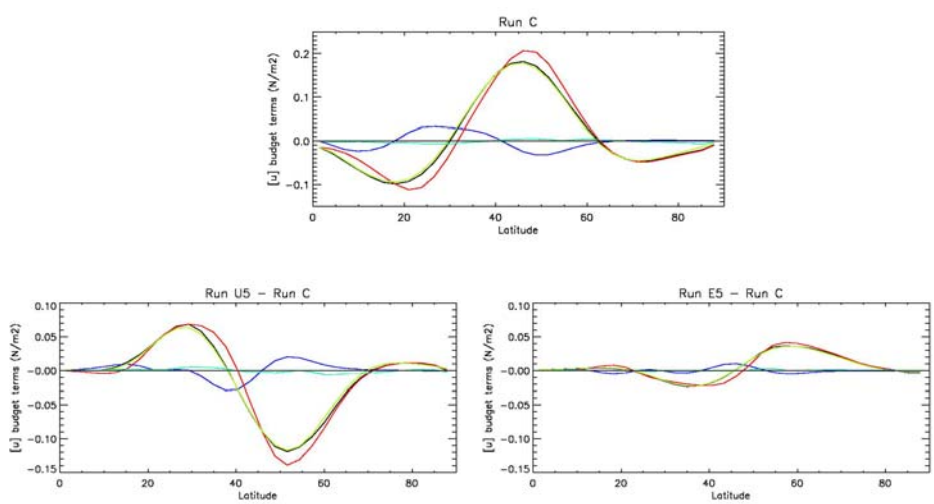

$$\frac{1}{g}\frac{\partial}{\partial t}\int_0^{p_s}[u]\,dp = C_{ZONAL} + C_{EDDY} - [\tau_{S\lambda}]$$

Figure 70: Vertically-integrated budget of components of the momentum equation: transport by eddies (red), transport by the zonal mean circulation (blue), dissipation by surface stress (green), sum of the eddy and zonal components (black), net rate of change of momentum (cyan), i.e. the difference between the black and green curves. Top: control run; bottom left: difference between uniform stratospheric heating case and the control; bottom right: difference between equatorial stratospheric heating case and the control (Haigh et al, 2005)

5.5 Role of Ionisation

Ions produced through the nucleonic cascade of cosmic rays in the troposphere rapidly interact with atmospheric molecules and are converted to complex cluster ions (Gringel et al. 1986; Hoppel et al. 1986). There are two loss terms for the ions; ion-ion recombination and ion-aerosol attachment. Ion production rates in the lower troposphere mean that the average lifetime of a small ion is up to 350 s. The ions act as charge carriers in the Global electric circuit which can generate charge build-up at cloud boundaries, and affect the processing of CCN/cloud droplets (Electroscavenging). Ions are also thought to play a role in stabilizing an initial atmospheric cluster until it is large enough to continue growing via neutral growth mechanisms into a particle/CCN (Ion Induced Nucleation). In addition, ions will attach to pre-existing aerosol nucleated through neutral processes, once charged there is a potential the aerosol's continued growth is enhanced (Charge Assisted Growth). These mechanisms are likely to have an impact on the number of aerosols acting as cloud condensation nuclei (CCN) at typical atmospheric super-saturations of a few percent [Viggiano and Arnold 1995]. In the following the important aspects of Ion Induced Nucleation, Charge Assisted Growth, and Electroscavenging will be discussed.

Ion Induced Nucleation (IIN)

Atmospheric aerosols are either released from the surface or are nucleated in-situ within the atmosphere. Bursts of nucleation have frequently been observed in the lower troposphere (Kulmala, 2004), and are thought to be an important source of CCN, particularly over maritime regions. The nucleation of new aerosol in the atmosphere is the result of a competition between condensation/coagulation growth processes and evaporation. Under typical atmospheric conditions H_2SO_4 and H_2O are thought to play an important role in the initial stages of new aerosol formation. However, initial clusters involving only a few H_2SO_4 molecules are more unstable than much larger clusters, due to the lower binding energies at the initial cluster surface. It is easier for a molecule to escape from a curved surface than a plane surface, thus the stability, which is related to curvature of a droplet, is size dependent. To over come this initial lack of stability through dissociation H_2SO_4 molecular concentrations, and hence collision rates with the initial ion clusters, must be high (>10^8/cc). However, typical atmospheric concentrations of the gas phase H_2SO_4 are too low (<10^7/cc) for clusters of a few molecules to be stable, thus the initial clusters should tend to evaporate and nucleation ought to be inhibited. Since observations indicate that in-situ nucleation is an important source of atmospheric aerosol, some additional process must be operating to stabilize the clusters during their initial growth until they are large enough to be stable in their own right and are considered nucleated. It is currently an open question as to how the initial clusters are stabilized until they reach this critical size. One mechanism that has been gaining increasing attention is the role of ionization during the early stages of nucleation, known as Ion Induced Nucleation (IIN). Since the majority of atmospheric ions are generated by cosmic rays, IIN processes could be important for understanding a sun-climate link.

Modelling the Physics of IIN

A number of theoretical models have been developed to explore IIN, and there are currently two models of particular note referred to here as Yu's model (Yu and Turco,

2000; Yu, 2006), and Lovejoy's model (Lovejoy et al 2004). A brief overview of the physics included in each of these models is given below.

Both models describe the full kinetic behaviour of cluster production at molecular resolution for a H_2SO_4/H_2O system under atmospheric conditions. The evolution of the size spectrum and composition of neutral and charged clusters are followed from a few molecules up to large particles (um). All clusters are allowed to grow through condensation and coagulation, and shrink through evaporation; small ion clusters are additionally lost through recombination or ion-aerosol attachment (Figure 71). Nucleation on ions is favoured because the charged clusters are more stable thermodynamically, and their growth rate enhanced and evaporation lowered due to the interaction between ions and polarisable vapour molecules. After the initial growth of small ion clusters, recombination generates large neutral clusters, but they will shrink due to evaporation if smaller than the critical size. The nucleation rate is then determined by the number of clusters exceeding the critical size after recombination. This is partly dependent on atmospheric ambient conditions and partly on the cluster thermodynamics described in the model. Thus IIN is essentially the ability of ions to help maintain the initial cluster, limit evaporation, and enhance initial cluster growth before recombining to produce a stable neutral aerosol.

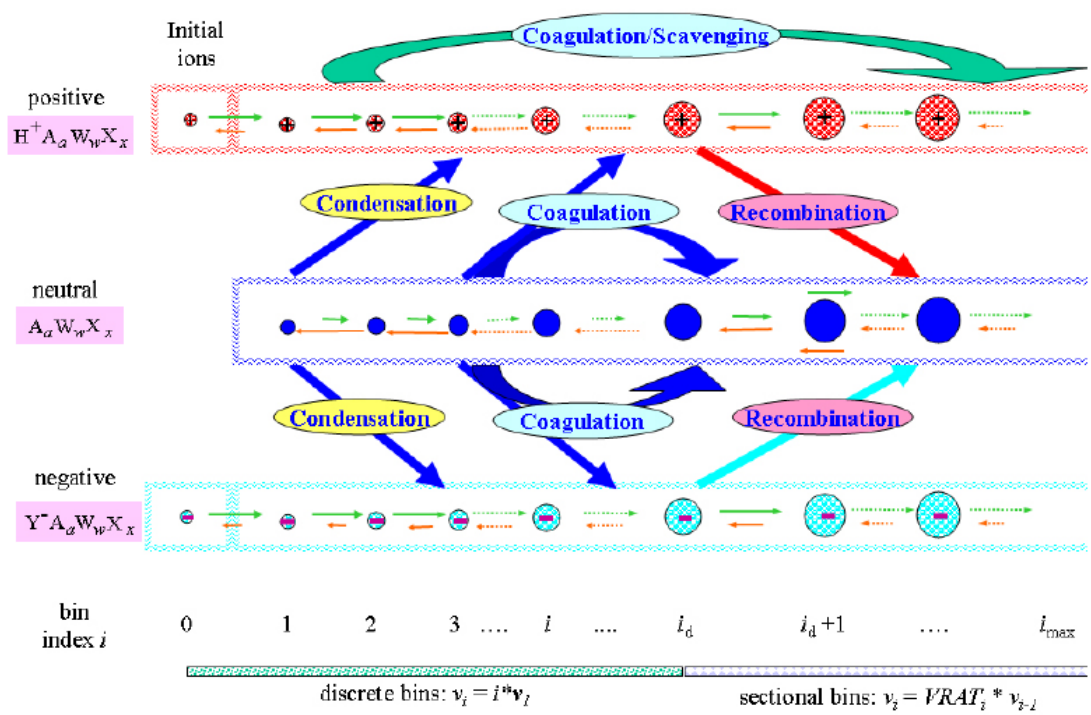

Figure 71: The kinematical models treat condensation, coagulation and recombination of charged and neutral clusters. Notice how the sizes of the small green arrows indicate increased probability for charged cluster coagulation and growth compared to neutral growth for small clusters. Yu's model predicts significant IIN under lower tropospheric conditions. Figure reproduced from Yu (2006).

Although the models of Yu and Lovejoy are similar, there is a major difference. Yu's model predicts significant growth of the cluster ions before recombination under lower Tropospheric conditions (potentially important for low clouds – see later) which provides

a significant source of new particle generation in the presence of ionisation. However, under similar conditions Lovejoy's model only finds a negligible contribution to nucleation from ions, but a relatively large contribution at mid-upper Tropospheric conditions (Figure 72). This appears to be a result of differences in the physical description of the cluster thermodynamics, and the treatment of positive ions which are explicitly allowed to evolve by Yu, but treated as a single species restricted to small ions in Lovejoy's model. However, there are large uncertainties in both these processes due to a lack of rigorous experimental data and lack of a suitably robust theoretical description of cluster thermodynamics that are valid under a wide range of atmospheric conditions

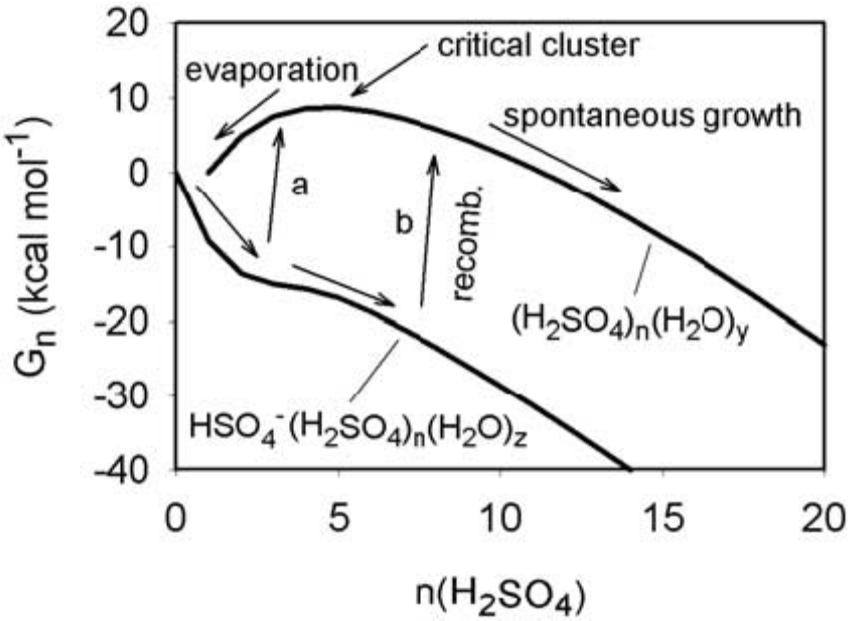

Figure 72: Gibbs free energy (G_n) versus number of H2SO4 molecules (n) in a cluster under upper tropospheric conditions. The upper branch indicates the energy barrier that must be negotiated by neutral particles before nucleation can occur. The lower branch is the equivalent energy curve in the presence of an ion – note the lack of energy barrier. Lovejoy's model suggests that under lower tropospheric conditions the energy barrier in the presence of an ion is similar to the neutral case thus limiting IIN. Figure taken from Lovejoy et al (2004).

To summarise, both models indicate that, based on current nucleation theory, there is a significant role for ionisation in the nucleation of new particles in the atmosphere, but that it is unclear as to where in the atmosphere the largest contribution should be expected.

Observational Evidence for IIN

Growth of atmospheric ions has been observed in a number of in-situ situations. At a ground based station in Tahkuse, Estonia, Horrak et al (1994; 1998; 2000), detected the growth of small ions from 1.6nm - 6nm (referred to as intermediate ions), sizes well above the critical cluster size. Both positive and negative ions were observed to grow through the intermediate ion size, however, charge asymmetry existed with higher concentrations of negative ions. It was speculated that this was due to the preferential condensation of different atmospheric trace gases onto one or other polarity.

Positively charged ion growth events have been reported in the upper troposphere by (Eickhorn et al 2002). Available instrumentation limited observations to only positive ions in the upper troposphere, thus growth events in other parts of the atmosphere or on negative ions are not ruled out. Figure 73 is a plot of two average ion spectra from this campaign, one describing the background small ion distribution (< 1 nm), and the other significant ion growth events leading to the formation of massive ions (>1.6nm). Initial ion growth between 300-1000amu (<1.4nm) was consistent with the uptake of H2SO4 under upper tropospheric conditions with realistic gas concentrations (Figure 74 dashed curve). However, condensation could not explain the growth of the massive ions. These largest ions were argued to have formed as the result of IIN producing large stable neutral particles through recombination, and then the subsequent attachment of a positive small ion rendering the particle detectable by the instrumentation.

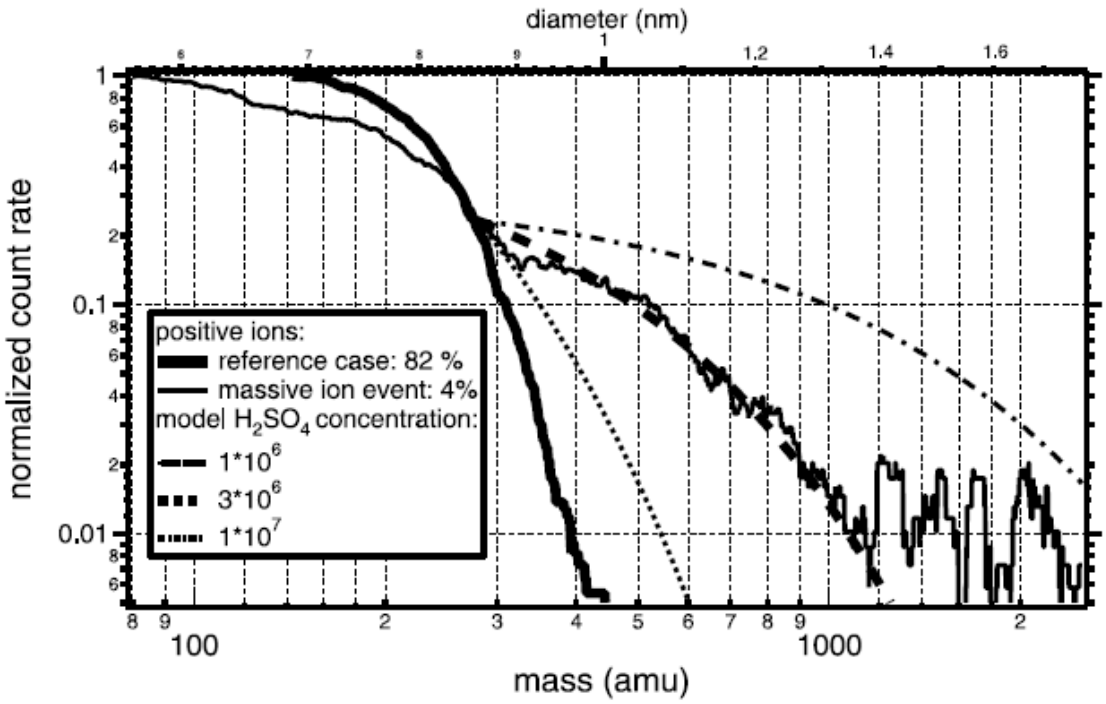

Figure 73: Positive ions (<2nm) versus normalised count rate detected in the upper troposphere (taken from Eickhorn et al (2002)). The thick solid curve represents the small ion spectrum typically found in 82% of the cloud free observations. The thin solid line indicates that massive ion growth was detected in 4% of the observations. Modelled ion spectra based on uptake of H2SO4 for various concentrations are indicated by the dashed lines.

Lee et al (2003) reported aircraft based observations of aerosol particles (both charged and neutral) in the size range 4 to 2000nm. They found very high concentrations of ultra-fine particles (< 9nm) with evidence of significant new particle nucleation in the upper troposphere/lower stratosphere (7-13km). In this campaign ions were not separately measured, however, Lovejoy's model (described in the previous section) was used to estimate the evolution of particle production and growth assuming IIN was an important mechanism. A remarkably good agreement was found between the simulations and observations up to 5 days after a nucleation event (Figure 74). Other nucleation mechanisms not involving ionisation were ruled out due to the low concentration of trace gases at these altitudes.

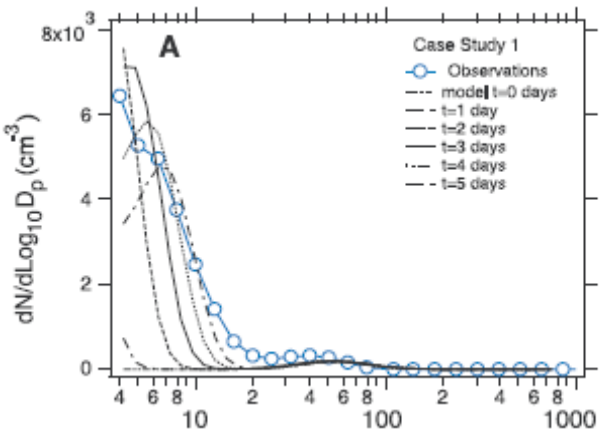

Figure 74: An example of observed particle growth in the upper troposphere and lower stratosphere measured from 4 nm and up to 2000 nm (blue curve), well above the nucleation size. Simulations using Lovejoy's IIN model (black curves) agree very well with the observations 5 days after a simulated nucleation event. Figure taken from Lee et al 2003.

Experimental Evidence of IIN

Until recently experimental efforts to explore the role of IIN had been performed under conditions that were not relevant for understanding atmospheric processes. Either unrealistically high levels of ionization were present or the concentrations of gases were far from those observed in the atmosphere. The major limiting factor has been the difficulty in controlling within a laboratory environment the very low levels of reactive gases that are present in the atmosphere. However, recent experimental efforts have now begun to explore nucleation under realistic atmospheric conditions, two of which are described below.

Ionization is not the only mechanism with the potential to stabilize the initial cluster growth. Other mechanisms have been proposed that involve the presence of trace amounts of various organic gases. The role of organic trace gases in stabilizing the nucleation of H_2SO_4/H_2O particles has been investigated in an atmospheric pressure flow tube by Berndt et al. (2006). Furan was used as the test organic and it was found that nucleation of particles in the flow tube was independent of its presence (Figure 75a). This suggests that organics are not necessarily needed, a null result which is consistent with the possibility of a mechanism involving ions. However, Berndt et al (2006) additionally measured the fractions of positively and negatively charged particles that were produced (Figure 75b).

An excess of negatively charged particles was observed between 2-3nm. However, the charged particle concentration only represented a small fraction (< 1%) of the total particle concentration. Based on this observation, Berndt et al (2006) maintained that IIN was of minor importance under their experimental conditions. However, their instrumentation was only able to detect particles, charged or neutral, down to diameters >2nm. So it is unclear why they rule out the possibility that IIN could have nucleated the particles sub 2nm that, following recombination, would then appear neutral in the instrumental detection limit above 2nm. The charge distribution observed in their experiment could then be explained from ion-aerosol attachment where the neutral

aerosol was initially formed under IIN; a similar argument was proposed by Eichkorn et al (2002) based on their in-situ observations of positive ions with diameters <2nm in the upper troposphere (see above).

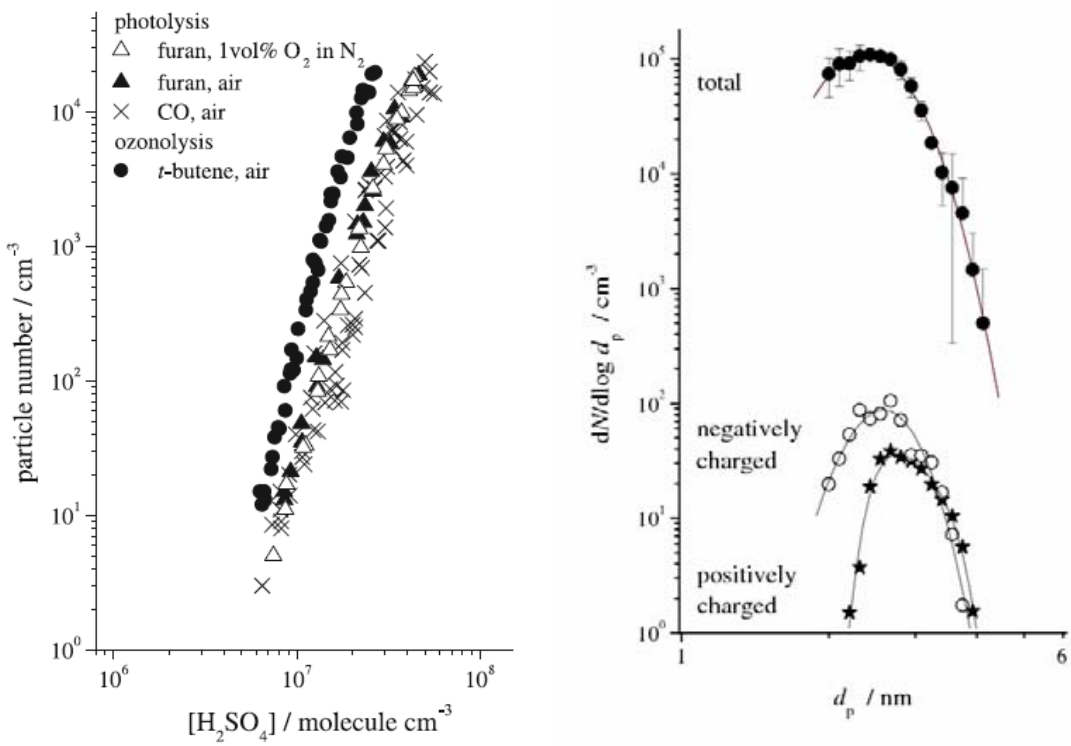

Figure 75: a – left panel) Number of H_2SO_4 molecules in a cluster versus particle concentration both with (triangles) and without (crosses) the presence of organics. The solid dots examine nucleation in the absence of UV illumination. In all cases little difference in nucleation and growth rates are observed. b – right panel) Particle diameter versus concentration for charged and total particle size distributions. Figures taken from Brandt et al (2006).

An experiment at DNSC has been designed to explicitly explore the role of ionisation in the initial nucleation process (Svensmark et al, 2006). The measurements were performed in a 7 m^3 chamber containing trace amounts of ozone, sulphur dioxide, and water vapour at concentrations relevant for the Earth's atmosphere. Ions were produced in the chamber by the naturally occurring galactic cosmic radiation and by the decay of the natural abundance of radon. The average production of ions could be additionally enhanced to between 1-60 ions/cc/s, levels that are relevant throughout the troposphere. Figure 76 indicates how aerosol concentrations (diameters > 3nm) are proportional to ion concentration within the chamber. Comparison with a simple growth model including condensation/coagulation processes provides an estimate of the nucleation rate, S, of particles that reach the critical cluster size. The results indicate that the production rate of new aerosol is proportional to the square root of the ion production rate.

The timescale for the production of a critically sized cluster was tested in the presence of an electric field applied across the chamber. By varying the field strength the lifetime of ions in the chamber could be reduced. With a suitably large field IIN should be shut down as the ions would not have time to nucleate a new particle before their removal from the chamber. The maximum field strength was 12000 V/m which is equivalent to an

ion lifetime of ≤ 2 secs, significantly less than the timescale for recombination (~300 secs) that limits the IIN mechanism described above. However, in the presence of this field particle concentrations were only reduced by 50%, and it was clear that significant nucleation involving ions was still occurring. The nucleation process under these experimental conditions definitely involved ions, not as a result of IIN, but through some other mechanism operating at a much faster time scale. It was speculated in Svensmark et al (2006) that the charge initially nucleated a cluster before detachment due to excitation by a thermal photon or the release of chemical energy within the initial cluster. The detached charge could then nucleate a new cluster, continuously repeating this cycle, until lost through recombination or aerosol attachment. These experimental results suggest that nucleation rates are limited by the residence time of a charge in a cluster necessary to produce a stable cluster. If, as the results suggest, this is much shorter than the recombination timescale, multiple nucleations from each individual charge is possible, leading to nucleation rates that are potentially much larger than the ion production rate. In contrast the maximum nucleation rate involving IIN would be limited by the ion production rate. So the proposed detachment mechanism acts as an amplification factor for new particle production involving atmospheric ionisation.

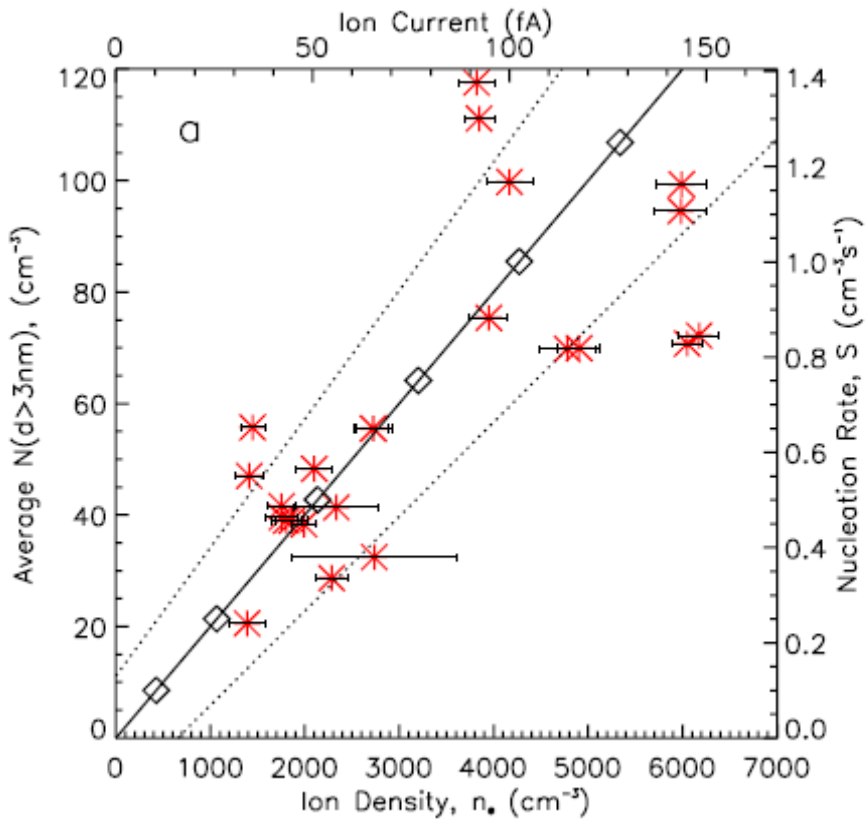

Figure 76: Ion density versus average aerosol concentration (diameter >3nm). The nucleation rate, S, on the right hand axis was estimated from a comparison with a simple growth model. The ion current on the upper axis was the physical parameter measured from which ion density was calculated. Figure taken from Svensmark et al 2006.

Low clouds

Yu's model suggests that CCN in the lower troposphere and marine boundary layer (below 5 km) are most sensitive to changes in ionisation. Under such conditions, an increase in GCR would lead to an increase in the number of aerosols, CCN and cloud droplets and hence a decrease in cloud droplet sizes. Ferek et al. (2000) have shown that an increase in aerosol concentrations due to ship exhaust can lead to drizzle suppression. This clearly has an impact on cloud microphysics and in turn implications for cloud properties. However, ship tracks are a large perturbation locally, whereas a possible GCR - CCN mechanism will be a small perturbation globally. If ionization from GCR can be shown to have a similar affect on the lower tropospheric aerosol distribution, and subsequently prolong a cloud's lifetime, it would be consistent with the cosmic ray - low cloud correlation (Marsh and Svensmark, 2000). An effect from ionisation on clouds would provide the link to climate with their strong impact on the radiative budget of the Earth.

In section 4.4 we analysed the low cloud cover with respect to correlations with various solar parameters (Figures 40 and 41 and Tables 10 and 11). If we restrict our analysis to the areas of Figure 41 where cosmic rays show a significant positive correlation with low clouds, i.e., mid-to-high latitudes, particularly over the oceans, we find an even stronger response – not in the original data, but rather in case where the solar cycle have been removed from the cloud and GCR/UV data. The response is a factor 3 stronger compared to global data.

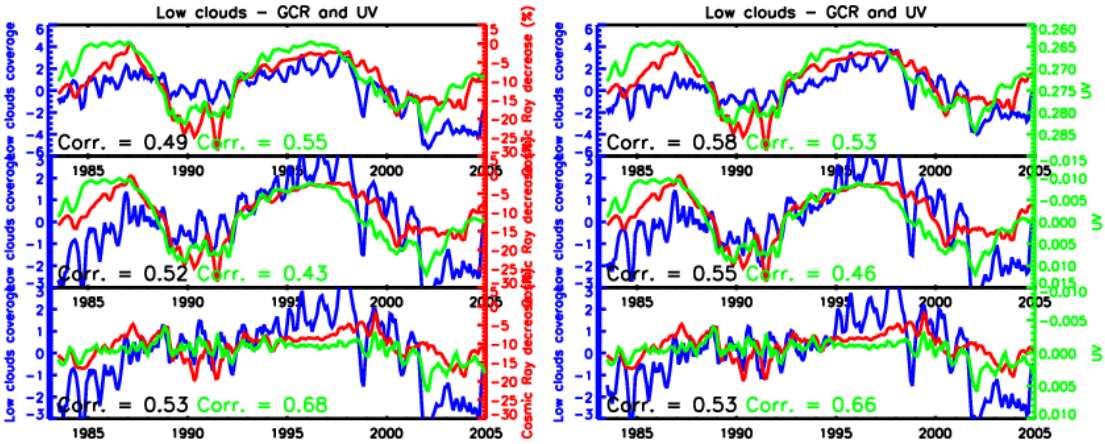

Figure 77: Correlation between GCR (red) and UV (green) and coverage of low clouds (blue). Similar to Figure 40, except that only areas with significant positive correlation with GCR is included in the analysis. Left: ISCCP data for coverage of low altitude clouds. From top: annual cycle removed, trend and internal modes removed, solar cycle removed. Right: same as left, but after adjustment with the SSM/I DMSP cloud data

5.6 Role of TSI

The total solar irradiance (TSI) is in a sense the most obvious solar parameter to single out for study when considering the Sun-climate connection. The power input received by the Earth from the Sun is the driver of Earth's climate system and the variations in TSI do correlate reasonably well with the variations seen in the climate. However, the brute variations in power received at Earth are not strong enough to explain the variations in climate that are observed. Variations in TSI over a solar cycle of 1.3 W/m^2 at the top of the atmosphere translates to 0.23 W/m^2 at the surface. With a climate sensitivity of 0.5-0.8 $K/(W/m^2)$ this corresponds to a change in tropospheric temperature of 0.14-0.18 K. The observed variations in tropospheric temperatures over a solar cycle are, however, approximately 0.5 K. For TSI to be the driver of the climate variations observed some sort of amplification or feedback mechanism must therefore be in place.

The influence of TSI on the climate is multifaceted. Variations in TSI translate to different heating in various layers of the atmosphere (though UV here plays the major role), heat absorption in the oceans with different time scales from those of the atmosphere, differential heating over land and oceans, etc. These primary influences from TSI will in turn alter such things as atmospheric circulation, water vapour content in the atmosphere, and cloud cover. Effects from these secondary phenomena may then feed back into the energy absorbed by the climate system from solar irradiation, for example via changes in the Albedo, possibly enhancing the effects of TSI variations.

Due to the geographically heterogeneous nature of solar influence on climate and the rather complicated feedback mechanisms involved in solar forcing of the climate any simple explanation of TSI-climate connections is likely to fail, except in limited cases such as variations in sea surface temperature that seem to be at least partly explainable by simple energy balance considerations.

TSI and tropospheric temperature

Satellite measurements of TSI started in November 1978 and have been continued since by various instruments. These instruments do not agree to better than 0.2% in the absolute value of TSI (see Figure 78), but in relative changes of TSI they agree to better than 0.01%. Fröhlich and Lean, 1998, and Lee III et al., 1995, have constructed continuous time series of TSI from these satellite data from 1978 to the present, fluctuating around 1367 W/m^2. Reconstructions of TSI based on proxy data, e.g., sunspot number, have been constructed going back through the Maunder minimum (Lean et al., 1995, Hoyt and Schatten, 1993, and others). These reconstructions agree qualitatively, though in absolute numbers there are significant differences. In fact, just going back 1-2 decades prior to the onset of satellite observations of TSI various reconstructions of TSI differ by as much as the variability within a solar cycle. This must be borne in mind when using reconstructed TSI for any climate correlation purpose.

Figure 79 shows TSI together with global mean tropospheric temperature anomaly. The correlation is reasonably good, 0.31, increasing to 0.61 when using a 12 month running mean of both TSI and temperature. Over a solar cycle TSI varies approximately 1.3 W/m^2 from solar min to solar max. With the geometric factor of ¼ and the Earth's Albedo of

0.7 this translates to a forcing of the atmosphere of 0.23 W/m^2. With a climate sensitivity of 0.6-0.8 K/(W/m^2), (e.g., Appendix 9.1, Houghton et al., 2001), estimated from the average response of climate models to a doubling of CO2 this translates to a response of 0.14-0.18 K between solar max and solar min. However, the tropospheric temperature varies with approximately 0.5 K over a solar cycle. A direct forcing from TSI is therefore not sufficient to explain the variation of tropospheric temperatures and some amplification mechanisms would be required for TSI to be the main driver of the tropospheric temperature variability.

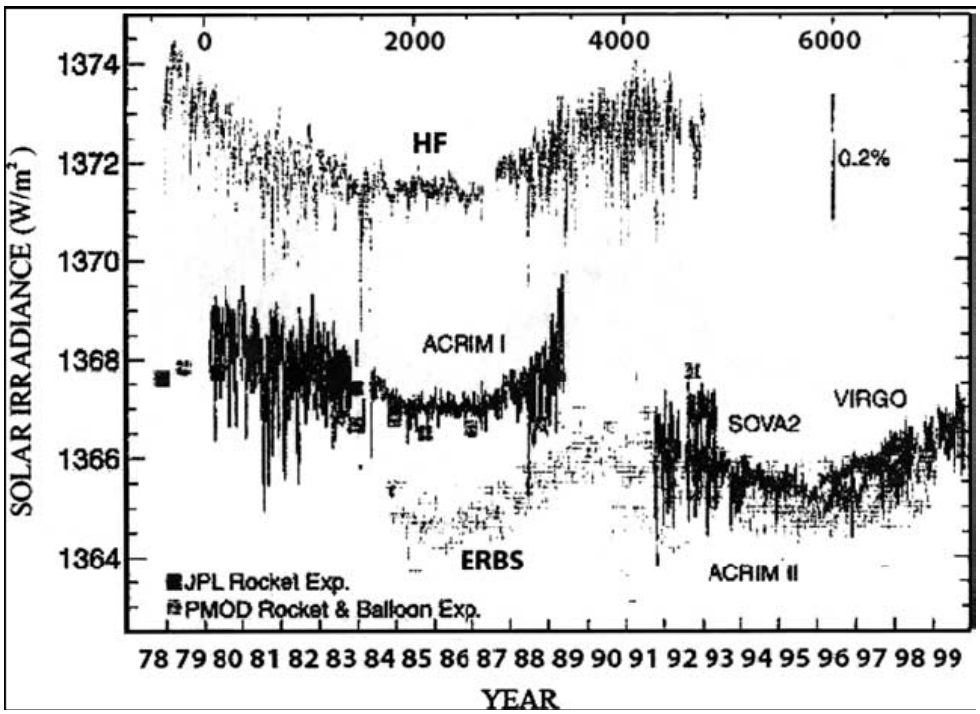

Figure 78: Daily average values of TSI from a number of radiometer experiments since 1978. From Fröhlich, 2000.

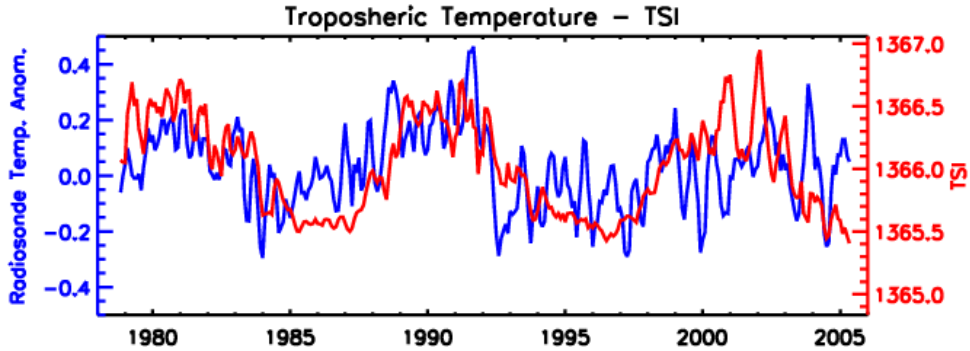

Figure 79: TSI and global tropospheric temperature anomaly. The temperature data have a linear trend and internal modes of variability removed. Correlation coefficient is equal to 0.31, increasing to 0.61 when using a 12 month running mean.

Sea surface temperatures

Sea surface temperatures display some correlation with changing solar activity. Using temperature data from ocean going ships and sunspot number as a measure for solar activity Reid (1987, 1991, 2000) has demonstrated this going back to the mid 19th century. Figure 80 shows the global sea surface temperature anomaly compared to sunspot number. In Figure 81 we show the SST temperature from the CRU surface temperature data set with TSI. The correlation is rather poor, 0.09, increasing only to 0.1 when using 12 month running averages. Introducing a lag increases the correlation to 0.13 for a lag of 12 months.

White et al. (1997) investigated the response of SST to changing solar activity using band-passed-filtered surface marine weather observations (1900-1991) and bathythermograph upper ocean temperature profiles (1955-1994). They found clear signals in power spectra, singular spectrum analysis, and empirical orthogonal functions corresponding to the solar 11- and 22-year cycles, see Figures 82 and 83. Moreover, they found that these signals were consistent across the three major oceanic basins. The band-passed-filtered data for the SST anomalies yielded solar-related components with amplitudes of 0.04 K and 0.07 K for the 11-year and 22-year cycles, respectively, associated with TSI amplitudes of 0.5 W/m^2 at the top of the atmosphere (1.0 W/m^2 max to min difference) corresponding to a climate sensitivity of the oceans of 0.08-0.14 K/(W/m^2).

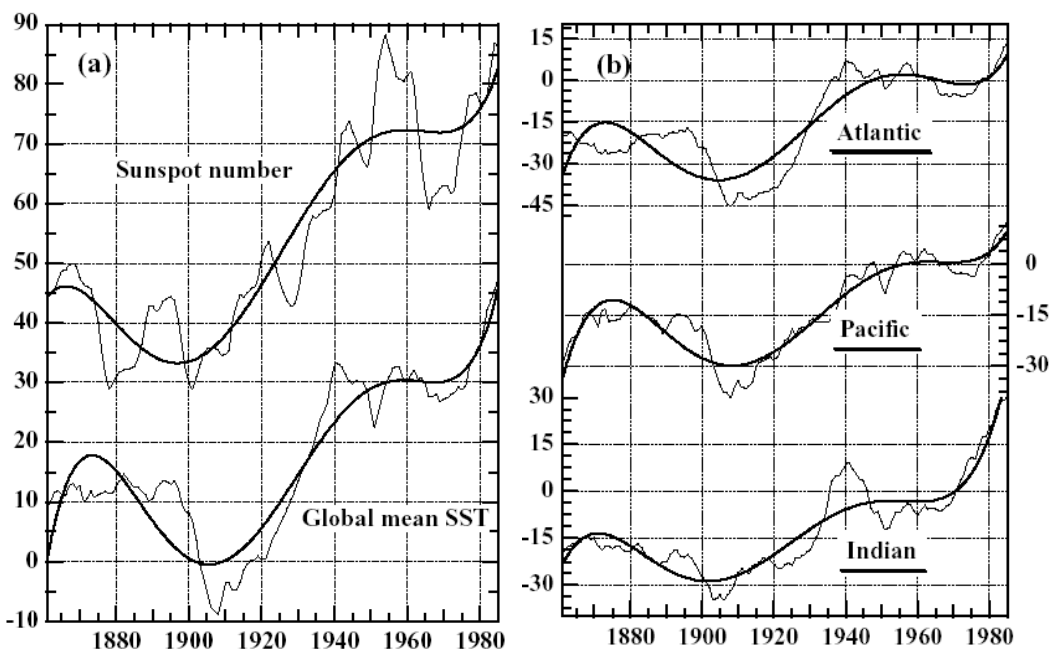

Figure 80: From Reid (2000). Sea surface temperature anomalies in 0.01 K (lower left: global average, right: basin averages) compared to sunspot number (upper left). To emphasize to the long term similarity between the data sets 7th degree polynomial (fat) have been fitted to the curves.

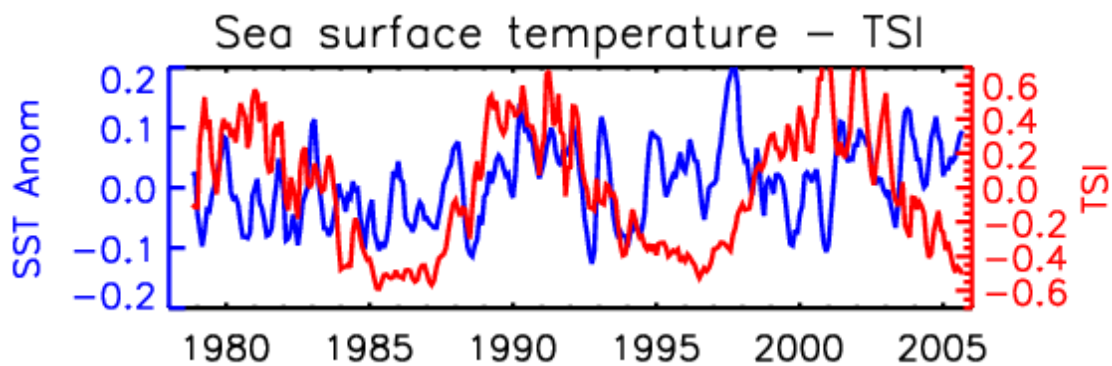

Figure 81: SST from the Climate Research Unit's surface temperature data set and TSI. The correlation over the past 25 years is rather poor with a coefficient of 0.09.

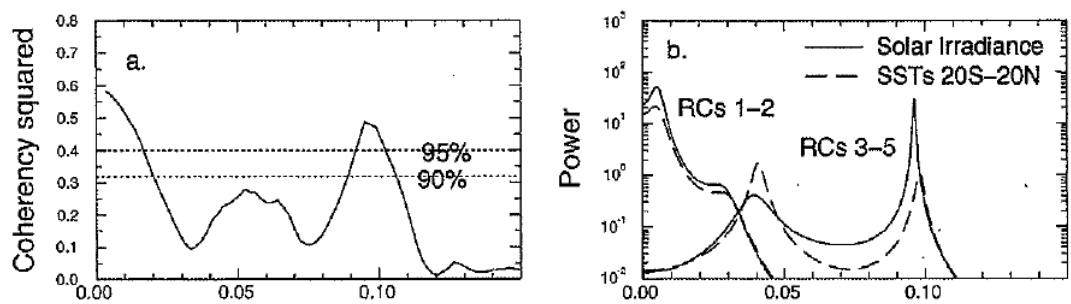

Figure 82: From White et al. (1997). Left: coherency spectrum for annual time series of global SST and TSI anomalies. Right: Maximum entropy spectrum of leading reconstructed components from two-channel singular spectrum analysis of SST and TSI. The peaks correspond to approximately 11- and 22-year cycles.

White et al. (1997) then consider the global average heat budget of the upper ocean (Gill, 1982) $\partial T/\partial t + KT = S/(\rho CH)$, where T is the temperature anomaly, S is the irradiance anomaly at the sea surface, ρ and C are the density and specific heat of sea water, H is the depth the solar signal penetrates uniformly into the upper ocean, and K is the inverse of the dissipation time scale. K^{-1} is estimated from the time lags observed in the singular spectrum analysis to be 1-1.5 years for the 11-year cycle and 2-3 years for the 22-year cycle and the penetration depth H is correlations in the bathythermograph data to be 40-60 m for the 11-year cycle and 40-80 m for the 22-year cycle. This results in an upper ocean response to a top of the atmosphere TSI signal of 0.5 W/m^2 of 0.01-0.03 K for the 11-year cycle and 0.02-0.05 K for the 22-year cycle. Furthermore, they find that the phase lags observed agree well with what comes out of considering the equilibration time scale from a Stefan-Boltzmann law calculation.

The model derived estimates of the sensitivity of the ocean temperatures to a TSI signal of 0.5 W/m^2 of is on the low side, 0.01-0.03 K compared to the observed 0.04 K for the 11-year cycle, and 0.02-0.05 K compared to the observed 0.07 K for the 22-year cycle. The simplicity of the model, however, may well be responsible for this. Feedback mechanisms with the atmosphere could change the model response to agree better with the observations.

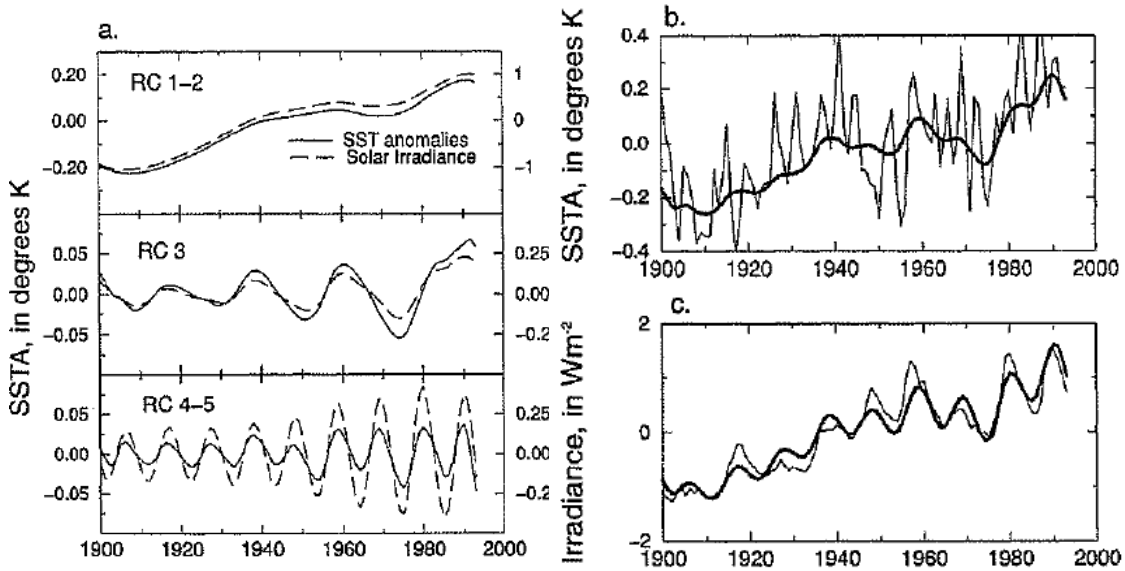

Figure 83: From White et al. (1997). Reconstructed components from singular spectrum analysis of SST and TSI. Left: the RCs of SST and TSI for RC=1-2, RC=3 and RC=4-5. Right: The RCs 1-6 for SST and TSI (fat curve) compared to the unfiltered data. The SST still have a considerable signal not account for by the RCs 1-6 whereas TSI is well described by RC 1-6.

TSI and GCMs

There are a large number of studies with the effects of changing TSI in general circulation models. Haigh (1999) gives a short introduction to some of these results. In general, the models all reproduce an increase in global average surface air temperature with increasing solar radiation, however they differ strongly in the geographical distribution of this warming, e.g., showing stronger responses in South America and the Arctic Ocean (Rind and Overpeck, 1993), mid- to high-latitudes (Nesme-Rimes et al., 1993), or northern hemisphere land areas (Cubasch et al., 1997). Haigh comments that the lack of a clear pattern between the models is an indicator "that the physical representations, in at least some of the models, are inadequate to the task."

GCMs are often applied in the detection and attribution of the component causes of climate change (see e.g. IPCC reports). In this technique the geographical *patterns* of response to particular forcing factors are pre-determined from the GCMs; it is assumed that the time-dependences of the forcing factors are known but that the *amplitudes* of the climate responses are unknown. The task is then essentially to perform a multiple regression analysis on a dataset to find which weighted combination of the response patterns best matches the data, taking into account known errors/uncertainties in both the data and patterns. Stott et al (2003), however, suggest that this method might have a bias against weak signals lost in the sampling noise. If that is the case these studies could underestimate the importance of natural factors and attributed a larger effect to anthropogenic causes of climate change. By running experiments in which natural forcings were enhanced Stott et al found that their model appears to be underestimating

the solar influence by a factor of 2 or 3, while slightly overestimating the role of green house gases (GHGs). The authors have some caveats and reservations about their results but note that the conclusion is supported by two other studies: Hill et al. (2001) find that models underestimate the solar response in tropospheric temperatures by a factor of 2 to 3, and North and Wu (2001) find an underestimate for near-surface temperatures of about 2.

Meehl et al. (2003) have investigated the climate response over the 20th century to both solar and greenhouse gas forcing. Using model runs of a fully coupled global ocean-atmosphere-sea ice-land surface model (Washington et al. 2000), with forcings from greenhouse gases+sulfate, from solar variations (TSI from Hoyt and Schatten, 1993), and from both they produced the global temperature anomalies shown in Figure 84. The combination of GHG+sulfate and solar forcing reproduces the observed surface temperature anomalies fairly well although the spread of uncertainty does not preclude the existence of an underestimate of the solar influence such as found by Stott et al (2003).

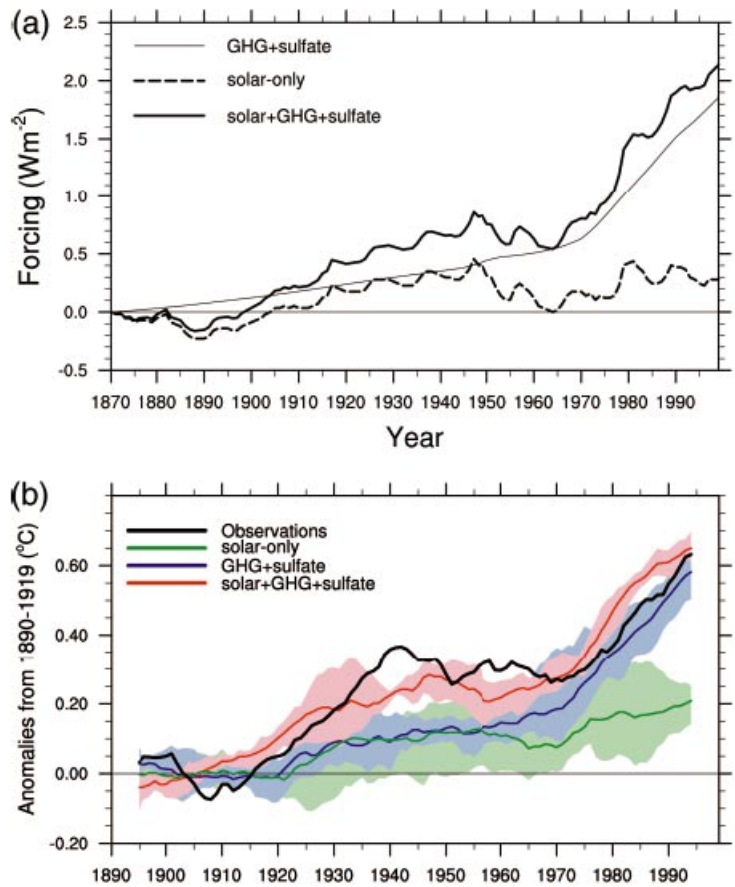

Figure 84: From Meehl et al., 2003. (a) Top of the troposphere radiative forcing used in the model for GHG+sulfate, solar, and both. (b) Global annual mean surface air temperature for observations and model outputs. Only the combined GHG and solar forcing reproduces the observations.

The authors use the separate runs for solar, GHG+sulfate, and solar+GHG+sulfate to focus on the seasonal and regional response for solar forcing in the early 20th century and GHG+sulfate late in the century. Of particular importance is an apparent non-linear effect of the solar forcing that is seen when comparing model runs with solar forcing only and residuals between model runs with solar+GHG+sulfate and GHG+sulfate only. The study shows that the effects of the solar forcing are considerably larger in the latter case, i.e., when the solar forcing is working together with greenhouse gases. The increased warming arising from the solar forcing occurs mainly at northern hemisphere high altitudes, with a maximum of 0.7 K in the late 1940s. This is an effect associated with an ice-Albedo feedback that has been observed in other model studies. To demonstrate the non-linear effect of using solar forcing only and solar forcing combined with GHG+sulfate the authors focused on the early 20th century where the solar forcing increased strongly. They showed that though the solar irradiation increased over the early 20th century this has not resulted in a net increase in solar irradiation absorbed at the surface. Small increases over the oceans are offset by similar decreases over land. This is associated with increases in cloud cover over land. The net infrared radiation has consistently increased with a similar effect whether the forcing is solar or GHG+sulfate. This increase in infrared radiation can be explained by ocean warming resulting in increases in water vapour and cloud cover over both land and oceans.

The response is quite different when the solar forcing is calculated as the difference between solar+GHG+sulfate and GHG+sulfate only. Now, the net solar radiation absorbed at the surface is consistently increasing over the early 20th century. At least for northern summer this is consistent with a decrease in cloud cover. It is also interesting to note that the land-ocean differential in net solar radiation is stronger in the solar residual case and that this could enhance the land-sea temperature gradients. Combined with the corresponding changes in net IR at the surface the solar-residual has a larger land forcing contrast in the northern summer season than the solar only case, and this possible non-linear behavior could have an effect on tropical monsoon areas.

6. Modelling

Global Climate Models (GCMs) are computer simulations of the state of the atmosphere-ocean system and its variability. They have become increasingly important as tools of the climate scientist. Using numerical representations of processes involved, GCMs enable studies of complex interactions within the climate system, their evolution and sensitivity to internal or external forcing factors.

The atmosphere is a continuous, compressible fluid resting on the surface of a rotating planet. By applying some of the basic laws of physics - conservation of energy, conservation of mass, Newton's 2nd law of motion and the ideal gas law – to this fluid we can acquire an understanding of the main features of the global atmospheric circulation. Global Climate Models (GCMs) simulate the state and evolution of the atmosphere through solving the equations of motion at all points on a grid discretised in space and time. The starting point, considering first only dry air, is equations of continuity and momentum, the equation of state for the atmosphere, and the First Law of Thermodynamics. These provide 6 equations for 6 unknowns, the velocity u (three components), the pressure p, the density ρ, and the temperature T. Given initial and boundary conditions, some properties of dry air (M, C_p, η) and, importantly, a grid of values of the diabatic heating rate Q the equations can be solved in space and iterated in time to produce 4-dimensional fields of the variables. There are, however, a number of complications that make this procedure somewhat less simple than it may first appear:

1. The specification of Q depends on model state. This requires that the radiative transfer equation be solved as a function of the model fields of temperature and composition at each time-step.
2. The presence of water is fundamental to the state of the atmosphere providing sources/sinks of latent heat and clouds which have a huge impact on Q. Thus water vapour has to be transported within the model and a scheme to represent convection and condensation needs to be included.
3. The discretisation in space and time results in rounding errors and also, possibly, numerically unstable solutions.
4. Some representations need to be included for factors which occur on scales smaller than the grid size but nevertheless impact the large scale, for example surface orography and turbulence.
5. Constraints on computer resources (processing speed, memory, storage) place limitations on what is possible, requiring compromises to be made in grid resolution and/or the detailed representation of particular processes.

Below is presented short description of these 5 points.

Radiative processes

The global average equilibrium temperature of the Earth is determined by a balance between the energy acquired by the absorption of incoming solar radiation and the energy

lost to space by the emission of thermal infrared radiation. The amount of solar energy absorbed depends both on the incoming irradiance and on the Earth's reflective properties. If either of these changes then the temperature structure of the atmosphere-surface system tends to adjust to restore the equilibrium. The value for the incoming radiation, 342 Wm^{-2}, is equivalent to a total solar irradiance at the Earth of 1368 Wm^{-2} averaged over the globe. Of this 31% (107 Wm^{-2}) is reflected back to space by clouds, aerosols, atmospheric molecules and the surface, with the clouds playing the most important role, so that only 235 Wm^{-2} is absorbed by the Earth system. 20% (67 Wm^{-2}) of the incident radiation is absorbed within the atmosphere leaving 49% (168 Wm^{-2}) to reach and heat the surface. The temperature and emissivity of the surface are such that 390 Wm^{-2} of infrared energy are emitted into the atmosphere. Only 40 Wm^{-2} of this, however, escapes to space with the remainder being absorbed by atmospheric gases and clouds. The atmosphere returns 324 Wm^{-2} to the surface. The energy balance at the surface is achieved by non-radiative processes such as evaporation and convection. The radiation balance at the top of the atmosphere is achieved by the 195 Wm^{-2} of heat energy emitted to space by the atmosphere and clouds.

Absorption by the atmosphere of solar radiation depends on the concentrations and spectral properties of the atmospheric constituents. Prominent absorption features are due to specific gases with molecular oxygen and ozone being the major absorbers in the ultraviolet and visible regions and water vapour and carbon dioxide more important in the near-infrared. The solar irradiance at any point depends on the properties and quantity of absorbing gases in the path above. If the solar spectral irradiance varies then, without a change composition, the spectral heating rate just varies in proportion to the irradiance. If, however, as is actually the case, the atmospheric composition also responds to solar variability for example through photochemistry then this will affect both radiative fluxes and heating rates in a non-linear fashion.

In order to simulate the radiation budget, and to calculate the radiative component of the diabatic heating term, Q, it is necessary to invoke the radiative transfer equation. This gives the change in intensity of radiation of wavelength λ in direction between positions s and s+ds. Even to evaluate this one equation requires a large number of computations but to evaluate the diabatic source term, Q, in a GCM it is necessary to integrate the expression over all angles and wavelengths. Clearly it is not computationally feasible to incorporate in a GCM the full details of the expression and a range of approximations need to be made. Some of these are listed, along with the associated reduction in typical numbers of calculations, in Table 16. Each approximation brings a loss of accuracy and the choice of radiation scheme will be determined by a compromise between required accuracy and computational demands. The final row of the Table gives the Newtonian cooling approximation in which heating is assumed proportional to local temperature. This is usually not sufficiently accurate (especially in the troposphere) and most GCMs adopt a band model approach. The number of spectral bands necessary also depends on the height regime of the model. For example, if it is intended to assess the effects of solar UV radiation in the middle atmosphere then extra shortwave bands need to be added to GCM radiation schemes which have been designed for use in the troposphere.

Approximation	Sum over spectral lines in expression for optical depth	Integration over height in expression for optical depth	Integration over height of irradiance contributions	Integration over zenith angle	Integration over wavelength	Total number of calculations	Number of exponentials in transmittance and Planck functions
None	1-10	10-100	10-100	1-10	10^4	$10^6 – 10^{10}$	10^5-10^6
Curtis-Godson	1-10	-	10-100	1-10	10^4	$10^5 – 10^8$	10^5-10^6
Diffusivity	1-10	-	10-100	-	10^4	$10^5 – 10^7$	10^5-10^6
Band model	-	-	10-100	-	1-10	$10 – 10^3$	$10 – 10^3$
Newtonian cooling	-	-	-	-	-	1	-

Table 16: Approximations in the radiative transfer equation (neglecting scattering) and the number of calculations needed for each component integral. Note that the total number is the product, not the sum, of the components because the integrals are nested. The final column gives the number of exponential functions that need to be estimated – each adding a further computational overhead.

Clouds

Clouds have a major impact on the heat and radiation budgets of the atmosphere. They transport latent heat from the oceans to the atmosphere. They reflect solar radiation back to space, reducing the net incoming radiative flux, and they trap infrared radiation, acting in a similar way to greenhouse gases. The magnitudes of these effects depend on the location, altitude, time of year and also the physical properties of the cloud.

Uncertainties and approximations in the representation of cloud formation and cloud radiative properties remain a major cause of uncertainty in current climate prediction models. Cloud formation depends on factors ranging from local topography, large scale flow and the temperature and humidity of air masses to the microphysical composition of particulates in the atmosphere. With grid sizes of the order of 100km in the horizontal and 1km in the vertical, there is no possibility of GCMs being able to reproduce realistic cloud structures down to convective scale so they include a variety of parameterizations for cloud prediction.

These schemes include methods for predicting the occurrence of cloud and precipitation and for representing the effects of sub-gridscale convection. There are many varieties of cloud prediction scheme; the simplest estimates high, medium, low and convective cloud cover based on empirical relationships between cloud, relative humidity and vertical velocity (e.g. Slingo 1987) and diagnose precipitation from cloud water (or ice) only. It is necessary also to include the effects of sub-gridscale convection because without these, averaged over a grid box, vertical velocities would be too slow to produce realistic transport of moisture, condensation and latent heat release. The convection schemes parameterize the vigorous vertical transports carried out by updrafts and downdrafts associated with individual clouds. Numerous assumptions are made in convection schemes which are adjusted to optimize the schemes' overall performance so that they may work well in some situations and not others.

On the largest spatial scales and annual timescales these parameterizations have limited success. Figure 85 shows the zonal annual mean cloud cover as observed and as predicted by an international selection of climate models. Most of the models reproduce the

maxima in cloud observed in the tropics and in mid-latitudes but all underestimate the amount of cloud in the tropics and sub-tropics and overestimate it in mid- to high latitudes. For local cloud on timescales of hours, however, the predictions can be very poor.

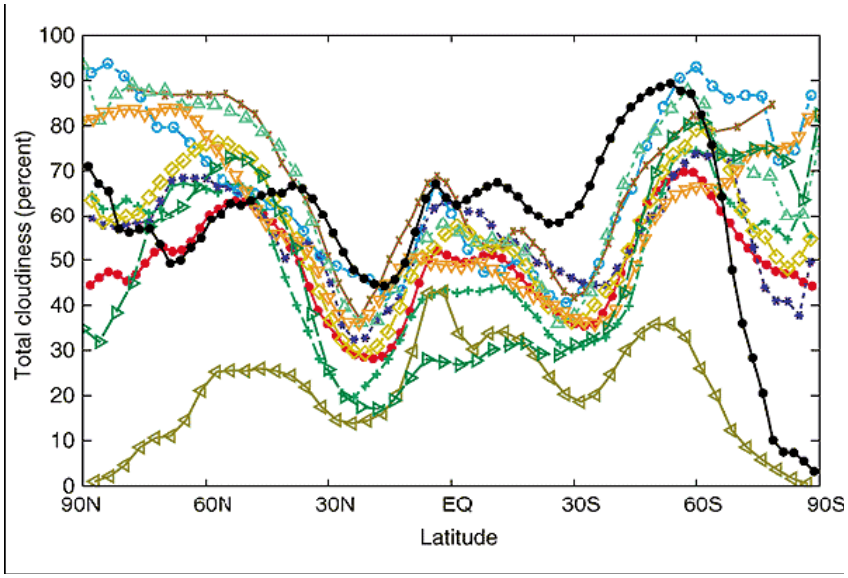

Figure 85: Zonal mean cloud cover from ISCCP data (in black) and as predicted by ten different global circulation models (coloured curves). From IPCC (2001).

Even disregarding the problems associated with predicting cloud distributions the models still need to calculate the effects of the cloud on the radiation fields. Again gross approximations have to be made in terms of the microphysical properties of the water or ice particles and the method by which to carry out necessary integrations over spectral and spatial variables.

Discretization

The equations of motion cannot be solved analytically so numerical techniques need to be employed. Approximate solutions can be found using finite difference or series expansion methods in which the continuous functions of the variables are replaced by values on a finite number of spatial and/or temporal nodes (see e.g. Jacobson, 1999). The finite difference approach involves mapping the variables onto a grid and replacing the differential operator, ∂, by a discrete difference, Δ. There is no unique way of accomplishing this and the choice of approximation will depend on requirements with regard to accuracy, stability and convergence for the equation(s) in question.

Numerous schemes have been constructed using various combinations of approximations for the time and space differentials. Higher order approximations tend to be more stable but to smooth out fine structure in the fields. The stability of a scheme also depends on the grid-spacing; for example, the finite difference form of the advection equation tends to become unstable if the time step is greater than the ratio of the grid length to the maximum speed (i.e. the shortest time taken to cross a grid box).

Turbulence

At the surface of the Earth the air flow is necessarily zero but in a thin (50-300m) layer above the surface wind speeds increase logarithmically with height creating a shear layer. This wind shear produces eddies, on all scales up from the molecular, which result in the turbulent transfer of heat and momentum both horizontally and vertically. Surface obstacles such as rocks, trees, buildings also give rise to wind shear and turbulence while surface heating causes thermal turbulence and convection throughout the atmospheric boundary layer (extending up to between 0.5 and 3km). Clearly it is not possible for a model with a horizontal grid spacing of hundreds of kilometers and a vertical resolution of a few kilometers to simulate the details of these eddies but some representation needs to be included of their bulk effect on the momentum and heat budgets. This is usually done using a tensor **K** of eddy diffusion coefficients so, for example, the momentum equation will include an additional term where the eddy diffusion coefficients can be specified as functions of location and season or determined as a function of model state (e.g. wind shear, static stability). This approach is also sometimes used at the top of a model domain, not so as to represent any physical process but merely to ensure that high wind speeds do not develop near the upper boundary.

Models of reduced complexity

For climate simulations with GCMs it is often desirable to carry out an ensemble of runs, each with slightly different initial conditions, such that the spread in results provides an indication of intrinsic uncertainty. This imposes a significant overhead in terms of computing requirements. Computational demands also constrain possibilities with regard to the inclusion of what would be regarded as the best possible representation of all the known relevant physical and chemical processes. In practice, however, the latter may not be desirable – sometimes interpreting GCM output is almost as difficult as interpreting data from the real atmosphere. Under such circumstances it is often more useful to use simplified models which focus on one (or more) aspects of a problem at the expense of the treatment of other features which are deemed to be less important in the particular context.

A common approach is to reduce the dimensionality of the model, at the expense of a complete representation of dynamical processes. For example, 2D (latitude-height) models, in which zonal mean quantities are considered, have been successfully used in studies of stratospheric photochemistry and radiative transfer, including the response to solar variability (see e.g. Haigh, 1994). Although there is no overt longitudinal variability in 2D models, the diurnal variation in solar zenith angle is included in the photochemical and radiation schemes. 1D (height only) Energy Balance Models, which have no transport apart from vertical diffusion, can provide a useful first order estimate of global mean response to radiative forcing perturbations.

Alternatively, if the focus of attention is on a process occurring in a particular region of the atmosphere, it may be useful to restrict the spatial extent of the model, although care must then be taken with boundary conditions. Some interesting work on links between solar variability, the QBO and polar stratospheric temperatures has been carried out with a model in which the lower boundary was set at the tropopause, thus avoiding the necessity to simulate the complex cloud-radiation and boundary layer effects within the troposphere and allowing long integrations to take place (Gray et al, 2005).

Another approach is to simplify the treatment of certain processes in order to focus on others. For example, studies of coupling between the tropical lower stratosphere and tropospheric circulations, aimed at investigating potential solar amplification mechanisms, have been carried out by Haigh et al (2005) using a model in which all diabatic processes have been reduced to Newtonian relaxation to a reference equilibrium temperature. This maintains the full representation of dynamical processes but avoids the necessity for detailed calculations of Q thus allowing numerous experiments to be carried out.

Modelling studies of the solar modulation of climate via UV have traditionally been carried out by first estimating the predicted ozone changes between solar minimum and solar maximum (or 20th century versus Maunder Minimum values) using 2-D models that include relatively sophisticated chemical schemes. These monthly-averaged, zonally-averaged ozone changes are then used as input to the radiation schemes of full GCM simulations. In this way, the temperature and circulation response to the ozone changes can be assessed, although there is no possibility for those temperature and circulation changes to interactively feed back onto the ozone distributions. The prime methodology employed to assess the impact of including these additional ozone changes is to carry out model simulations with only TSI changes and compare them with simulations with both TSI and ozone changes. Most 'process' modelling studies, that seek to simulate the solar signal and thence explore the process mechanisms, employ models that extend from the ground to around 80 km in order to fully resolve the ozone distribution in the stratosphere. Most of the modelling studies are unable to reproduce the secondary temperature (and ozone) maximum in the lower stratosphere. This is important because it not only represents a deficiency in the simulation of the middle atmosphere itself but also means that the stratospheric anomaly required as forcing for any stratosphere-troposphere coupling mechanisms is not adequately provided. It suggests an underestimation of the modelled dynamical feedback through a modification of the meridional circulation and this requires further investigation. There are also many deficiencies in the model simulations of the interaction between the solar and QBO influences (Labitzke et al. 2002) and these may be related to the same dynamical problems. Very few of the models employed include an adequate gravity wave parameterization scheme and this may be one factor that requires improvement (Arnold and Robinson, 2003).
Because of computing resource constraints, GCM simulations of solar influence have usually consisted of two 20-30 year runs, under perpetual solar minimum conditions and perpetual solar maximum conditions respectively, and the difference between the two runs used as an estimate of the peak-to-peak solar signal. By running for many years in 'perpetual' mode like this, the statistical significance of the results is substantially improved. In order to gain the equivalent statistical significance from a single simulation in which the time-varying 11-year solar signal is imposed, the simulation would need to be many hundreds of years long. Employing a coupled ocean-atmosphere model in which the ocean temperatures can adjust to the imposed solar changes is inappropriate for integrations of this type employed for 11-year solar cycle studies, because the atmosphere is never actually in solar minimum or maximum for long enough for the ocean to adjust to any great extent. In this case, the models are used with observed or climatological-

mean sea surface temperatures imposed at their lower boundaries. On the other hand, estimates of longer term solar changes, such as those between 20th century and Maunder Minimum values, are more appropriately carried out using a coupled model in which the ocean temperatures are able to respond and feedback onto the atmosphere component of the model.
Recently, improved computing capabilities have allowed the development of GCMs that include fully-coupled chemistry schemes so that improved feedback is possible not only from the ozone changes on to the temperature and circulation patterns but vice versa. However, the use of these fully-interactive chemistry GCMs for studies of the solar cycle influence is still at a relatively immature stage (e.g. Labitzke et al. 2002, Tourpali et al. 2003, Egorova et al. 2004, Haigh et al. 2004, Langematz et al. 2005, Schmidt et al. 2006) and runs with both coupled oceans and chemistry have yet to be carried out.

Below are given tables on the solar forcing parameters that could be investigated in GCM experiments (Table 17), the relevant physical mechanisms (Table 18), and proposed GCM experiments (Table 19).

Table 17: Solar forcing parameter requirements for each Mechanism.

Mechanism	Solar input	Time-scale	Requirements	Availability
TSI	Total solar irradiance	11-year cycle	Many cycles $\Delta t \sim 1$ month	Yes, for nearly 3 cycles, although absolute value and underlying trends not well established.
		Multi-decade to century	$\Delta t \sim 1$ year (annual cycle imposed)	Yes – based on proxy solar activity measures - but absolute value not known and large uncertainties in secular trend.
Radiative heating of the middle and lower atmosphere	UV/visible spectral irradiance	27-day cycle	$\nu \sim 4{,}000 - 86{,}000\text{cm}^{-1}$ $\Delta\nu \sim 4{,}000\text{cm}^{-1}$ Many cycles (at solar max) $\Delta t \sim 1$ day	Yes, for 3 solar maxima.
		11-year cycle	$\nu \sim 4{,}000 - 86{,}000\text{cm}^{-1}$ $\Delta\nu \sim 4{,}000\text{cm}^{-1}$ Many cycles $\Delta t \sim 1$ month	Yes, for nearly 3 cycles, but data not contiguous and uncertainties in spectrum.
		Multi-decade to century	$\nu \sim 4{,}000 - 86{,}000\text{cm}^{-1}$ $\Delta\nu \sim 4{,}000\text{cm}^{-1}$ $\Delta t \sim 1$ month	No

UV production / destruction of ozone	UV spectral irradiance	Solar flares	$\nu \sim 14{,}000 - 23{,}000\text{cm}^{-1}$ $\Delta\nu \sim 200\text{cm}^{-1}$ and $\nu \sim 28{,}000 - 86{,}000\text{cm}^{-1}$ $\Delta\nu \sim 500\text{cm}^{-1}$ Many flares $\Delta t \sim 1$ hour	Records of flare events but not of spectra.
		27-day cycle	$\nu \sim 14{,}000 - 23{,}000\text{cm}^{-1}$ $\Delta\nu \sim 200\text{cm}^{-1}$ and $\nu \sim 28{,}000 - 86{,}000\text{cm}^{-1}$ $\Delta\nu \sim 500\text{cm}^{-1}$ Many cycles (at solar max) $\Delta t \sim 1$ day	Yes, for 3 solar maxima.
		11-year cycle	$\nu \sim 14{,}000 - 23{,}000\text{cm}^{-1}$ $\Delta\nu \sim 200\text{cm}^{-1}$ and $\nu \sim 28{,}000 - 86{,}000\text{cm}^{-1}$ $\Delta\nu \sim 500\text{cm}^{-1}$ $\Delta\nu \sim 400\text{cm}^{-1}$ Many cycles $\Delta t \sim 1$ month	Yes, for nearly 3 cycles, but data not contiguous and uncertainties in spectrum.
SPEs destruction of ozone	Solar proton flux spectra	Several days (for each event)	$E \sim 0.5$ - 500MeV $\Delta E/E \sim 1$ Many events $\Delta t \sim 1$ day Geographical distribution of insertion locations.	Yes
Solar wind	V and Bz	Months	Daily	Yes, since 1962
Ionisation	Solar-modulated cosmic rays	Forbush decreases	Many events $\Delta t \sim 1$ hour	Yes, 50 years data, but only indirectly in the form of neutron counts
		11-year cycle	Many cycles $\Delta t \sim 1$ month	Yes, but only indirectly in the form of neutron counts

Table 18 Fundamental physical/chemical processes associated with each mechanism.

Mechanism	Process	Inputs	Outputs
TSI	Variations of heating of land and sea surface; influence on cycle atmospheric and oceanic circulation and on hydrological cycle.	Temporal variations in TSI.	Response in temperature, wind, precipitation, ocean currents.
UV	Direct heating by UV.	UV spectral irradiance. Distributions of radiatively active gases (esp. ozone). Cloud distribution and radiative properties.	Heating rates as a function of latitude, longitude, altitude and time.
	Dynamical coupling (within the middle atmosphere).	Solar heating rate anomalies as a function of position and time (with and without ozone response).	Response of the middle atmosphere to solar UV variation: temperatures, wind and wave activity. Any additional effects due to ozone changes.
	Stratosphere-troposphere dynamical coupling.	Solar heating rate anomalies plus the response to these of stratospheric temperatures and winds.	Response of tropospheric circulations to perturbations in the stratosphere.
	Production of ozone by UV.	UV spectral irradiance as a function of time. Distributions of source gases and temperature.	Photochemical production rate of ozone as a function of latitude, longitude, altitude and time.
	Ozone transport.	Dynamical response of atmosphere to enhanced UV (i.e. changes in wind distribution).	Response of ozone concentration distribution to solar UV as a function of latitude, longitude, altitude and time.
SPEs	Destruction of ozone by SPEs.	SPE flux spectra. Distributions (climatology) of temperature, wind and chemically active constituents.	Response of NO_x and O_3 to solar proton events.

Solar wind	Reconnection	V and Bz	Magnetospheric/ionospheric disturbances: downward propagation and influence on polar dynamics.
Ionisation	Cosmic ray induced ionization plus ion induced nucleation	Ionization (cosmic rays) Aerosol and source gas concentrations Water vapour concentration	Cloud distribution and properties

Table 19: Proposed GCM experiments to test mechanisms.

Mechanism	**Process**	**GCM experiment**	**GCM type/specification**	**Notes**
TSI	Effects of different TSI on atmosphere-ocean system.	Time slice runs at low and high TSI values.	"Standard" climate model extending from surface to mid-stratosphere, with coupled ocean. [We refer to this model as M0]	> 20 year runs.
	Effects of time-varying TSI on atmosphere-ocean system.	Decadal-centennial scale response.	M0	Need ensemble of runs plus statistics from very long (~1000 year) control run of model.
UV	Effects of enhanced UV on the dynamical structure of the middle and lower atmosphere.	Time slice runs at low and high (spectrally-resolved) UV.	M0 without coupled ocean but extending from surface to mesopause. Good vertical resolution (need intrinsic QBO). Radiation scheme with adequate spectral resolution. [M1]	> 40 year runs.

		Mechanistic studies of wave effects in middle atmosphere.	Stripped-down M1. E.g. raise lower boundary to tropopause, remove tropospheric physics (clouds etc)	Multiple runs to investigate statistics of wave propagation, sudden stratospheric warmings, link to radiative forcing distribution.
		11-year cycle modulations	M1	> 20 cycles (~200 years).
		Role of ocean in 11-year cycle.	M1 with coupled ocean. [M2]	ditto
		Decadal-centennial scale response to solar UV.	M2	Need ensemble of runs plus statistics from very long (~1000 year) control run of model.
	Coupling between dynamics and chemistry (ozone)	Time slice solar max and solar min runs, response of oceans.	M1 with coupled chemistry scheme [M3]	> 20 year runs.
		27-day cycle modulations	M3	~ 20 year run
		11-year cycle modulations	M3	

	Fully-coupled atmosphere-ocean-chemistry	Decadal-centennial scale.	M2 with coupled chemistry. [M4]	Long runs with coupled oceans and chemistry not currently feasible. Could (i) repeat centennial run of M2 with prescribed (varying) ozone or (ii) time slice runs of M4 with high and low solar activity.
	Stratosphere-troposphere dynamical coupling.	Mechanistic studies of tropospheric response to perturbations in stratosphere.	Adapted M1. E.g. lower top to mid-stratosphere, increase vertical resolution near tropopause, simplify radiation scheme.	Multiple runs to investigate dynamical processes, especially wave propagation, response to stratospheric heating.
SPEs	Destruction of ozone by SPEs.	Effect of enhanced NO_x, including subsequent transport of low O_3 air.	M3 extended upwards into ionosphere [M5] or M3 with specified downward flux of NO_x.	Each run few months. Need ensembles to confirm statistics.
		Combined effects of UV and SPEs.	ditto	Ensemble of >20 year time slice solar max and solar min runs with SPEs added in solar max runs.
Solar wind	Reconnection, planetary waves	CME frequency/ proton events	M5	>40 years

Ionisation	Cosmic ray modulation of cloud cover.	Impact of ionisation on local cloud (timescale of Forbush decreases)	M0 plus specified ion-induced aerosol. [Parameterisations of aerosol "indirect" effect on cloud already exist.]	Ensemble of many events
		Impact of ionisation on cloud plus cloud-radiation feedbacks	ditto	Ensemble of >20 year time slice solar max and solar min runs with GCRs increased in solar min runs.

7. Conclusions and Recommendations

Through the ISAC study the team has reached a number of conclusions below we summarize the most important of these. It is then followed by recommendations. As this is an ESA funded study, one recommendation deserves to be highlighted: better, easier, more user-friendly access to existing data sets. The norm for US generated data sets are easy to access, easy to download, well organised. European data sets are lacking in this these respects. Too often the data are, when freely available, not organised with the end user in mind.

Conclusions

The Sun:

- Sunspot number catches only part of solar activity
- The Sun's magnetic field drives short term changes
- Use therefore magnetic data for Sun-Climate studies
- Solar output predictability is at most years ahead
- Due to the complexity and time-varying nature of the Sun solar-climate coupling must be expected to be very complex and probably changing with time

Correlations:

- The overall solar cycle dominates solar-climate correlations.
- Statistically robust signals of the impact of solar variability have been detected throughout the stratosphere and troposphere in temperature, wind and atmospheric circulation. These include, when the Sun is more active,:
    - a warming of the upper and lower stratosphere in low-to-middle latitudes
    - a strengthening of the winter stratospheric polar night jet
    - vertical bands of warming in the mid-latitude troposphere
    - a weakening and poleward expansion of the tropical Hadley cells and a poleward shift of the Ferrel cells
    - a more positive tendency of the North Atlantic Oscillation
    - the solar signal in stratospheric temperatures and in the tropospheric polar modes of variability is modulated by the phase of the quasi-biennial oscillation
- Direct heating by absorption of solar ultraviolet radiation can explain most of the temperature response in the upper stratosphere but not the signals in the lower stratosphere and troposphere.
- When removing the solar cycle the most robust tropospheric correlations are seen with UV and cosmic rays.
- UV and GCR show negative(positive) bands of correlations with low clouds at mid-to-high latitudes. These bands are strengthened by removal of the solar cycle.

- On the surface only rather weak correlations are observed. This is to some extent due to the short time span of the available parameters such as the NDVI (vegetation), snow and ice data.
- At solar min/max a zonally averaged temperatures under solar max/min conditions show a negative/positive correlation with UV in the troposphere and similar, but with opposite sign with GCR.

Mechanisms, Models and Methods

- Correlation studies inherently assume a linear response to changes in forcing parameters. Any non-linear behaviour of the climate system is bound to cause problems.
- There are serious discrepancies between the solar signal in stratospheric ozone derived from satellite measurements and that suggested by chemistry-climate models.
- Uncertainty in the ozone signal also implies uncertainty in the value of solar radiative forcing of the troposphere.
- Some of the ozone discrepancy may be related to inadequate treatment in the models of the effects of solar energetic particles but these are unlikely to explain the ozone minimum shown in the tropical middle stratosphere.
- Solar signals near the tropical stratopause can be transmitted to the polar and tropical lower stratosphere through mechanisms involving wave-mean flow interactions.
- Perturbations to the winter stratospheric polar vortex appear to propagate downwards into the troposphere although the mechanisms involved are not clear.
- Heating of the tropical lower stratosphere can influence the temperature, wind and circulation of the troposphere through dynamical coupling that appears to depend on perturbing the behaviour of synoptic-scale eddies.

Recommendations

Methods

- In future analyses of solar climate relations it would be fruitful to
    - use wavelet methods
    - use solar magnetic field data
- To understand solar activity use MHD and low-dimensional models.
- To analyse solar activity use multi-resolution analysis of all scales and extend time series through reconstructions by using indicators.
- Solar output quantities EM (SOHO, SDO), SEPs (ACE, Rhessi, Stereo) and SW (SOHO, Ulysses, ACE) would preferably be presented in synoptic maps.
- Coupled chemistry-climate modelling studies of the response of the middle atmosphere to variations in solar UV and energetic particles are needed to disentangle radiative, photochemical and dynamical influences on temperature, wind and composition

- Fully-coupled ocean-atmosphere-chemistry simulations are desirable but currently limited by computational demands.
- Coupled thermosphere-ionosphere-mesosphere-stratosphere modelling simulations to investigate atmospheric coupling processes.
- The use of simpler mechanistic models to identify and diagnose particular mechanisms operating.
- A better understanding of the role of clouds in the climate, particularly with respect to feedbacks between different solar-climate mechanisms, is needed in order to distinguish the solar signal in these mechanisms.

Observations

- Future observations of solar activity: carry out high resolution (Hinode, Solar Orbiter) and 3D real-time synoptic observations of the flow and magnetic field (SDO).
- Continued measurements of solar irradiance from satellites, along with robust inter-calibration of instruments, are essential for refining estimates of solar input to the Earth, its temporal variability and spectral composition
- Continued measurements of stratospheric ozone (and other minor constituents) from satellites, along with robust inter-calibration of instruments, are needed to advance understanding of the ozone response to the Sun.
- Combined aerosol and cloud observations particularly in the lower troposphere.

Data

- Through better understanding of the Sun construct robust reconstruction of TSI using indicators.
- Through continued observations and inter-calibration create a reliable and well-organised data set of clouds (type, distribution, properties).
- Through continued observations and inter-calibration create a reliable and well-organised data set of clouds (type, distribution, properties).
- Better, easier, more user-friendly access to existing data sets.

References

Abbot, C. G., and F. E. Fowle, Income and outgo of heat from the earth, and the dependence of its temperature thereon, Annals of the Astrophysical Observatory, 2, 159–176, 1908.

Abbot, C. G., and F. E. Fowle, Volcanoes and climate, Smithsonian Miscellaneous Collections, 60(29), 1–24, 1913.

Arnold, N. F. and T. R. Robinson, Solar cycle changes to planetary wave propagation and their influence on the middle atmosphere circulation, *Annales Geophysicae-Atmospheres Hydrospheres and Space Sciences, 16*(1), 69-76, 1998.

Arnold, N. F. and T. R. Robinson, Solar magnetic flux influences on the dynamics of the winter middle atmosphere, *Geophysical Research Letters, 28*(12), 2381-2384, 2001.

Arnold, N.F. and T.R. Robinson, 2003. Solar cycle modulation of the winter stratosphere: the role of atmospheric gravity waves. *Adv. Space. Sci*., **31**, 2121-2126.

Balachandran, N. K. and D. Rind, Modeling the Effects of Uv Variability and the QBO on the Troposphere-Stratosphere System .1. the Middle Atmosphere, *Journal of Climate, 8*(8), 2058-2079, 1995.

Balachandran, N. K., D. Rind, P. Lonergan and D. T. Shindell, Effects of solar cycle variability on the lower stratosphere anti the troposphere, *Journal of Geophysical Research-Atmospheres, 104*(D22), 27321-27339, 1999

Baldwin, M. P. and T. J. Dunkerton, Stratospheric harbingers of anomalous weather regimes, *Science*, *294*, 581-584, 2001.

Bazilevskaya, G. A., Observations of variability in cosmic rays, Space Science Reviews, 94, 25–38, 2000.

Beer, J., Long-term indirect indices of solar variability, Space Science Reviews, 94, 53–66, 2000.

Berger, A., Imbrie, J., Hays, J., Kukla, G., and B. Saltzman, Milankovitch and Climate, in NATO ASI, Series, Vol. 126, pp. 895, D. Reidel Publishing Company, Dordrecht, 1984.

Berndt T., Böge O., and Stratmann F., Formation of atmospheric H2SO4/H2O particles in the absence of organics: A laboratory study, *Geophysical Research Letters*, vol. 33, l15817, doi:10.1029/2006gl026660, 2006

Bigelow, F. H., The relations between the meteorological elements of the United States and the solar radiation, The American Journal of Science, 25(149), 413–430, 1908.

Black, R. X., B. A. McDaniel, 2004: Diagnostic case studies of the Northern Annular Mode. *J. Clim*. **17**, 3990-4004.

Boberg, F. and H. Lundstedt, Solar wind variations related to fluctuations of the North Atlantic Oscillation, *Geophysical Research Letters, 29*(15), 2002.

Boberg, F. and H. Lundstedt, Solar wind electric field modulation of the NAO: A correlation analysis in the lower atmosphere, *Geophysical Research Letters, 30*(15), 2003.

Bucha, V. and V. Bucha, Geomagnetic forcing of changes in climate and in the atmospheric circulation, *Journal of Atmospheric and Solar-Terrestrial Physics, 60*(2), 145-169, 1998.

Carslaw, K. S., R. G. Harrison and J. Kirkby, Cosmic rays, clouds, and climate, *Science, 298*(5599), 1732-1737, 2002.

Castanheira, J. M., H. F. Graf, 2003: North Pacific-North Atlantic relationships under stratospheric control? *J. Geophys. Res*. **108**, Art. No. 4036.

Crooks S. A. and L. J. Gray, Characterization of the 11-year solar signal using a multiple regression analysis of the ERA-40 dataset, *Journal of Climate, 18*, 996-1015, 2005.

Crooks, S.A. and L.J. Gray, 2004: Characterisation of the 11-year solar signal using a multiple regression analysis of the ERA-40 dataset. *J. Clim*. **18**, 996-1015.

Cubasch, U., R. Voss, G.C. Hegerl, J. Waszkewitz, and T.J. Crowley, Simulation of the influence of solar radiation variations on the global climate with an ocean-atmosphere general circulation model, *Clim. Dyn., 13*, 757-767, 1997.

Deland, M. T. and R. P. Cebula, Composite Mg-Ii Solar-Activity Index for Solar Cycle-21 and Cycle-22, *Journal of Geophysical Research-Atmospheres, 98*(D7), 12809-12823, 1993.

Delmonte, B., Petit, J.R., Krinner, G., Maggi, V., Jouzel, J., and R. Udisti, Ice core evidence for secular variability and 200-year dipolar oscillations in atmospheric circulation over East Antarctica during Holocene, submitted to Climate dynamics, 2005.

Damon, P. E., and J. L. Jirikowic, The Sun as a low-frequency harmonic oscillator, Radiocarbon, 34(2), 199–205, 1992.

Denton, G., and W. Karlen, Quaternary Res. 3., No. 2, 155, 1973.

Dickinson, R. E., Solar Variability and the Lower Atmosphere, *Bulletin of the American Meteorological Society, 56*(12), 1240-1248, 1975.

Ebisuzaki, W., A method to estimate the statistical significance of a correlation when the data are serially correlated, *Journal of Climate, 10*(9), 2147-2153, 1997.

Eddy, J. A., The Maunder Minimum, *Science, 192*(4245), 1189-1202, 1976.

Egorova, T., E. Rozanov, E. Manzini, M. Haberreiter, W. Schmutz, V. Zubov and T. Peter, Chemical and dynamical response to the 11-year variability of the solar irradiance simulated with a chemistry-climate model, Geophysical Research Letters, 31(6), 2004.

Eichkorn, S., S. Wilhelm, H. Aufmhoff, K. H. Wohlfrom and F. Arnold, Cosmic ray-induced aerosol-formation: First observational evidence from aircraft-based ion mass spectrometer measurements in the upper troposphere, *Geophysical Research Letters, 29*(14), 2002.

Fairbridge, R.W., Encyclopedia of Atmospheric Sciences and Astrogeology, Encyclopedia of Earth Sciences Series, Vol. 2, edited by R.W. Fairbridge, Reinhold, New York, 1967.

Farrar, P. D., Are cosmic rays influencing oceanic cloud coverage - or is it only El Nino?, *Climatic Change, 47*(1-2), 7-15, 2000.

Ferek, R.J., T. Garrett, P.V. Hobbs, S. Strader, D. Johnson, J.P. Taylor, K. Nielsen, A.S. Ackerman, Y. Kogan, Q. Liu, B.A. Albrecht, and D. Babb. Drizzle suppression in ship tracks. J. Atmos. Sci. 57, 2707-2728, doi:10.1175/1520-0469(2000)057, 2000

Fioletov V.E., D.W. Tarasick and I. Petropavlovskikh, 2006: Estimating ozone variability and instrument uncertainties from SBUV(/2), ozonesonde, Umkehr, and SAGE II measurements: Short-term variations. *J. Geophys. Res.* **111**, Art. No. D02305.

Foster, J. C., J. M. Holt and R. G. Musgrove, Ionospheric Convection Associated with Discrete Levels of Particle-Precipitation, *Geophysical Research Letters, 13*(7), 656-659, 1986.

Frick, P., D. Galyagin, D. V. Hoyt, E. Nesme-Ribes, K. H. Schatten, D. Sokoloff, and V. Zakharov, Wavelet analysis of solar activity recorded by sunspot groups, Astronomy & Astrophysics, 328, 670–681, 1997

Friis-Christensen, E. and K. Lassen, Length of the Solar-Cycle - An Indicator of Solar-Activity Closely Associated with Climate, *Science, 254*(5032), 698-700, 1991.

Fröhlich, C., Observations of irradiance variations, *Space Science Review 94*, 15–24, 2000.

Fröhlich, C. and J. Lean, The Sun's total irradiance: Cycles, trends and related climate change uncertainties since 1976, *Geophysical Research Letters, 25*(23), 4377-4380, 1998.

Fröhlich, C. and J. Lean, Solar irradiance variability and climate, *Astronomische Nachrichten, 323*(3-4), 203-212, 2002.

Fuller-Rowell, T., and D. S. Evans, Height-Integrated Pedersen and Hall Conductivity Patterns Inferred from the TIROS-NOAA Satellite Data, *Journal of Geophysical Research, 92*, 7606-7618, 1987.

Gill, A.E., *Atmosphere-Ocean Dynamics*, Academic, San Diego, California, 1982.

Gillett N. P., B. D. Santer, and A. J. Weaver, *Nature, 432*, doi:10.1038/nature03209, 2004.

Gleisner H, and P. Thejll, Patterns of tropospheric response to solar variability. *Geophysical Research Letters, 30***,** art. no. 1711, 2003.

Gray L. J. , S. Crooks, C. Pascoe, S. Sparrow, and M. Palmer, Solar and QBO influences on the timing of stratospheric sudden warmings, *Journal of Atmospheric Science 61*, 2777-2796, 2004.

Gray, L J, J D Haigh and R G Harrison, 2005. Review of the influences of solar changes on the Earth's climate. Hadley Centre Technical Note 62, Met Office, Exeter

Gringel, W., J. M. Rosen and D. J. Hofmann, Electrical Structure from 0 to 30 Kilometers, in The Earth's Electrical Environment, pp. 166-182, National Academy Press, Washington,D.C., 1986.

Haigh J. D., The impact of solar variability on climate, *Science*, *272*, 981-984, 1996.

Haigh, J. D., 1999: A GCM study of climate change in response to the 11-year solar cycle. *Quart. J. Roy. Meteorol. Soc.* **125**, 871-892.

Haigh, J. D., Modelling the impact of solar variability on climate, *Journal of Atmospheric and Solar-Terrestrial Physics, 61*(1-2), 63-72, 1999.

Haigh, J. D., 2003: The effects of solar variability on the Earth's climate. *Phil. Trans. Roy. Soc A.* **361**, 95-111.

Haigh, J. D., The effects of solar variability on the Earth's climate, *Philosophical Transactions of the Royal Society of London Series A-Mathematical Physical and Engineering Sciences, 361*(1802), 95-111, 2003.

Haigh, J. D., M. Blackburn and R. Day, 2005: The response of tropospheric circulation to perturbations in lower stratospheric temperature. *J. Clim.* **18**, 3672–3691.

Haigh, J. D. and H. K. Roscoe, Solar influences on polar modes of variability, *Meteorologische Zeitschrift*, *15*, 371-378, 2006.

Harrison, G., Twentieth century secular decrease in the atmospheric potential gradient, *Geophysical Research Letters, 29*(14), 2002.

Harrison, R. G. and K. S. Carslaw, Ion-aerosol-cloud processes in the lower atmosphere, *Reviews of Geophysics, 41*(3), 2003.

Hartley, D. E., J. Villarin, R. X. Black, C. A. Davis, 1998: A new perspective on the dynamical link between the stratosphere and troposphere. *Nature* **391**, 471-474.

Herman, J. R. and R. A. Goldberg, Sun, weather, and climate, NASA, Washington DC, 1978.

Herschel, W., On the Method of Observing the Changes That Happen to the Fixed Stars; With Some Remarks on the Stability of the Light of Our Sun. To Which is Added, a Catalogue of Comparative Brightness, for Ascertaining the Permanency of the Lustre of Stars., *Philosophical Transactions of the Royal Society of London, 86*, 166-226, 1796.

Higgins, R. W., J. E. Janowiak, and Y.-P. Yao, A gridded hourly precipitation data base for the United States (1963-1993), NCEP/Climate Prediction Center Atlas 1, *http://www.cpc.ncep.noaa.gov/research_papers/ncep_cpc_atlas/1/,* 1996.

Hill, D. C., M. R. Allen, N. P. Gillet, S. F. B. Tett, P. A. Stott, G. S. Jones, W. J. Ingram and J. F. B. Mitchell, Natural and Anthropogenic causes of recent climate change, in Detecting and Modelling Regional Climate Change, edited by M. B. India and D. L. Bonillo, pp. 275-290, Springer-Verlag, 2001.

Hood, L.L., 2004. Effects of solar UV variability on the stratosphere. In 'Solar variability and its effect on the Earth's atmosphere and climate system. *Geophysical Monograph* **141** American Geophysical Union, Washington D.C., Eds. J. Pap, P. Fox, C. Frolich, H. Hudson, J. Kuhn, J. McCormack, G. North, W. Sprigg and S. Wu.Haigh J. D., The role of stratospheric ozone in modulating the solar radiative forcing of climate, *Nature*, *370*, 544-546, 1994.

Hood, L. L., J. L. Jirikowic and J. P. McCormack, Quasi-Decadal Variability of the Stratosphere - Influence of Long-Term Solar Ultraviolet Variations, *Journal of the Atmospheric Sciences, 50*(24), 3941-3958, 1993.

Hoppel, W. A., R. V. Anderson and J. C. Willet, Atmospheric electricity in the planetary boundary layer, in The Earth's Electrical Environment, pp. 149-165, National Academy Press, Washington,D.C., 1986.

Horrak U., Salm J. and Tammet H., Bursts of intermediate ions in atmospheric air., *Journal of Geophysical Research,* 103 D12, 13909-13915, 1998

Horrak, U., Salm, J., & Tammet, H.. Statistical characterisation of air ion mobility spectra at Tahkuse observatory: Classification of air ions. *Journal of Geophysical Research* D, 105, 9291–9302., 2000

Horrak, Iher, Luts Salm and Tammet, Mobility spectrum of air ions at Tahkuse Observatory, *Journal of Geophysical Research* ,Vol 99, No. d5, pages 10,697-10, 700, May, 1994

Houghton, J. T., Y. Ding, D. J. Griggs, M. Noguer, P. J. van der Linden and D. Xiaosu, Climate Change 2001: The Scientific Basis, p. -881, Cambridge University Press, 2001.

Hoyt, D. V. and K. H. Schatten, New Information on Solar-Activity, 1779-1818, from Herschel, William Unpublished Notebooks, *Astrophysical Journal, 384*(1), 361-384, 1992.

Hoyt, D. V. and Schatten, K. H., A discussion of plausible solar irradiance variations, 1700-1992. *Journal of Geophysical Research 98*, 18 895-18 906, 1993.

Hoyt, D. V. and K. H. Schatten, The role of the sun in climate change, Oxford University Press, New York, 1997.Hurrell, J. W., Decadal Trends in the North-Atlantic Oscillation - Regional Temperatures and Precipitation, *Science, 269*(5224), 676-679, 1995.

Hoyt, D.,V. and K.H. Schatten, The role of the sun in climate change, Oxford University Press, New York, 1997.

IPCC Intergovernmental Panel on Climate Change 4th Assessment Report, 2007.

Jacobson MZ 1999 Fundamentals of Atmospheric Modelling. CUP

Jorgensen, T. S. and A. W. Hansen, Comments on "Variation of cosmic ray flux and global cloud coverage - a missing link in solar-climate relationships" by Henrik Svensmark and Eigil Friis-Christensen [Journal of Atmospheric and Solar-Terrestrial Physics 59 (1997) 1225-1232], *Journal of Atmospheric and Solar-Terrestrial Physics, 62*(1), 73-77, 2000.

Keckhut, P., C. Cagnazzo, M.-L. Chanin, C. Claud and A. Hauchecorne, 2004: The 11-year solar-cycle effects on temperature in the upper stratosphere and mesosphere. Part I: Assessment of observations. *J. Atmos. Sol. Terr. Phys.* **67**, 940-947.

Kelly, P. M., Solar influence on North Atlantic mean sea level pressure, Nature, 269, 320–322, 1977.

Kernthaler, S. C., R. Toumi and J. D. Haigh, Some doubts concerning a link between cosmic ray fluxes and global cloudiness, *Geophysical Research Letters, 26*(7), 863-865, 1999.

Klein, S. A. and D. L. Hartmann, Spurious Changes in the ISCCP Dataset, *Geophysical Research Letters, 20*(6), 455-458, 1993.

Kniveton, D. R., Precipitation, cloud cover and Forbush decreases in galactic cosmic rays, *Journal of Atmospheric and Solar-Terrestrial Physics, 66*(13-14), 1135-1142, 2004.

Kniveton, D. R. and M. C. Todd, On the relationship of cosmic ray flux and precipitation, *Geophysical Research Letters, 28*(8), 1527-1530, 2001.

Kodera, K., 1995: On the origin and nature of the interannual variability of the winter stratospheric circulation in the Northern Hemisphere. *J. Geophys. Res.* **100**, 14077-14087.

Kodera, K., 2002: Solar cycle modulation of the North Atlantic Oscillation: Implication in the spatial structure of the NAO. *Geophys. Res. Lett.* **29**, Art. No. 1218.

Kodera, K. and Y. Kuroda, Dynamical response to the solar cycle, *Journal of Geophysical Research*, *107*, art. No. 2224, 2002.

Kristjansson, J. E., A. Staple, J. Kristiansen and E. Kaas, A new look at possible connections between solar activity, clouds and climate, *Geophysical Research Letters, 29*(23), 2002.

Kuang, Z. M., Y. B. Jiang and Y. L. Yung, Cloud optical thickness variations during 1983-1991: Solar cycle or ENSO?, *Geophysical Research Letters, 25*(9), 1415-1417, 1998.

Kudela, K., Rybak, J., Anatalova, A. and M. Storini, Time evolution of low-frequency periodicities in cosmic ray intensity, Solar Physics, 2005, 165-175, 2002.

Kuroda, Y., K. Kodera, 1998: Interannual variability in the troposphere and stratosphere of the southern hemisphere winter. *J. Geophys. Res.* **103**, 13787-13799.

Kulmala M., Kerminen V., Anttila T., Laaksonen A., and O'Dowd C., Organic aerosol formation via sulphate cluster activation, *Journal of Geophysical Research*, vol. 109, d04205, doi:10.1029/2003JD003961, 2004

Labitzke, K., Sunspots, the QBO, and the Stratospheric Temperature in the North Polar-Region, *Geophysical Research Letters, 14*(5), 535-537, 1987.

Labitzke, K., 2004: On the signal of the 11-year sunspot cycle in the stratosphere over the Antarctic and its modulation by the Quasi-Biennial Oscillation (QBO). *Meteorol. Z.* **13**, 263-270.

Labitzke, K. and K. Matthes, Eleven-year solar cycle variations in the atmosphere: observations, mechanisms and models, *Holocene, 13*(3), 311-317, 2003.

Labitzke, K., H. van Loon, 1982: On the association between the QBO and the extratropical stratosphere. *J. Atmos. Terr. Phys.* **54**, 1453-1463.

Labitzke, K. and H. van Loon, Associations Between the 11-Year Solar-Cycle, the QBO and the Atmosphere .1. the Troposphere and Stratosphere in the Northern Hemisphere in Winter, *Journal of Atmospheric and Terrestrial Physics, 50*(3), 197-206, 1988.

Labitzke, K. and H. van Loon, Connection Between The Troposphere And Stratosphere On A Decadal Scale, *Tellus A 47*, 275-286, 1995.

Labitzke, K. and H. van Loon, The signal of the 11-year sunspot cycle in the upper troposphere lower stratosphere, *Space Science Reviews, 80*(3-4), 393-410, 1997.

Labitzke, K., H. van Loon, 1999: The stratosphere (Phenomena, History and Relevance). Springer Verlag Berlin Heidelberg New York, 179pp.

Langematz, U., J.L. Grenfell, K. Matthes, P. Mieth, M. Kunze, B. Steil, C. Bruhl, 2005. Chemical effects in 11-year solar cycle simulations with the Freie Universitat Berlin Climate Middle Atmosphere Model with inline chemistry (FUB-CMAM-CHEM) *Geophys. Res. Lett.*, **32**, art. no. L13803.

Larkin, A., J. D. Haigh, and S. Djavidnia, The effect of solar UV irradiance variations on the Earth's atmosphere, *Space Science Reviews*, *94*, 199-214, 2000.

Lean, J., J. Beer, and R. Bradley, Reconstruction of solar irradiance since 1610: Implications for climate change, Geophysical Research Letters, 22(23), 3195–3198, 1995.

Lean, J. L., G. J. Rottman, H. L. Kyle, T. N. Woods, J. R. Hickey and L. C. Puga, Detection and parameterization of variations in solar mid- and near-ultraviolet radiation (200-400 nm), *Journal of Geophysical Research-Atmospheres, 102*(D25), 29939-29956, 1997.

Lee III, R. B., M. A. Gibson, R. S. Wilson, and S. Thomas, Long-term total solar irradiance variability during sunspot cycle 22, *Journal of Geophysical Research, 100*(A2), 1667–1675, 1995.

Lee, S. H., J. M. Reeves, J. C. Wilson, D. E. Hunton, A. A. Viggiano, T. M. Miller, J. O. Ballenthin and L. R. Lait, Particle formation by ion nucleation in the upper troposphere and lower stratosphere, *Science, 301*(5641), 1886-1889, 2003.

Lee, H., A. K. Smith, 2003: Simulation of the combined effects of solar cycle, quasi-biennial oscillation and volcanic forcing on stratospheric ozone changes in recent decades. *J. Geophys. Res.* **108**, 4049, doi:10.1029/2001JD001503.

Liszka, L., Cognitive information processing in space physics and astrophysics, Pachart Publishing House, Tucson, 2003.

Lockyer, N., and W. J. S. Lockyer, On solar changes of temperature and variations of rainfall in the region surrounding the Indian Ocean. I., Nature, 63, 107–109, 1901.

Lovejoy, E.R., J. Curtius, and K.D. Froyd, Atmospheric ion-induced nucleation of sulfuric acid and water, *Journal Of Geophysical Research*, 109, D08204, doi:10.1029/2003JD004460, 2004.

Lundstedt, H., L. Liszka, and R. Lundin, Solar activity explored with new wavelet methods, Annales Geophysicae, 23, 1505–1511, 2005.

Lundstedt, H., L. Liszka, R. Lundin, and R. Muscheler, Long-term solar magnetic activity explored with wavelet methods, Annales Geophysicae, 24, 1–10, 2006.

McCracken, K. G., G. A. M. Dreschhoff, D. F. Smart, and M. A. Shea, Solar cosmic ray events for the period 1561–1994: 2. The Gleissberg periodicity, Journal of Geophysical Research, 106(A10), 21,599–21,609, 2001.

de la Fuentes Marcos, R., and C. de la Fuentes Marcos, On the correlation between recent star formation rate in the Solar Neighbourhood and the glaciation period record on Earth, New Astronomy, 10(1), 53-66, 2004.

Marsh, N. and H. Svensmark, Cosmic rays, clouds, and climate, *Space Science Reviews, 94*(1-2), 215-230, 2000a.

Marsh, N. and H. Svensmark, Low cloud properties influenced by cosmic rays, *Physical Review Letters, 85*(23), 5004-5007, 2000b.

Marsh, N. and H. Svensmark, Galactic cosmic ray and El Nino Southern Oscillation trends in International Satellite Cloud Climatology Project D2 low-cloud properties, *Journal of Geophysical Research-Atmospheres, 108*(D6), 2003a.

Marsh, N. and H. Svensmark, Solar influence on Earth's climate, *Space Science Reviews, 107*(1-2), 317-325, 2003b.

Marsh, N. and H. Svensmark, Comment on "Solar influences on cosmic rays and cloud formation: A reassessment" by Bomin Sun and Raymond S. Bradley, *Journal of Geophysical Research-Atmospheres, 109*(D14), 2004a.

Marsh, N. and H. Svensmark, Long-term Stability of ISCCP-D2 IR cloud data: a possible artefact, *Journal of Geophysical Research-Atmospheres, 108*, 2004b.

Marshall, J., Y. Kushner, D. Battisti, P. Chang, A. Czaja, R. Dickson, J. Hurrell, M. McCartney, R. Saravanan and M. Visbeck, North Atlantic climate variability: Phenomena, impacts and mechanisms, *International Journal of Climatology, 21*(15), 1863-1898, 2001.

Matthes, K., U. Langematz, L. L. Gray, K. Kodera and K. Labitzke, Improved 11-year solar signal in the freie universitat Berlin climate middle atmosphere model (FUB-CMAM), *Journal of Geophysical Research-Atmospheres, 109*(D6), 2004.

Meehl, G.A., W.M. Washington, T.M.L. Wigley, J.M. Arblaster, A. Dai, Solar and Greenhouse Gas Forcing and Climate Response in the Twentieth Century, *J. of Clim., 16*, 426-444, 2003.

Mitchell, J.M., Stockton, C. W., and D.M. Meko, Evidence of a 22-year rhythm of drought in the western United States related to the hale solar cycle since the 17th century, in Solar-Terrestrial Influences on Weather and Climate, ed. B. M. McCormac and T. A. Seliga, D. Reidel publishing Company, 1979.

Muscheler, R., Beer, J., and B. Kromer, Long-term Climate Variations and Solar Effects, in Proc., ISCS 2003 symposium, Solar Variability as an Input to Earth's Environment, Tatranska Lomnica, Slovakia, 23-28 June 2003, ESA SP-535, September 2003.

Neff, U., S. J. Burns, A. Mangini, M. Mudelsee, D. Fleitmann and A. Matter, Strong coherence between solar variability and the monsoon in Oman between 9 and 6 kyr ago, *Nature, 411*(6835), 290-293, 2001.

Nesme-Rimes, E., E.N. Ferriera, R. Sadourny, H. LeTreut, and Z.X. Li, Solar dynamics and its impact on solar irradiance and the terrestrial climate*, J. Geophys. Res., 98,* 18923-18935, 1993.

Nordmann, C., Connection between sun-spots and atmospheric temperature, Nature, 68, 162, 1903.

North, G. R. and Q. G. Wu, Detecting climate signals using space-time EOFs, *Journal of Climate, 14*(8), 1839-1863, 2001.

Ogurtsov, M. G., Y. A. Nagovitsyn, G. E. Kocharov, and H. Jungner, Long-period cycles of the Sun's activity recorded in direct solar data and proxies, Solar Physics, 211, 371–394, 2002.

Palle Bago, E. and C. J. Butler, The influence of cosmic rays on terrestrial clouds and global warming, *Astronomy and Geophysics, 41*(4), 4, 2000.

Paularena, K.I., Szabo, A., and J.D.L. Richardson, J. Geophys., Res., 22, 3001, 1995.

Peixoto, J. P. and A. H. Oort, Physics of Climate, *Reviews of Modern Physics, 56*(3), 365-429, 1984.

Peristykh, A. N., and P. E. Damon, Persistence of the Gleissberg 88-year solar cycle over the last 12,000 years: Evidence from cosmogenic isotopes, Journal of Geophysical Research, 108(A1), doi:10.1029/2002JA009390, 2003.

Petit, J., Jouzel, J., Raynaud, D., Barkov, N. I., Barnola, J.M., Basile, I., Bender, M., Chappellaz, J., Davis, M., Delaygue, G., Delmotte, M., Kotlyakov, V.M., Legrand, M., Lipenkov, V.Y., Lorius,C., Pepin, L., Ritz, C., Saltzmann, E. and M. Stievenard, Climate and atmospheric history of the past 420,000 years from the Vostock ice core, Antarctica, Nature, 399, 429-436, 1999.

Pudovkin, M. I. and S. V. Veretenenko, Variations of the cosmic rays as one of the possible links between the solar activity and the lower atmosphere, *Advances in Space Research, 17*(11), 161-164, 1996.

Pustilnik, L. A. and G. Y. Din, Influence of Solar Activity on State of Wheat Market in Medieval England, 2003.

Randel, W. J., F. Wu, D. J. Gaffen, 2000: Interannual variability of the tropical tropopause derived from radiosonde data and NCEP reanalyses. *J. Geophys. Res.* **105**, 15509-15523.

Reames, D. V., Solar energetic particle variations, Advances in Space Research, 34, 381–390, 2004.

Reid, G. C., Influence of Solar Variability on Global Sea-Surface Temperatures, *Nature, 329*(6135), 142-143, 1987.

Reid, G. C., Solar Total Irradiance Variations and the Global Sea-Surface Temperature Record, *Journal of Geophysical Research-Atmospheres, 96*(D2), 2835-2844, 1991.

Reid, G. C., Solar variability and the Earth's climate: Introduction and overview, *Space Science Reviews, 94*(1-2), 1-11, 2000.

Richter, C. M., Sonnenflecken, Erdmagnetismus und Luftdruck, Meteorologische Zeitschrift, 19, 386–389, 1902.

Rind, D. and J. Overpeck, Hypothesised causes of decade-to-century-scale climate variability: climate model results, *Quat. Sci. Rev*., 12, 357-374, 1993.

Roldugin, V. C. and B. A. Tinsley, Atmospheric transparency changes associated with solar wind-induced atmospheric electricity variations, *Journal of Atmospheric and Solar-Terrestrial Physics, 66*(13-14), 1143-1149, 2004.

Rossow, W. B. and R. A. Schiffer, ISCCP Cloud Data Products, *Bulletin of the American Meteorological Society, 72*(1), 2-20, 1991.

Rossow, W. B., A. W. Walker, D. E. Beuschel and M. D. Roiter, International Satellite Cloud Climatology Project(ISCCP) : documentation of new cloud datasets, p. -115, World Meteorological Organization, Geneva, 1996.

Sato, M., J. E. Hansen, M. P. Mccormick and J. B. Pollack, Stratospheric Aerosol Optical Depths, 1850-1990, *Journal of Geophysical Research-Atmospheres, 98*(D12), 22987-22994, 1993.

Schmidt, H., G. P. Brasseur, M. Charron, E. Manzini, M. A. Giorgetta, T. Diehl, V. I. Fomichev, D. Kinnison, D. Marsh, S. Walters, 2006. The HAMMONIA Chemistry Climate Model: Sensitivity of the Mesopause Region to the 11-Year Solar Cycle and CO2 Doubling. *J. Clim.*, **19**, 3903-3931.

Schuster, A., The periodicity of sun-spots, The Astrophysical Journal, 23(2), 101–109, 1906.

Shaviv, N. J., The spiral structure of the Milky Way, cosmic rays, and ice age epochs on Earth, *New Astronomy, 8*(1), 39-77, 2003a.

Shaviv, N. J., Toward a solution to the early faint Sun paradox: A lower cosmic ray flux from a stronger solar wind, *Journal of Geophysical Research-Space Physics, 108*(A12), 2003b.

Shindell, D., D. Rind, N. Balachandran, J. Lean and P. Lonergan, Solar cycle variability, ozone, and climate, *Science, 284*(5412), 305-308, 1999.

Slingo JM 1987 The development and verification of a cloud prediction scheme for the ECMWF. *Q.J.Roy.Meteorol.Soc.* **113,** 899-927.

Solanki, S. K., M. Schüssler, and M. Fligge, Evolution of the Sun's large-scale magnetic field since the Maunder Minimum, Nature, 408, 445–447, 2000.

Stott, P. A., G. S. Jones and J. F. B. Mitchell, Do models underestimate the solar contribution to recent climate change?, *Journal of Climate, 16*(24), 4079-4093, 2003.

Sun, B. M. and R. S. Bradley, Solar influences on cosmic rays and cloud formation: A reassessment, *Journal of Geophysical Research-Atmospheres, 107*(D14), 2002.

Sun, B. M. and R. S. Bradley, Reply to comment by N. D. Marsh and H. Svensmark on "Solar influences on cosmic rays and cloud formation: A reassessment", *Journal of Geophysical Research-Atmospheres, 109*(D14), 2004.

Svensmark, H., Influence of cosmic rays on Earth's climate, *Physical Review Letters, 81*(22), 5027-5030, 1998.

Svensmark et al,, Experimental Evidence for the role of Ions in Particle Nucleation under Atmospheric Conditions, *Proceedings of Royal Society A, Physical and Engineering Sciences* , 2006

Svensmark, H. and E. Friis-Christensen, Variation of cosmic ray flux and global cloud coverage - A missing link in solar-climate relationships, *Journal of Atmospheric and Solar-Terrestrial Physics, 59*(11), 1225-1232, 1997.

Svensmark, H. and E. Friis-Christensen, Reply to comments on "Variation of cosmic ray flux and global cloud coverage - a missing link in solar-climate relationships", *Journal of Atmospheric and Solar-Terrestrial Physics, 62*(1), 79-80, 2000.

Thejll, P. and K. Lassen, Solar forcing of the Northern hemisphere land air temperature: New data, *Journal of Atmospheric and Solar-Terrestrial Physics, 62*(13), 1207-1213, 2000.

Thejll, P., B. Christiansen, H. Gleisner, 2003: On correlations between the North Atlantic Oscillation, geopotential heights, and geomagnetic activity. *Geophys. Res. Lett.* **30**: Art. No. 1347.

Thompson, D. W. J., S Solomon, 2002: Interpretation of recent Southern Hemisphere climate change. *Science* **296**, 895-899.

Thompson, D. W. J., M. P. Baldwin, S Solomon, 2005: Stratosphere-troposphere coupling in the Southern Hemisphere. *J. Atmos. Sci.* **62**, 708-715.

Thompson, D. W. J.and S. Solomon, Recent stratospheric climate trends as evidenced in radiosonde data: Global structure and tropospheric linkages, *Journal of Climate, 18*, 4785-4795, 2005.

Tinsley, B. A., Solar wind modulation of the global electric circuit and apparent effects on cloud microphysics, latent heat release, and tropospheric dynamics, *Journal of Geomagnetism and Geoelectricity, 48*(1), 165-175, 1996a.

Tinsley, B. A., Solar wind modulation of the global electric circuit and apparent effects on cloud microphysics, latent heat release, and tropospheric dynamics, *Journal of Geomagnetism and Geoelectricity, 48*(1), 165-175, 1996b.

Tinsley, B. A., Correlations of atmospheric dynamics with solar wind-induced changes of air-earth current density into cloud tops, *Journal of Geophysical Research-Atmospheres, 101*(D23), 29701-29714, 1996c.

Tinsley, B. A., Influence of solar wind on the global electric circuit, and inferred effects on cloud microphysics, temperature, and dynamics in the troposphere, *Space Science Reviews, 94*(1-2), 231-258, 2000.

Tinsley, B. A., G. M. Brown, and P. H. Scherrer, Solar variability influences on weather and climate: Possible connections through cosmic ray fluxes and storm intensification, Journal of Geophysical Research, 94(D12), 14,783–14,792, 1989.

Tinsley, B. A. and G. W. Deen, Apparent Tropospheric Response to Mev-Gev Particle-Flux Variations - A Connection Via Electrofreezing of Supercooled Water in High-Level Clouds, *Journal of Geophysical Research-Atmospheres, 96*(D12), 22283-22296, 1991.

Tobiska, W. K., Validating the solar EUV proxy, E-10.7, *Journal of Geophysical Research-Space Physics, 106*(A12), 29969-29978, 2001.

Tourpali, K., C. J. E. Schuurmans, R. van Dorland, B. Steil and C. Bruhl, Stratospheric and tropospheric response to enhanced solar UV radiation: A model study, *Geophysical Research Letters, 30*(5), 2003.

Usoskin, I. G., N. Marsh, G. A. Kovaltsov, K. Mursula and O. G. Gladysheva, Latitudinal dependence of low cloud amount on cosmic ray induced ionization, *Geophysical Research Letters, 31*(16), 2004.

Usoskin, I. G., O. G. Gladysheva, and G. A. Kovaltsov, Cosmic ray-induced ionization of the atmosphere: spatial and temporal changes, *Journal of Atmospheric and Solar-Terrestrial Physics, 66,* 1791-1796, 2004.

van Loon, H., K. Labitzke, 1994: The 10-12 year atmospheric oscillation. *Meteorol. Z.* **3**, 259-278.

Verschuren, D., K. R. Laird and B. F. Cumming, Rainfall and drought in equatorial east Africa during the past 1,100 years, *Nature, 403*(6768), 410-414, 2000.

Viereck, R. A. and L. C. Puga, The NOAA Mg II core-to-wing solar index: Construction of a 20-year time series of chromospheric variability from multiple satellites, *Journal of Geophysical Research-Space Physics, 104*(A5), 9995-10005, 1999.

Viggiano, A. A. and F. Arnold, Ion Chemistry and Composition of the Atmosphere, in Handbook of Atmospheric Electrodynamics, edited by H. Volland, pp. 1-26, CRC Press, Washington,D.C., 1995.

Wagner, G., J. Beer, J. Masarik, R. Muscheler, P. W. Kubik, W. Mende, C. Laj, G. M. Raisbeck, and F. Yiou, Presence of the solar de Vries cycle (_205 years) during the last ice age, Geophysical Research Letters, 28(2), 303–306, doi:10.1029/2000GL006116, 2001.

Wang, Y. M., J. L. Lean, and N. R. Sheeley, Modeling the sun's magnetic field and irradiance since 1713, *Astrophysical Journal 625*, 522-538, 2005.

Washington, W.M., et al., Parallel climate model (PCM) control and transient simulations, *Climate Dynamics, 16,* 755-774, 2000.

White, W. B., J. Lean, D. R. Cayan and M. D. Dettinger, Response of global upper ocean temperature to changing solar irradiance, *Journal of Geophysical Research-Oceans, 102*(C2), 3255-3266, 1997.

Wilcox, J. M., P. H. Scherrer, L. Svalgaard, W. O. Roberts, R. H. Olson, and R. L. Jenne, Influence of solar magnetic sector structure on terrestrial atmospheric vorticity, Journal of the Atmospheric Sciences, 31(2), 581–588, 1974.

Williams, V., J. Austin and J. D. Haigh, Model simulations of the impact of the 27-day solar rotation period on stratospheric ozone and temperature, *Ozone Variations of Solar Origin, 27*(12), 1933-1942, 2001.

WMO 2007 Scientific Assessment of Ozone Depletion: World Meteorological Organisation Global Ozone Monitoring Project Report No. 50, 2006.

Yu, F. Q., Altitude variations of cosmic ray induced production of aerosols: Implications for global cloudiness and climate, *Journal of Geophysical Research-Space Physics, 107*(A7), 2002a.

Yu, F. Q., Altitude variations of cosmic ray induced production of aerosols: Implications for global cloudiness and climate, *Journal of Geophysical Research-Space Physics, 107*(A7), 2002b.

Yu, F., Binary H2SO4-H2O homogeneous nucleation rates based on a kinetic quasi-unary model: Look-up tables, *Journal of Geophysical Research,* doi:10.1029/2005JD006358, in press. 2006

Yu, F., and R. P. Turco, Ultrafine aerosol formation via ion-mediated nucleation, *Geophysical Research Letters*, 27, 883. 2000

Yu, F., and R. P. Turco, From molecular clusters to nanoparticles: The role of ambient ionization in tropospheric aerosol formation, *Journal of Geophysical Research*, 106, 4797, 2001.

DNSC Scientific Report Series

DNSC Report Series is an informal report series, published at irregular intervals. This publication is copyrighted and may therefore only be reproduced electronically or in other media if this corresponds to direct citation and includes a full reference to the publication, i.e. individual pictures or brief quotations from the text.

1/2005 Khan, Shfaqat Abbas, Surface deformations analyzed using GPS time series

1/2007 Olsen, Nils, Terence J. Sabaka, and Luis R. Gaya-Pique,
Study of an Improved Comprehensive Magnetic Field Inversion Analysis for *Swarm*

2/2007 Christiansen, Freddy, Joanna D. Haigh, and Henrik Lundstedt,
Influence of Solar Activity Cycles on Earth's Climate

Danish National Space Center
Juliane Maries Vej 30
DK-2100 København Ø
Phone +45 3532 5700
Fax + 45 3532 2475
Mail office@space.dtu.dk
www.space.dtu.dk